COVALENTLY BONDED PROTEIN SURFACES ON POLY(METHYL METHACRYLATE): CHARACTERIZATION BY X-RAY PHOTOELECTRON SPECTROSCOPY AND ATOMIC FORCE MICROSCOPY

by

Geoffrey Winston Nelson

A thesis submitted to the Department of Chemistry

In conformity with the requirements for

the degree of Master of Science.

Queen's University

Kingston, Ontario, Canada

(September, 2008)

Abstract

X-ray photoelectron spectroscopy (XPS) and atomic force microscopy (AFM) have been used to characterize a poly(methyl methacrylate) (PMMA) surface with covalently attached proteins. Protein-terminated PMMA surfaces have possible applications as substrates for bio-reactive surfaces or biosensors. The PMMA surfaces were first aminated using hexamethyldiamine; the resulting $-NH_2$ sites were reacted with the hetero-bifunctional cross-linker Sulfo-EMCS. The N-hydroxysuccinimide ester terminal and maleimide terminal groups of Sulfo-EMCS can react with surface amine groups and sulfhydryl-containing proteins respectively. A surface that has covalently bonded with such proteins is interesting, as it may be used to develop techniques to compare the mechanical properties of proteins that have similar functions, but different structures. This study characterizes *Thermotoga maritima* β-glucosidase 1 (TmGH1), which belongs to a family of proteins that facilitate hydrolysis of glucose-related monomers with retention of conformation. The resulting surfaces were characterized by XPS to monitor surface composition and coverage. Tapping and contact-mode AFM methods were used to image the surface and obtain force curves. Data that suggests the creation of a covalently bonded surface of TmGH1 on PMMA has been obtained, as well as force curves using dodecanethiol-terminated AFM tips that suggest specific unfolding events when a mechanical force is applied to TmGH1. These results have applications to the further investigation of protein folding and unfolding mechanisms of family GH1 proteins using AFM-related techniques.

Acknowledgements

I would like to thank my supervisor, Dr. J. Hugh Horton, for his many years of guidance and mentorship during my undergraduate and graduate years at Queen's University. This thesis would not have been completed without the educational and enjoyable discussions we have had regarding this thesis.

I would also like to thank my supervisory committee members, Dr. Hesp and Dr. Liu, for their advice at the mid-point of this project. I would also like to thank Lyndsay Hull for supplying some solvents and providing access to equipment necessary for the experiments. The teamwork of the Horton Group has helped facilitate many aspects of experimentation, so I would like to thank Sorin Nita, Peiling Sun, Dan Wang and Mohammed Bhuiyan. Of course, this project would not have been possible without the synthesis of proteins completed by Dr. David Zechel, Meagan Perry and Shu Mei He of Queen's University.

The support of my family and friends throughout my time at Queen's University has been marvelous; it gives me much strength and motivation to know that they love me and believe in my abilities. Queen's University will always have a place in my heart, because of the many people I have been fortunate to meet during my time here.

Finally, I wish to acknowledge the financial support of Queen's University and the Faculty of Graduate Studies. Also, the support of Queen's Residence Life for the past two years has allowed me to continue part-time work as a Residence Don, while remaining a graduate student.

Table of Contents

List of Figures

List of Tables

Chapter 1

Introduction

Polymers are macromolecules comprised of repeating chemical units (monomers) that are covalently-linked together. Polymer chemistry can be found all around us: polysaccharides (starch, cellulose, RNA, DNA), polypeptides (proteins and enzymes), natural products (rubber and silk), and industrial products (nylon, synthetic textiles, vulcanized rubber and plastics). Some of these polymers can form solid structures with useful physical and chemical properties. In particular, the related surfaces chemistry is of interest to those that wish to modify polymer surfaces to achieve a chemical goal. One such goal is the covalent immobilization of proteins on polymer surfaces for the purpose of creating an analytical device or to investigate protein response to mechanical forces. This thesis aims to immobilize proteins onto a polymer substrate for the purpose of surface characterization. Imaging and mechanical force experiments using atomic force microscopy (AFM) and surface analysis using X-ray photoelectron spectroscopy (XPS) are conducted on prepared samples.

The polymer substrate that is to be modified is a surface of poly (methyl methacrylate) (Figure 1.1), or PMMA. It has been used in analytical chemistry applications that focus on biological molecules, such as microfluidics,[1,2,3,4] mass spectrometry,[5] bio-reactive surfaces,[6, 7] and non-specific adhesion of biological molecules.[7] A trend in all of these applications is the modification of PMMA to accept non-specific and/or specific protein interactions. A notable example of a specific, biological PMMA interaction is the procedure proposed by Fixe *et al.* to chemically modified PMMA to accept thiol-terminated DNA.[8] The PMMA surfaces in this thesis were modified using a protocol that converted the original ester-terminated surface into a maleimide terminated surface, which can then covalently bond to a cysteine terminated protein (Figure 1.2).

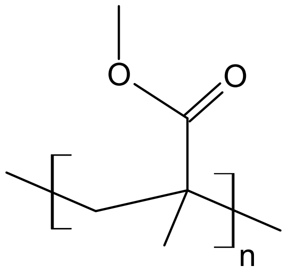

Figure 1.1: poly(methyl methacrylate)

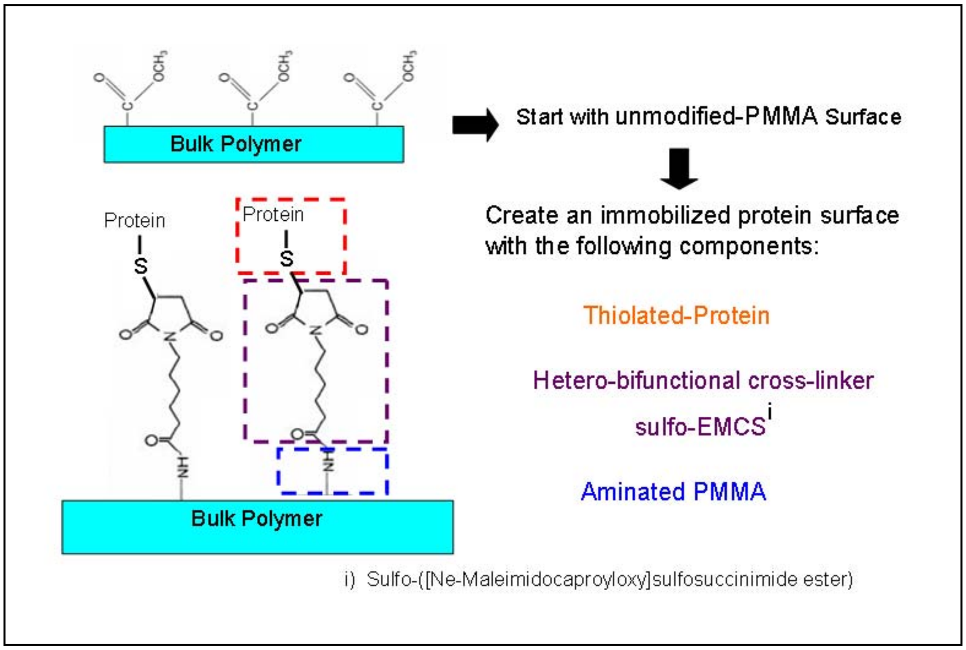

Figure 1.2: Summary of the surface modification procedure.

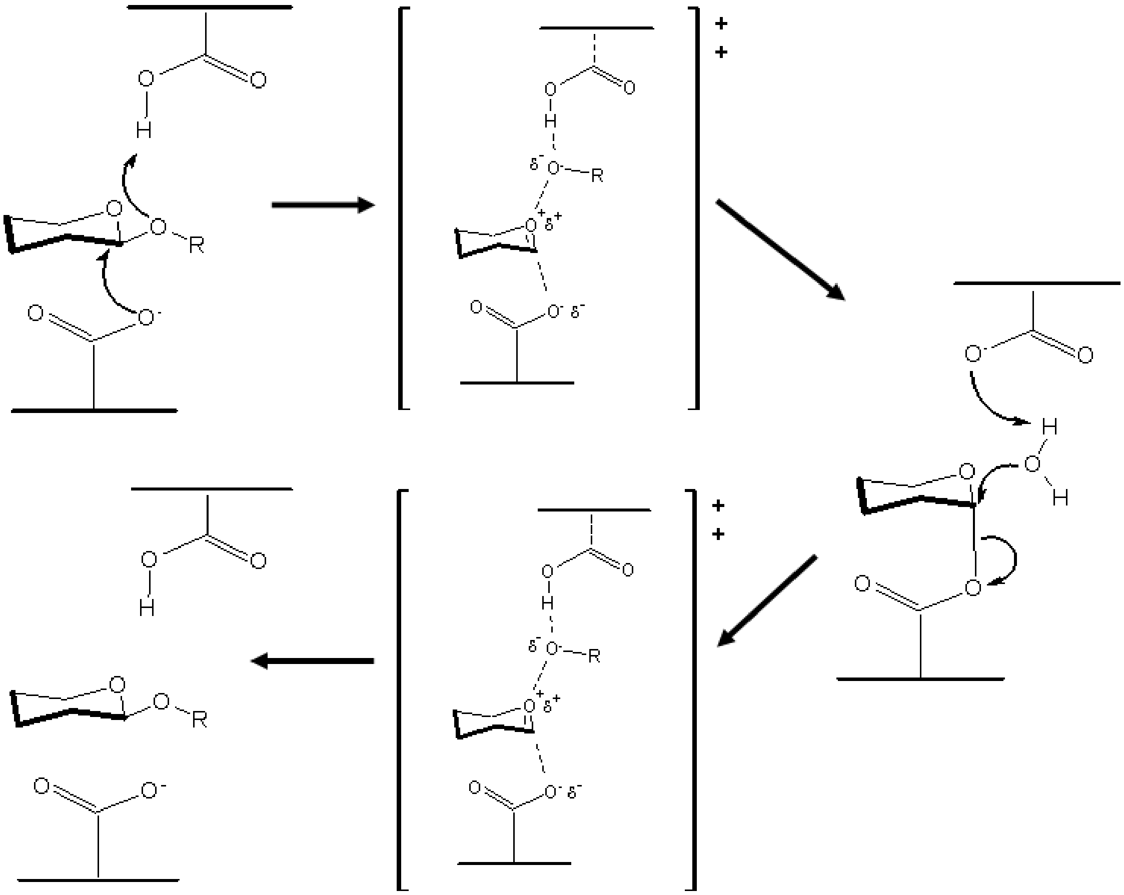

Figure 1.3: The mechanism of β-glycoside hydrolysis with net retention of anomeric configuration is shown above.[10]

The protein that is to be attached to the modified PMMA substrate is *Thermotoga maritima* β-glucosidase (TmGH1). This protein is a single-domain glycoside hydrolase, which is a family of proteins known to increase the rate of glycoside bond hydrolysis by a factor of 10^{17}.[9] The mechanism of the glycosidic hydrolysis is shown in Figure 1.3, above, as it is applied to β-glucosidase hydrolysis.[10] TmGH1 can be compared to other proteins within the family, such as *Agrobacterium feacalis* β-glucosidase (Abg), based on structure and response to environmental stimuli, such as temperature. For example, TmGH1 is stable up to 100 ºC (‘thermostable’; stable up to 100 ºC) and Abg is only stable to approximately 36 ºC (mesophile; stable up to 37 ºC). This presents the opportunity to investigate any structural differences between members of this family of proteins using known atomic force microscopy techniques, starting with TmGh1.[11] As well, specific XPS and AFM studies on surfaces covered with TmGH1 have not, to my knowledge, been conducted yet.

The protocol for PMMA surface modification to attach TmGH1 and other proteins has some novel applications and potential advantages over current methods used for other AFM and XPS studies. First, most AFM experiments with proteins use gold or silicon as the underlying substrate and the replacement of these substrates with less expensive and more chemically reactive substrates is attractive to researchers who wish to investigate a large number and variety of biological structures. The current inability to resolve unfolding events of solitary, single domain proteins using AFM limits the ‘resolution’ of mechanical AFM studies to multiple proteins attached to each other in a chain-like manner. Unfolding events have been visualized for chains of single domain proteins, but not for a single unit of the chain.[102] The ability to probe a single protein would be a truer representation of the unfolding forces involved and it could also open an avenue towards the probing of the chemistry of individual binding sites. In order to facilitate this ability, the distance between proteins needs to be minimized, while maximizing the probability of a tip-protein interaction. As well, the robustness of the protein-substrate bond needs to be improved, to withstand tip-sample interactions long enough for an unfolding event to be seen. The use of a cross-linker is thought to increase the chances of a specific protein-substrate interaction and a substrate containing a cross-linker is thought to reduce the surface density of the proteins to limit protein-protein interactions. The goal is to observe unfolding events within an individual single-domain protein and this thesis aims to show an alternative method for attaching proteins to surfaces for mechanical investigations to achieve this goal.

While the AFM technique is often used to image and mechanically probe protein surfaces, the X-ray photoelectron spectroscopy (XPS) technique to study related surfaces is not as popular. XPS is not commonly used for proteins due to surface charging effects for non-conductive surfaces (which limit the resolution of the XPS technique) and the need for expensive apparatus to maintain high vacuum environments during experimentation. On the other hand, the XPS can offer chemical sensitivity and (limited) depth information that is not available via traditional AFM methods. The XPS technique will be used to compare the relative surface composition of different protein surfaces, identify possibly active and inactive (denatured) protein surfaces, and also suggest chemical orientation of the proteins with respect to the surface. A contribution will be made towards the more routine use of XPS to investigate protein structure and surface chemistry. Used together, AFM and XPS can provide both mechanical and chemical information about the surfaces studied here, and they both have extended applications to other systems.

1.1 Organization of Thesis

The protocols for creating a protein-terminated PMMA surface will be presented in this thesis. The surfaces will be characterized by XPS and AFM methods. The XPS method will determine the chemical composition of the surfaces and the AFM experiments will image and probe the response of attached proteins to mechanical force. The chemical modification of polymers for a variety of applications is a growing field and will be reviewed in this chapter, along with a review of investigations of protein structure using AFM. In Chapter 2, the theory and experimental methods involved in surface preparation and XPS theory will be discussed. Chapter 3 contains the XPS results and discussion of their significance. The AFM experiments and theory are explained in Chapter 4 and the results of those experiments are presented and discussed in Chapter 5. Brief conclusions will be made in Chapter 6 to summarize the results and significance of the thesis work.

1.2 Substrates for Attachment of Biomolecules

Polymers are macromolecules that are comprised of repeating chemical units (monomers) that are covalently-linked to each other. The surface modification of polymers to change or improve their adhesion qualities is required for some of these applications. A comprehensive review of “polymer surface modification for the attachment of bioactive compounds”, written by Goddard and Hotchkiss, places these experimental works on PMMA into a broader context.[12] Polymers can be used for biological applications in the medical and analytical fields of this particular research field.[12] The goal of attaching and characterizing TmGh1 and other proteins on PMMA would be a specific addition to the literature with regards to future applications to analytical and medical devices.

There seems to be two broad interests in the field of polymer chemistry for biological modification. Some intend to effect mass changes to polymer surfaces with a broad range of chemical functionality and uses. Examples of broad applications, include: the use of polymers to prevent a wide variety biological and environmental corrosion of undersea pipelines (ShawCor Ltd.; pipeline company); the near ubiquitous use of Teflon as a chemical resistant coating on household cooking items; and schemes to improve the general ‘stickiness’ of polymers for ‘saran wrap’ or other similar uses. At another extreme is polymer research that is aimed for very narrow interests and much research regarding the binding of proteins to substrates using specific methodologies falls into this category. The specific biochemistry of individual molecules must be considered when choosing a modification scheme. In the case of proteins, polymers must be chosen with consideration to protein terminal functional groups, intended application, and conservation of biological functionality.

Silicon and gold have been popular and traditional substrates for protein surfaces. Silicon has been used to bind to biological molecules through the modification of Si surfaces by organic functional groups. One approach has been to use hydrogen-terminated Si substrates to bind to ω – functionalized 1-alkanes using thermal or photochemical hydrosilation reactions, which is a surface that has been previously studied by our group with the goal of binding to biological molecules.[95] It is notable that H-terminated Si surfaces have the advantage of being relatively homogeneous surfaces that are free of oxides; this has the potential to facilitate the creation of reproducible arrays of biological molecules, such as DNA, on surfaces of Si.[13-15] Oxidized silicon substrates contain layers of Si-O-Si and Si-OH bonds, which can serve as points of attachment for biological molecules, but these surfaces are limited by their amorphous structure (disorder). However, ordered self-assembled monolayers on Si surfaces can be created by exposure of oxidized Si to organosilane reagents (e.g. chloro and methoxy-silanes) to create Si-O-Si bonds between the attached molecule and the Si substrate.[16] While this is relatively simple wet chemistry, the resultant surfaces are limited by the inhomogeneity of the preceding oxidized silicon surface and unwanted polymerization side-reactions.[14] There are a couple disadvantages of silicon substrates: first, the density of attachment points (individual Si or Si oxides) is lower than Au or polymers, which can limit applications that require a higher density of functional groups on surfaces; second, while simple, the chemistry involved with Si substrates utilizes harsh conditions (NH_4F, H_2O_2, H_2SO_4) to create H-terminated surfaces.

Gold has been used for the direct and indirect attachment of biological molecules. It is well known that thiol-terminated molecules can bind to Au through a sulfide bond. There are two popular methods used to attach biological molecules to an Au substrate: using self-assembled monolayers (SAMs) to attach proteins indirectly to Au or intentionally using thiol-terminated biological molecules to facilitate direct attachment to Au. Self-assembly on Au is the process where by small, thiol-terminate molecules - mostly alkanethiols – order themselves onto the substrate. Thiols terminated with various functional groups (e.g. amines, carboxylic acids, protein binding sites etc.) have been used to construct biologically active and inactive surfaces.[17] Thiol-terminated biotin (a protein binding group) was self-assembled with a molecule that resists protein adhesion (thiol-terminated oligo-ethylene glycol), to create a surface that could selectively bind the protein streptavidin, while maintaining the bioactivity of the protein.[16] Methyl and hexa-ethylene glycol terminated alkanethiol self-assembled monolayers (SAMs) were compared in terms of their abilities to adsorb RNase A; using florescence tags, it was determined that methyl-terminated surfaces showed evidence of protein adhesion, but not for the hexa-ethylene glycol surface.[18] The classic examples of direct adhesion of proteins to Au are found within the literature on AFM unfolding experiments using multi-domain proteins. A chain of proteins are bound to the Au surface through the sulfide bond and then are mechanically pulled from the surface using an AFM cantilever.[11,19] The use of silicon and gold as substrates for protein attachment is well established, but their expense, lack of optical transparency, among other reasons has motivated the search for alternative substrates for biological surfaces.

Polymers are the most commonly chosen alternative to Si and Au substrates due to their low cost, ease of device construction, ease of chemical modification, and, in some cases, optical transparency.[1,12] In particular, the use of polymers in analytical and medical devices to date have demonstrated the vast utility of these materials towards the manufacture of reliable, low-cost analytical devices with microstructures, such as channels. These are commonly formed through replica molding,[18] hot embossing,[1, 4] laser ablation,[20] and other methods which are reviewed here.[21] Compared to Si or Au, polymers suffer from the disadvantages of increased surface roughness, surface inhomogeneity, sensitivity to organic solvents, acids and bases, and unwanted side reactions during chemical modification (e.g. cross-linking, other functional groups etc.).[12, 21] To minimize these disadvantages, two approaches are taken: either synthesize a new polymer to achieve both the bulk and surface characteristics desired; or modify the first few micrometers (or less) of the surface of a bulk polymer to change its surface chemistry, while retaining most bulk properties. In most cases, such as in this thesis, it is easier to create a surface modification scheme than it is to synthesize a novel polymer.

1.3 Polymers Substrates and Chemical Modification (Biological)

There are a wide variety of polymers in use for the purpose of creating surfaces modified with biological molecules. Recently, Hotchkiss and Goddard have prepared an exhaustive review of this topic.[12] They have identified a number of polymers of interest to researchers within their review, but since our research has applications to biosensors and immobilized enzymes, the polymers that are of most interest are: Poly (dimethyl siloxane) (PDMS), Poly (tetrafluoroethylene) (PTFE) , Poly (pyrrole) (PPY), and Poly (methyl methacrylate) (PMMA).[12] Discussion will focus on the most popular substrates, which are PDMS and PMMA, however information on PTFE and PPY can be found in the Hotchkiss review; the focus on PDMS and PMMA has been that of our group and collaborators on previous projects.[1, 6, 22, 23] The choice of either PDMS or PMMA must take into consideration the goals of the project and the chemistry involved with the creation of a protein-terminated surface.

PDMS is one of the most popular substrates for the creation of biosensors and analytical devices, including microelectro-mechanical systems (MEMS) and fluorescent biosensors.[21] It is a polymer which is comprised of a backbone of Si-O-Si chains that are terminated by methyl groups. PDMS is a cheaper substrate than glass and can be fabricated using molding, casting or hot embossing techniques.[21] PDMS is quite hydrophobic compared to glass and this limits its ability to adhere to proteins.[21] Chemical modifications are employed to impart functional groups on the surface, such as the amine and sulfonic acid terminated PDMS surfaces previously studied by our group,[22] UV initiated graft polymerization, photolithography, silane chemistry (including SAMs) and oxidation of PDMS are all examples of other modifications of PDMS surfaces.[12, 21] PDMS is indeed a versatile substrate, but the methyl side chains of PDMS do require modification to either impart hydrophilicity or facilitate chemical functionality by simple organic chemistry.

Poly(methyl methacrylate) is comprised of repeating units of the methyl methacrylate monomer, which is shown in Figure 1.1. This polymer has a number of advantages as a substrate for various analytical devices: it has a high transparency (useful for optical detectors), low fluorescent background, easily moldable into different shapes (e.g. “Lab on Chip” creation) and ester side-chains that can be chemically modified to bond to biomolecules.[4] The ester side-chains also impart a hydrophilic property to the bulk material. The main disadvantage of using unmodified PMMA as a substrate is its low binding efficiency for biomolecules, as evidenced by poor attachment to anti-bodies.[4] It thus becomes important to use a chemical modification scheme to bind PMMA to biomolecules. This can be done using fairly benign organic chemistry strategies (e.g. hydrolysis, aminolysis), with a minimal time cost or expensive apparatus.

However, one must consider the possibility of polymer swelling with prolonged exposure to organic or aqueous solvents. Polymer swelling in PDMS is minimal in aqueous solutions. Also, the ease of chemical modification of the ester side-chains opens the possibility of numerous and unwanted side reactions during modification. PMMA is seen as an attractive substrate both because it has been shown to be a good platform for analytical devices, but also that the established chemistry to modify the surface to accept biological molecules is relatively benign. It is important for a protein-terminated PMMA device to be easily manufactured, have low cost, and yet still have specific binding characteristics to the proteins of interest here.

1.3.1 Chemical Modification of PMMA for Biomolecules

Chemical reactions involving PMMA centre around the modification of the carboxylic ester functionality on monomer side-chains. Ionized gas treatments[24] , UV radiation,[25] Laser radiation,[26] Wet chemical,[1] Organosilanes,[21] and the use of molecular tethers[8] are all techniques known to modify the PMMA ester group for a variety of purposes. There are advantages and disadvantages to each method, which are outlined in detail by Goddard and Hotchkiss (along with applications to these methods).[12]

1.3.1.1 Ionized Gas Treatments

There are three possible types of ionized gas treatments that can be used: Plasma, Corona discharge, and Flame treatment. The plasma treatment involves exposing the polymer substrate to a highly-charged and energized gaseous environment.[12] Particles, such as electrons and charged ions react with the surface to impart functionality based on the gas used in the procedure. The gases that are commonly used are Ar, N_2, O_2, H_2O, CO_2, and NH_3 ions and the extent of imparted functionality is also based on the operating conditions. For example, N_2 plasma has been used to increase the nitrogen component of PMMA and a variety of other polymers.[27] A comprehensive study of the effects of Noble gas, O_2 and N_2 plasma treatments on PMMA was made by Groning et *al.* where they demonstrated that plasma results in ester loss and that experimental conditions determine the resultant surface conditions.[28] Plasma treatment on PMMA is also used as a precursor to UV-graft polymerization or silanization.[12] Plasma treatments do suffer from poor reproducibility, expensive vacuum apparatus, and the potential for unwanted side reactions (i.e. radical reactions) or functionalities.

Corona discharge and flame methods are less used to modify PMMA and other polymers. The Corona-discharge method passes a current through electrodes which electrically induce the formation of charged particles in air, which are then streamed over the samples under atmospheric conditions.[12] The charged air causes a wide range of surface oxidation products, but this is also a disadvantage since specific functionality is often not a result. Compared to the more popular plasma method, corona methods suffer from contamination by the use of atmospheric conditions. An example of the use of corona discharge as a precursor to UV-graft polymerization of PMMA is a study by Ichijima et al..[21] Flame treatment usually utilizes a methane-flame to burn oxygen-enriched air, which is then passed over the sample. The polymers that are exposed to this treatment show an increase in oxidation products.[12] This simple technique has been used to change the wettability of PMMA in what seems to be an effective, low cost manner.[21] The flame treatment is less specific than plasma treatments, but in a similar manner to corona treatments, it represents a cheaper and less complicated alternative for imparting non-specific chemical modification to PMMA surfaces. In industry, these ionized gas treatments are often used to grossly increase the ability of PMMA to adhere to various coatings.[24] Despite access to plasma treatment methods by ozone, none of the ionized gas methods were used due to the non-specific nature of these treatments.

1.3.1.2 UV-radiation and Laser radiation

Prolonged exposure to UV light can form radicals on the surface of PMMA, which can then react to the surrounding environment or act as the first step towards the graft-polymerization.[12] Carboxylic acid groups have been added to PMMA using this technique.[21] UV-radiation induced photo-chemical reactions can also be controlled to functionalize micrometer to millimeter sized functionalized sites on the surface of PMMA.[21] Laser radiation using UV wavelengths can also be used to either physically ablate polymer surfaces or effect chemical changes. A relevant use of laser radiation to change the performance of a PMMA microfluidic device was demonstrated by Johnson et. al..[21] They showed that intersections of channels (90^0 turns) within a microfluidic device could be selectively modified by precise laser placement in order to reduce the effects of band broadening and also increase the efficiency of separations compared to unmodified micro-channels. This demonstrates the potential that laser radiation has for precise control over the UV modification of PMMA without ablating the surface.

The advantage of the UV and laser radiation methods is that it is easy to use and does not require wet chemical techniques. On the other hand, the technique has a number of disadvantages: first, the optical transparency of polymers can change, which would limit the post-treatment detection of biological molecules by optical methods; second, polymer degradation, which in the case of PMMA includes chain-scission and the lost of ester groups.[12] Polymer degradation needs to be avoided to ensure a robust platform for experiment and to limit the effects of polymer swelling by organic solvents.

1.3.1.3 Organosilanes

Organosilanes are a group of molecules that have the basic form $R_nSi(OR)_4$ and a commonly encountered sub-group, chlorosilanes, has the form $R_nH_mSiCl_4$; in both cases R is an organic functional group and OR can be a methoxy, ethoxy or acetoxy group. These molecules are known to form self-assembled monolayers on Si in a highly ordered fashion through a silanization reaction.[12] The product of these reactions is a Si-O-R, Si-O-Si, or even an Si-S-metal linkage, depending on the materials involved. This type of chemistry is used to functionalize polymer surfaces, particularly glass and PDMS, to promote adhesion to other substrates. Wet chemical approaches for silanization have been traditionally employed, but recent advances make chemical vapor deposition of silanes possible.[29] In the case of PMMA, pre-treatment by plasma treatments[29] or lithium aluminum hydride[12] have been shown to be reactive towards organosilanes. A diverse variety of terminal groups have been attached to PMMA, including perfluoroalkyl ($-C_nF_{2n+2}$), amino ($-NH_2$) and sulfhydryl (-SH) groups, by the utilization of silane chemistry.[29]

It is possible to conceive a protein-terminated PMMA surface having the same structure as proposed in this thesis, but through the use of either an amino terminated silane (amino propyltrimethoxy silane) or a maleimide-terminated silane.[30] While this is an alternative technique than the wet chemical approach taken in this thesis, organosilane chemistry still relies on pre-activation of the PMMA surface with plasma techniques, which is an added step and complication compared to the scheme developed in this thesis.

1.3.1.4 Wet Chemical Modifications

The wet chemical approach was chosen for tethering proteins to PMMA. This method is useful due to the ease of synthetic effort, readily available materials and the ability to modify both the surface and bulk properties of the polymer. As well, chemical reactions can occur at atmospheric conditions without use of advanced equipment. Issues that can arise when using wet chemical techniques to modify PMMA include: non-specific modifications in some instances; ester side-chain orientation; the use of hazardous solvents and reagents; polymer swelling or dissolution under prolonged exposure to solvents. Regardless, the wet chemical technique is a proven choice for PMMA modification.[12]

A variety of polymer modifications can be achieved using the wet chemical method. Ester groups of PMMA can hydrolysis to form carboxylic acid terminated surfaces[1, 6] or aminolysis with a primary amine.[8] Reagents such as concentrated sodium hydroxide and sulfuric acid can facilitate base and acid hydrolysis of PMMA respectively.[1] Lithium aluminum hydride in ether can also hydrolyze PMMA to produce a surface of carboxylic acids.[29] The aminolysis reaction is primarily used to create an amine-terminated surface, which can be done using 1,6 hexanediamine, ethylenediamine, N-aminoethyl-1,3-propanediamine and lithiated diamines.[12] Both hydrolysis and aminolysis have been used as pre-cursors to the attachment of homo or hetero cross-linkers, proteins, enzymes, DNA and other biological molecules to polymer surfaces.[12] While it is clear that both hydrolysis and aminolysis reactions can be used to adhere biological molecules to PMMA, the aminolysis reaction has the advantage of introducing nitrogen to a PMMA surface, which can be easily characterized using XPS between unmodified and modified samples.

1.3.1.5 Tethering and the use of a Hetero-bifunctional Cross-linker

While direct attachment of proteins to an oxidized or amine-terminated PMMA surface is possible using aminolysis and hydrolysis reactions, there are problems with direct attachments of proteins to such substrates. These include reduced bio-activity of attached proteins, over-functionalization of the surface, and unwanted non-specific protein-surface or surface-AFM tip interactions.[12] Attachment of biomolecules directly to unmodified PMMA, or even functionalized PMMA, could lead to denaturation of the protein by hydrophobic surface forces.[12] It seems that tethering bioactive compounds to surfaces using a linker molecule (also known as a spacer molecule) reduces steric effects and improves bioactivity.[12, 8] In their related review, Goddard and Hotchkiss[12] identify key effects of tethering on bioactivity and their use avoids protein denaturing and over-functionalization of a surface.[12] In terms of the acquisition of AFM data, it is important to reduce the magnitude and frequency of non-specific surface forces since they can interfere with protein force data collected in the region of 0-30 nm from the surface.[11] The approach normally taken to magnify the protein force data is to connect proteins into repeating chains of individual proteins.[31] This leads to the visualization of multiple force curves whose signal to noise ratio is quite high. However, the preparation of tandem repeats of proteins increases preparation time and intensity. Tethering a single protein to the surface could be to be an alternative approach which achieves a similar effect – lowering the non-specific interactions (i.e. background noise). A protein tethered to the surface should reduce steric interactions and non-specific interactions between a protein, other proteins, and the underlying PMMA substrate. The use of a cross-linker within the surface modification scheme is a key component of this work, and this chemical modification of PMMA is intended to preserve the bioactivity of proteins both for an analytical device and for the detection of protein response to mechanical force.

A use of a spacer unit or tether unit is necessary to mitigate these effects. The use of the hetero-bifunctional cross-linker Sulfo-EMCS has been used to covalently immobilize amine and thiol terminated DNA to PMMA.[8] The reaction was based on known aminolysis reactions of esters in the presence of electron donators, at basic pH conditions.[8] While this method is successful for DNA attachment, the high pH conditions (~pH 11) could affect the bio-mechanical properties of proteins in any adaption of the methodology. Also, this method uses the direct attachment of an electron donor to one of the terminal ends of DNA, which would most likely interfere with the bio-mechanical experiments using the AFM. Regardless, tethering is an attractive modification to PMMA and the method of Fixe *et al.* has been changed to facilitate the attachment of TmGH1 to a PMMA substrate.[8]

1.4 Characterization of Bio-Active Protein Surfaces

There are many surface characterization techniques, including atomic force microscopy (AFM), scanning tunneling microscopy (STM), infrared methods (FTIR, RAIRS), X-ray photoelectron spectroscopy (XPS), Auger electron spectroscopy (AES), transmission electron microscopy (TEM) and scanning electron microscopy (SEM), and optical methods (contact angle, fluorescence etc.). While many of these methods could have been used to characterize bioactive surfaces, the focus will be on AFM and XPS. Auger Electron Spectroscopy will also be mentioned briefly as it was used to characterize the chemical nature of sulfur on the modified surfaces.

1.4.1 Atomic Force Microscopy: Protein Force Curve Experiments

Atomic force microscopy (AFM) was developed by Binning *et al.* [32] as an alternative to the scanning tunneling microscope (STM)[33] for insulators and other poorly conducting surfaces. Since then, the AFM has been used to image a wide variety of surfaces, including polymers and biological molecules. There are two commonly used modes of AFM experiments: contact mode and tapping mode. The basic design of a contact mode AFM experiment is as follows: a flexible, but micrometer-sized tip approaches a surface by use of piezo-electric motors, capable of small changes in distance. A laser beam is aimed at the tip and reflected onto a photo-diode array. When the tip is in contact with the surface it is deflected from a horizontal position; this deflection is measured as a change in the laser position on the photo-diode detector. The tip can be moved away from the surface and the tip will continue to show deflection until it "snaps" out of contact with the surface. A calibrated force-distance curve can be obtained from the resultant data. In the tapping (or non-contact) mode, the AFM tip is oscillated by acoustic (AC-mode) or magnetic (MAC-mode) source at the resonance frequency of the tip. The tip is then placed above the surface and changes in the tip amplitude and phase are recorded. This mode allows images to be made of the surface that have nanometer resolution.[30]

The unfolding of proteins and imaging of proteins using AFM has been reviewed by many[33-35] and has also been featured in an issue of *Current Opinion on Structural Biology* (Issue 1, Volume 13). The AFM technique was first used to investigate the folding pathway of the domains of a single protein (immunoglobulin (Ig) domains of titin – a muscle protein) by Rief *et al.* in 1997.[33] There were two important outcomes of that experiment: the separation of individual protein domains leads to a characteristic saw-tooth pattern in the force-distance curve; and that unfolding forces depended on pulling speed. Both of these features were later related to the 'energy landscape' of unfolding proteins, as reviewed by Zhaung and Rief.[33] Subsequent experiments developed an understanding of protein unfolding dynamics, including further studies of titin (Ig and Fibronectin-type III domains (FnIII), both β-type folds), [31,36,37] tenascin (FnIII domains).[38] As well the following proteins and domains have been studied with success: the RNase barnase,[11] ankyrin (ANK) domains,[39] and T4 lysosome (α-type domains).[38] RNA has been reversibly unfolded using single force microscopy (SFM) techniques by Liphardt *et* *al.* in 2002.[30] Also, protein and inhibitor systems have been studied using the single molecule force microscopy capabilities of the AFM.[30] The aim of all of these papers and reviews has been two fold: to develop the AFM technique for proteins and to develop an understanding of the mechanical and thermodynamic relationships involved with the experiments.[33, 40]

1.4.2 X-ray Photoelectron Spectroscopy: Polymers and Proteins

X-ray photoelectron spectroscopy is a method of determining chemical composition of surfaces. Kai Siegbahn developed this technique in the mid 1960's and he was acknowledged for his research in the field with a Noble Prize in 1981.[41] When a sample is bombarded with high energy X-rays, electrons from core atomic levels are ejected from the surface. The kinetic energies of ejected photoelectrons are characteristic of the element from which the photoelectron originated. A combination of detection apparatus and computer software allows spectra to be obtained that show the chemical composition, oxidation states and relative quantities of elements within a sample. XPS is complementary with AFM because it provides some chemical information that is unattainable with the AFM technique and other scanning probe methods. XPS has been used to analyze the surface chemistry of polymers, and to a lesser extent, proteins.

XPS as an analytical tool works best when using conducting samples, but the surface chemistry of non-conducting samples, particularly polymers, have been studied in depth. In the case of polymers, there exists a wide range of resources and examples that address chemical composition, polymer XPS spectra and various experimental issues.[41,42] In the case of PMMA, the XPS spectrum of unmodified PMMA is often shown as a reference before any surface modifications are conducted on this particular substrate, thus it serves as a notable example of polymeric XPS analysis.[24, 43] The XPS technique has been used to characterize a variety of modified polymer surfaces, due the surface sensitivity (~ first 10 nm) of the method. In the case of polymers, the XPS spectrum is used to identify the nature of the carbon, oxygen, and nitrogen composition, along with that of other elements of interest, such as fluorine in fluropolymers. More recently, there have been advances in modifying XPS to serve as a chemically sensitive imaging device for the characterization of polymeric materials.[25] The major issue that arises during XPS analysis of polymers is that the non-conducting nature of these substrates can lead to surface charging or polymer degradation. The former problem is overcome through the use of electron flood guns while the latter is dependent on the material and exposure time to the X-ray radiation.[44] XPS is used here to characterize modified and unmodified PMMA surfaces.

The ability of XPS to identify elemental composition, relative quantification, and possible surface functional groups has been useful in biochemical analysis. An early review on the subject of biomaterial characterization by XPS is written by Ratner[96] and a more recent review written by Merrett *et al.* offers a more modern perspective on the field.[97] Throughout the literature, it is clear that XPS is an important characterization tool for biomaterials and this is demonstrated by its use to determine protein orientation using bound metals[98] protein adsorption phenomena onto other polymers,[99] and even biological samples that have been prepared by cryogenic freezing.[100] While the XPS is sensitive to the surface chemistry of biomaterials and related devices, it is equally sensitive to surface contamination by the ambient environment; this limitation is overcome through careful sample preparation and limiting exposure time to atmospheric conditions. In this thesis, the biological surface that is studied is a TmGh1-terminated surface and it will be characterized using the XPS technique.

1.5 TmGH1

Nature requires the ability to break down glucose and glucose monomers of related polymers, in order to gain energy or as a precursor to other biological functions. The β - Glucosidase Hydrolases are an important group of enzymes that hydrolyze glucose monomers and they are important to a variety of species in nature, including archaea, bacteria, plants, mammals and insects; for example lactase-phlorizin hydrolases is a component of the human digestion system and cellobiases in bacteria break down cellulose for energy needs.[45]

Thermotoga maritima β - Glycosidase Hydrolase 1 is a protein belonging to Family 1 and clan GH-A based on its amino acid sequence and tertiary structure (shorted to GH-1).[46] The GH-1 structure was first elucidated from GH1 produced by white clover for a suspected plant defense mechanism.[30] This report demonstrated that the protein had a single domain comprised of a mixture of α-helicies and β-sheets that formed a barrel-like structure (TIM barrel of 8 α-helicies and 8 β-sheets) and an overall globular, torid shape.[30, 46] There is a pocket near the C-terminus of the protein which contains two glutamic acid units and a variety of other polar, aromatic and charged species.[46] One glutamic acid unit acts as a nucleophile and the other as a acid/base catalyst for the hydrolysis of glucose with retention of configuration of the molecule.[45]

While GH-1 proteins are mostly found as individual protein monomers, it is important for the AFM studies to acknowledge that they can also form oligomers in solutions.[46]

Current research on the GH-1 proteins and, particularly TmGH1, has been generally limited to solution based chemical analysis or structural analysis by X-ray diffraction techniques. General reviews of the mechanistic pathway of the hydrolysis of glycosides can be found in various papers.[9, 45] These reviews confirm the general scheme of Figure 1.3 for the hydrolysis of a glucose unit for a GH-1 protein. In the case of TmGH1 there are some published and unpublished structural databases on The Protein Database that show the structure of TmGH1 complexed with a variety of inhibitors (isofagomine and 1-deoxynojirimycin).[47] These structural studies need to be considered in context with kinetic studies of inhibitors of the GH-1 β-glucosidases by kinetic or thermodynamic experiments, including those using salicortin,[48] idsofagomine Lactam,[49] tetrahydrooxazine and derivatives,[10] and the aforementioned Isofagamine and 1-deoxynojirimycin.[47] In the last case, it is suggested that TmGH1 inhibition pathway is still under recent investigation regarding its enthalpy, entropy, kinetic, thermodynamic and active site properties; continued study would aid in the design of optimal inhibitors for a variety of β-glucosidases. To my knowledge, there are no known mechanical AFM studies of GH-1 proteins or XPS studies on GH-1 proteins. There are AFM imaging studies of GH-1 proteins and one in particular uses inactive GH-1 proteins to observe the structure of a carbohydrate.[50] The AFM has also been used to image the binding events leading to the hydrolysis of glucose within glucosylceramide by β-glucosidase that has been activated by another protein.[51] One of the disadvantages of AFM is the inability to probe the 3 dimensional, internal structure of proteins, but the AFM protein pulling experiments show promise in determining the mechanical properties of the GH-1 structure.

Chapter 2

XPS Experimental and Theory

2.1 Surface Modification Protocols

All surfaces, glassware, tweezers and scissors were pre-cleaned with copious amounts of ddH_2O (de-ionized and distilled H_2O) and MeOH. Afterwards, they were dried with N_2 gas from a cylinder source. There were two types of underlying substrates used: mica (V-4 Grade, SPI Supplies) and Au (111) (Georg Albert PVD–Beschichtungen; sputter-coated, 300 nm thick on mica). Both surfaces were used to support spin-coated PMMA and modified PMMA samples, but the former was used for non-XPS experiments and the latter was used for XPS experiments. The Au served as an internal binding energy standard for XPS experiments as discussed in section 3.1. If prepared samples could not be placed immediately into the XPS preparation chamber, then they were placed into two plastic bags filled with nitrogen gas to preserve sample integrity. A general schematic of the protein-terminated PMMA surface is shown in Figure 1.2. The modification of PMMA to immobilize proteins is primarily based on two methodologies: gross-modification of PMMA for microfluidic applications, by Brown *et al.*[1], and the modification of PMMA to make a covalent attachment of DNA to PMMA surfaces by Fixe *et al.*.[8]

Henry *et al.* proposed a method for spin-coating PMMA onto Au or mica[3]; this procedure was followed with little modification. PMMA was provided by Warehoused Plastics Ltd. (Toronto) and was dissolved in dichloromethane (CH_2Cl_2) to a concentration of 0.5 mg/mL. The solution was sonicated until the PMMA was dissolved (approximately 30 minutes to 1 hour). The PMMA/CH_2Cl_2 solution should be stored under a fume hood due to its carcinogenic risk. Mica or Au (111) samples were cut using scissors to an approximate size of 1 cm by 1cm. These substrates were placed in a spin coater (Model: WS-200-4N-PP-RV, Laurell Technologies Corp.) that used a vacuum to hold the samples in place during rotation. If the samples were too small for the spin-coater sample holder, then samples were attached to a larger, clean piece of mica using double sided tape. PMMA was spin-coated onto the substrates at 2200 rpm for 70 seconds per droplet of PMMA solution. The total amount of solution placed on the spinning mica varied from 100 µL to 600 µL, in 100 µL or 200 µL increments, depending on the experiment. The samples were then cleaned with H_2O and MeOH, and dried with N_2 gas.

There were a variety of treatments used to modify the PMMA surface. A summary of all the surface treatments is shown in Table 2.1 and outlined in more detail in Appendix A. The PMMA substrates were oxidized using a 1.0 M solution of sulfuric acid (H_2SO_4 ,1.0 M) for 1 , 5, or 20 minutes at 298 K or 333 K.[1] A typical hot water bath and hot plate was used to heat 20 mL of H_2SO_4 to 333 K, while avoiding any mixing of sulfuric acid and water. Samples were washed with copious amounts of H_2O after treatment. In order to create NH_2-terminated surfaces, PMMA or oxidized-PMMA was exposed to a 1.0 M or 2.0 M solution of ethylenediamine (Sigma Aldrich – Reagent Plus. >99%) in DMSO (Sigma Aldrich), as suggested by various sources.[1, 3, 8] The solution was sonicated for 15 minutes and then the samples were exposed to the solution for a variety of timeframes (1, 2, 5, 10, 20 minutes) and at two temperatures (298 K or 333 K). Experiments occurring at 333 K required the ethylenediamine solution to be pre-heated using a hot plate. The sample was then placed into solution and the entire beaker was put into an oven set at 333 K for the reaction time. It should be noted that most samples were prepared with one exposure to ethylenediamine, but samples B2, W1 and W2 in Appendix A represent a single sample that was sequentially treated with the diamine solution, in order to compare the XPS signals of single and multiple treatment protocols. Some samples were treated with aqueous 1.0M NaOH standardized solution (pH 12.5), for 1 minute or 10 minutes, with the intention of reducing NH_3^+ groups that may have been present after normal preparation of the amine-terminated samples. Other samples were placed in a vacuum oven for at least 1 hour at 333K in order to evaporate residual DMSO solvent that may interfere with the S 2p XPS spectrum of the samples.

Sulfo-EMCS (N-[ε-maleimidocaproyloxy]sulfosuccinimide ester, M.W. 410.33 g mol^{-1}, 50 mg bottle; Pierce) is a moisture sensitive compound that required storage in a dessicator at 4 °C. A stock solution of 10 mM Sulfo-EMCS was made by dissolving the compound in a 50 mM borate buffer (pH 9.02). From this stock solution, 1 mM and 0.1 mM solutions of Sulfo-EMCS/buffer were made as required. NH_2-terminated PMMA samples were exposed to the buffer solution for 2 hours (recommended by Fixe *et al.*[8]) or 4 hours, at room temperature. Samples were then washed in two separate borate buffer solutions for 5 minutes each; they were then rinsed with copious amounts of ddH_2O and dried with N_2 gas. Some samples were placed in a vacuum oven (at least 1 hour, usually overnight) to reduce the potential contamination of the sample by NHS (N-hydroxysuccinimide) or DMSO residuals on the surface.

Modification	Purpose
Au under mica	Minimize Charging on XPS Samples
Spin-Coat PMMA	Thin Layer of PMMA on mica or Au/mica
Varying volume and size of droplets spin coated onto mica	Vary thickness of PMMA on surface
1.0 M Sulfuric Acid	To oxidize PMMA surface
1.0 M Ethylenediamine	To terminated surface with -NH_2 and attach sulfate end of Sulfo-EMCS to surface
1.0 M NaOH treatment	To minimize amount of -NH_3^+ on surface in order to maximize locations for Sulfo-EMCS to chemisorb
Sulfo EMCS	Hetero-bifunctional cross-linker to link substrate to thiol-terminated proteins and as a spacer to minimize protein interactions on surface.
TmGH1	Thermostable glucosidase
Abg	Mesophile glucosidase
phnH	This protein has two terminal cysteine groups (with -SH terminal ends); used to determine the orientation of TmGH1 on surface by comparing the XPS S2p signals of TmGH1 (one terminal cysteine group) to phnH
Volume	Increase concentration of functional groups on surface
Time	Increase or minimize extent of a reaction
Temperature	Increase extent of a reaction
Buffers	To prevent denaturization of proteins on surface or to maximize extent of reactions
Protein directly exposed to surfaces other than Sulfo-EMCS terminated PMMA (such as Au, PMMA, and NH2-PMMA)	Used in attempts to identify a covalent bond between surface and protein

Table 2.1: Summary of the surface modifications required to attach a thiol-terminated protein to PMMA

The proteins, TmGH1, Abg, and phnH were prepared by Meagan Perry and Shu Mei He of the Zechel Group at Queen’s University. The key structural feature of these proteins is that they are cysteine terminated at either one end (TmGH1 and Abg) or both ends (phnH). All protein solutions were flash-frozen using liquid nitrogen and stored in a -80 °C freezer inside small (~1mL) vials. When needed, solutions were thawed at room temperature and extracted from the vials using a micropipetter. TmGH1 was dissolved in a 50 mM sodium phosphate (Na_2HPO_4) buffer (pH 7.0) to a concentration of 22.4 μM (stock solution), which was then diluted to a concentration of 3.73 μM. A 43.2 μM solution of phnH was created using a 50 mM HEPES buffer (N-2-Hydroxyethylpiperazine-N'-2-ethanesulfonic acid, pH 7.5), with 150 mM of NaCl. This stock solution was diluted to 1.66 μM and 7.2 μM for experiments. Protein solutions were sonicated for 15 minutes prior to treating the samples. All samples were treated for 30 minutes and then washed twice, for 5 minutes each time, in the appropriate buffer solution. Afterwards, the samples were cleaned with ddH_2O/MeOH and placed in a vacuum oven for at least 1 hour. Samples that had the potential to specifically bind to these proteins were terminated with either Au (111) or Sulfo-EMCS. A variety of samples are to be studied in this thesis and the names of the samples surfaces will related to the compounds used to make them:

- PMMA
- NH_2-terminated PMMA (post-ethylenediamine treatment)
- Sulfo-EMCS terminated PMMA (post-Sulfo EMCS treatment, note that surface is terminated with a maleimide group)
- Protein-terminated PMMA (protein can be replaced with TmGH1, phnH or Abg)
- TmGH1-terminated Au (TmGH1 directly attached to Au)
- TmGH1-terminated PMMA (TmGH1 directly attached to PMMA)

- TmGH1-terminated NH_2-PMMA (TmGH1 directly attached to NH_2-terminated PMMA)

A full list of the studied samples is found in Appendix A and a general summary of the procedure used to make them can be found in Figure 2.1.

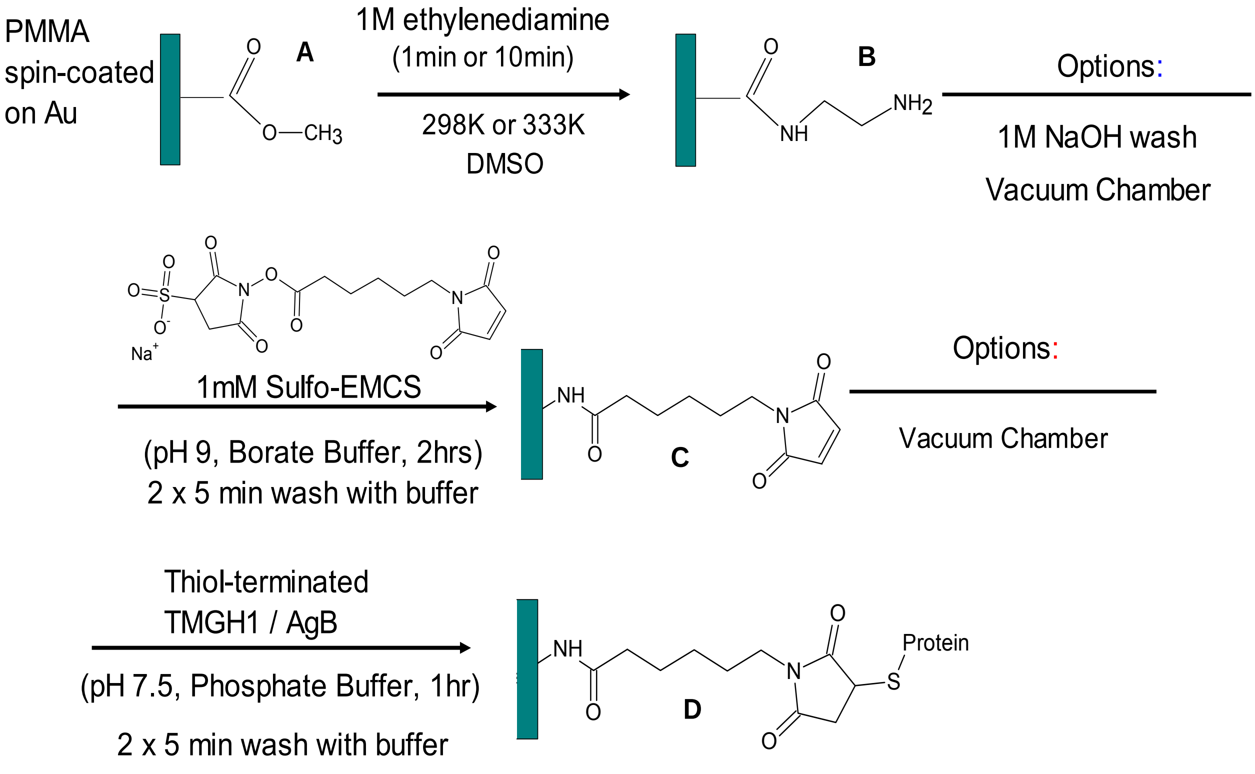

Figure 2.1: A schematic shows the surface modfication process that has been developed, including modifications used to optimize technique. There are four primary surfaces studied by XPS and AFM: (A) PMMA; (B) NH_2-terminated PMMA; (*C)* Sulfo-EMCS-terminated PMMA; (D) protein-terminated PMMA.

2.2 XPS

This section of the chapter will introduce the theory and practical considerations for the XPS system. Section 2.2.1 will introduce the basic XPS theory, section 2.2.2 will describe and explain how the XPS apparatus collects a signal, section 2.2.3 will explain the analysis methodologies employed in this thesis, and section 2.2.4 will describe the experimental set-up for the XPS apparatus used to collect the presented spectra.

2.2.1 XPS Theory

X-ray photoelectron spectroscopy is a method of determining chemical composition of surfaces. This method was developed for routine evaluation of surfaces by Kai Siegbahn in the mid 1960's and his efforts were rewarded with a Noble Prize in 1981.[52] The X-ray photoelectron process was known to exist previously, but the use of soft X-rays from Mg Kα (1253.6 eV) and Al Kα (1486.7 eV) sources, rather than the hard X-ray sources like Mo Kα (17.5 keV), and the development of better magnetic analyzers contributed to the advancement of the XPS technique. Also, the achievement of resolutions of 1.0 eV or better was crucial to the ubiquitous use of XPS for surface characterization.[52]

There are many handbooks and articles which describe the XPS process. Briggs *et al.*[41] and Moulder *et al.*[53] are excellent references for introductory and advanced reading on the technique. In general, high resolution XPS data is obtained by using an instrument that can generate low energy X-rays (typically produced from Mg Kα (1253.6 eV) or Al Kα (1486.7 eV) sources). These X-rays are directed towards a sample, which leads to the excitation of core-state electrons (1s, 2s, 2p, etc.). These electrons are ejected from the sample with a kinetic energy, K_E, and they are called photoelectrons. The kinetic energy of an ejected electron can be related to its binding energy, B_E:

$$K_E = h\nu - B_E - \Phi \qquad (1)$$

Where hν is the excitation energy of the incoming X-ray and Φ is the spectrometer workfunction (described below). Figure 2.2 shows the X-ray photoelectron process and the instrumentation required to detect ejected photoelectrons.

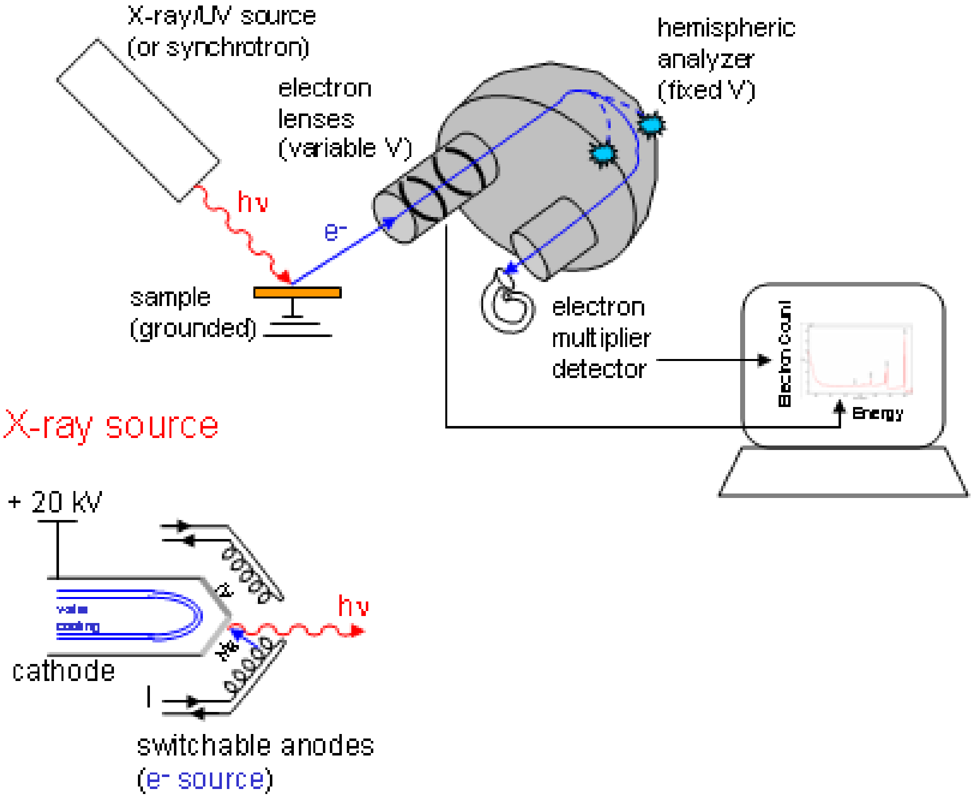

Figure 2.2: Schematic of an XPS analysis system. (courtesy of Dr. J.H. Horton, Queen's University, Department of Chemistry)

Each element has a unique XPS spectral signature, which means that the binding energy of the obtained peaks can be used to identify surface composition and chemical states of elements in the surface region. If a particular element in a sample exists in a number of different chemical states, then a variety of photoelectron binding energies for that element may be detected. Electrons in tightly bound, core states will have a lower detected kinetic energy and a higher binding energy and vice versa. For example, a photoelectron from a 2s orbital would have a higher binding energy than a photoelectron from a 4f orbital of the same element. The 3d photoelectron from a metal oxide would generally have a higher binding energy than the 3d photoelectron from the same metal in its elemental form. The intensity of a photoelectron signal is dependent on a number of factors: the amount of the element present on the sample surfaces, the cross section for photoelectron excitation, and the photoelectron escape depth or attenuation length. The cross-section value has been quantified by Schofield or Wagner sensitivity values[54, 55]; the physical meaning and use of these values will be explained later in section 2.2.3. Emitted photoelectrons can also be involved in inelastic scattering processes, which reduces the intensity of signal from lower depths in the sample. This can be quantified by the photoelectron escape depth, which is also known as the electron attenuation length (EAL).[56] This is the distance that a photoelectron travels before its intensity drops to 1/*e* of its original value. Values for the EAL for many elements can be found by using the corresponding NIST database.[57] The use of the EAL parameter is explained in Appendix B as it regards the NIST EAL database instructions found there.

Photoelectron peaks are not the only feature of an XPS spectrum; there are secondary processes that must be considered before assigning peaks or correcting the background. The first consideration is the work function of the spectrometer. The work function is the minimum amount of energy required to eject one electron from the valence band to the vacuum level. Spectrometers are usually calibrated for this workfunction value using a calibration standard, such as an Ag sample (Ag 3d$_{5/2}$ photoelectron peak, 368.1 eV) or other metals. The second feature is surface charging, which is of importance in non-conducting samples, such as the polymers used here. Upon ejection, a photoelectron leaves behind a "positive-hole" in a core orbital, which contributes to the generation of positive charge throughout the sample. This positive charge can cause photoelectrons to lose kinetic energy due to electrostatic attraction between photoelectrons and a positive surface as they emerge from the sample. This leads to a systematic shift of the spectrum to a higher binding energy. Surface charging can be corrected by calibrating the entire spectrum to a known standard binding energy, such as the adventious C1s (285.0 eV), Au 4f$_{7/2}$ peak (84.0 eV), or some other standard binding energy.[58] The entire spectrum itself is referenced to the value of the Fermi level, which is 0 eV.

Auger electron transitions are also excited by X-ray photoelectrons and appear as peaks in the resultant spectra. An Auger electron is emitted after absorbing the energy of an electron that has fallen into a positive-hole left by an emitted photoelectron (see Figure 2.3). The kinetic energies of those peaks can be described by the expression:

$$E_K = E_1 - E_3 - E_2 - \Phi \qquad (2)$$

where E_1 is the binding energy of the emitted photoelectron, E_3 is the binding energy of the electron that has fallen into the positive-hole created by the photoelectron emission,

E_2 is the binding energy of the emitted Auger electron, and Φ is the workfunction. Some of these Auger peaks have been identified in Figure 2.4 for a gold surface and a PMMA surface. A cursory use Auger electron spectroscopy is made, but this is not the focus of this thesis. For more information it is useful to consult Briggs and Grant.[58-60]

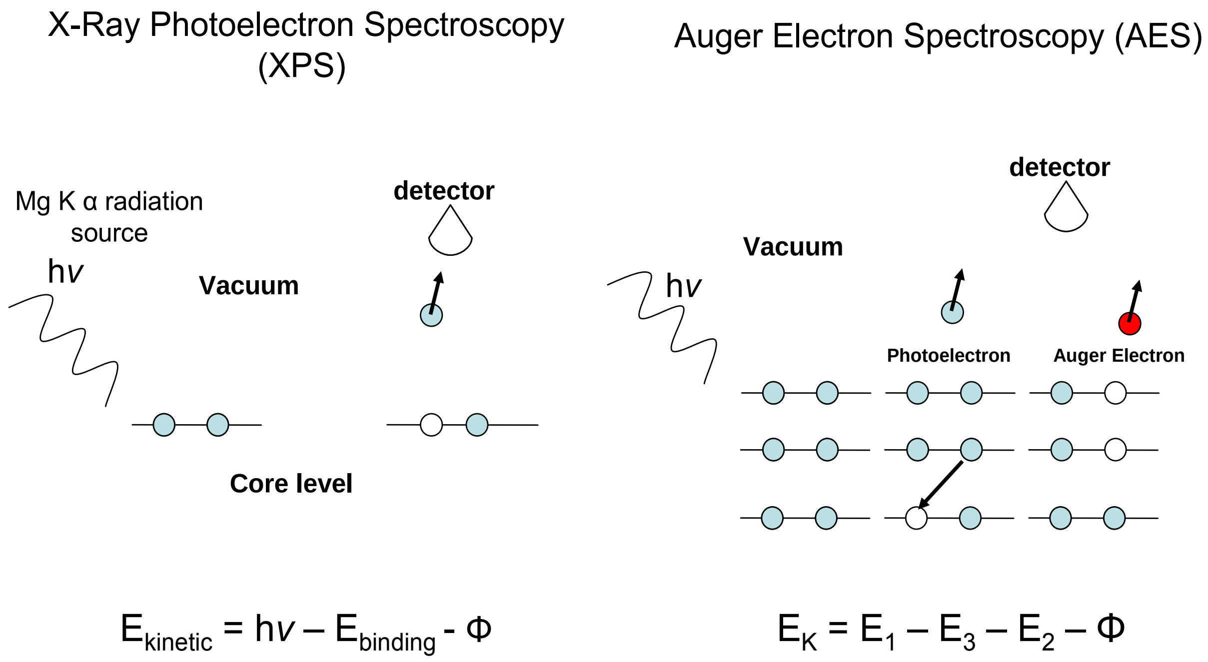

Figure 2.3: Schematic representation of XPS and AES phenomena

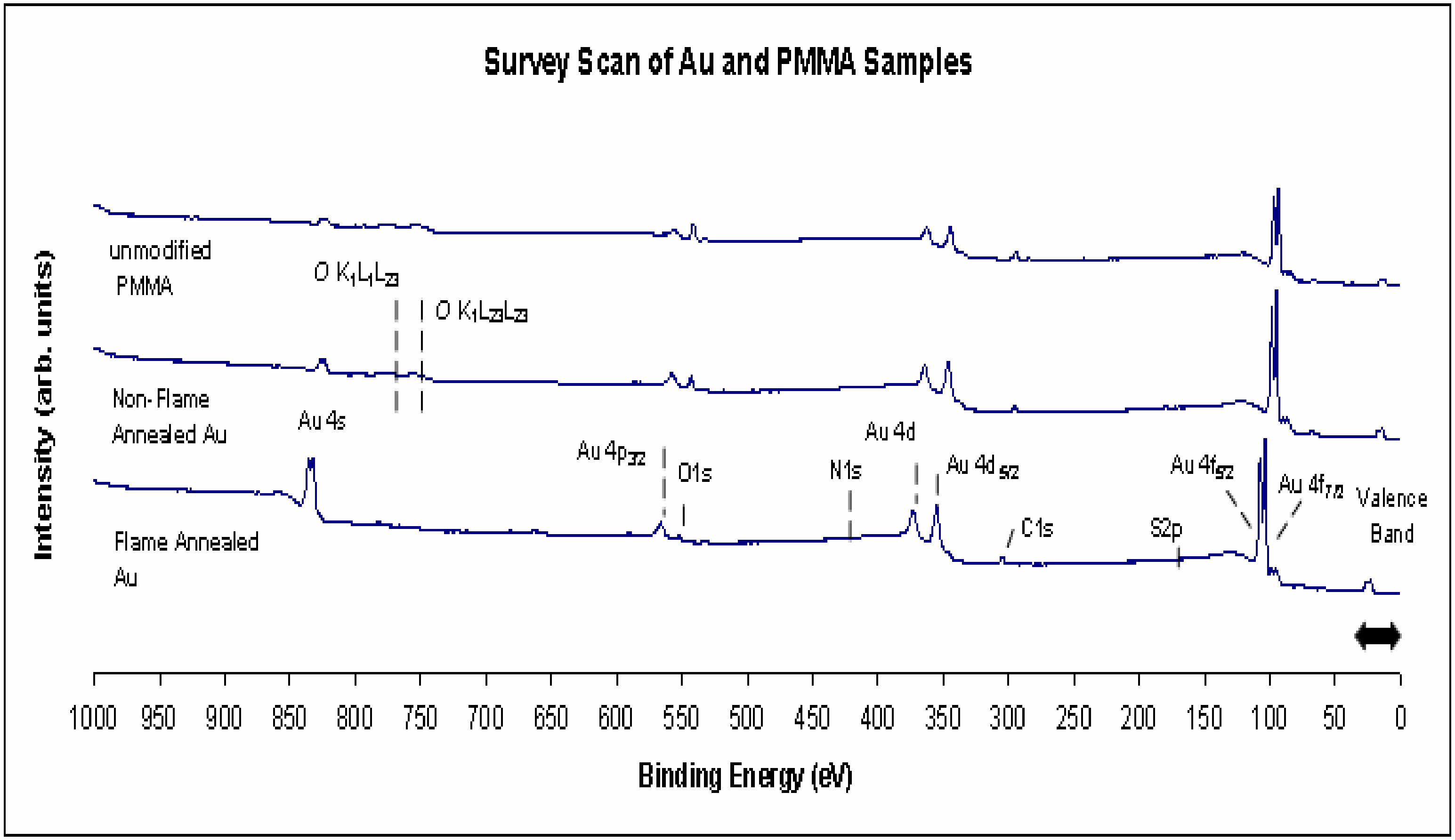

Figure 2.4: An XPS survey scan of Flame-annealed Au, Non-Flame Annealed Au, and unmodified PMMA samples (Mg K α source). Significant XPS and Auger peaks have been identified and peaks discussed in detail in this thesis are indicated in bold.

Multiplet splitting is another common feature of photoelectron peaks, and they arise from the close binding energies of orbitals split by spin-orbit coupling (e.g. $2p_{1/2}$ and $2p_{3/2}$ of a sulfur 2p signal). X-ray satellites from non-monochromatic X-rays, 'shake-up' transitions (peaks that arise from photoelectron interaction with π-systems) at binding energies higher than the main photoelectron peak, and the background electron emission (Bremsstrahlung radiation) are all described elsewhere and their effects are corrected by the application of appropriate background subtraction methods.[58, 61, 62]

2.2.2 XPS Instrumentation

This section will focus on the details of the XPS instrumentation and here the components of the XPS apparatus and the applicable theory will be explained in detail. It is instructive to examine the instrumentation that generates the X-ray excitation energy and analyzes the resultant photoelectron signal. Figure 2.2 shows the five main components of the XPS spectrometer: X-ray source, sample stage, the hemispherical analyzer and detector, and control and analysis system. The control of the XPS spectrometer will be integrated into the discussions of the other components of the spectrometer and the analysis of spectra will be described in section 2.2.2.

In an X-ray photoelectron spectrometer a sample is bombarded by X-rays, which leads to the ejection of photoelectrons, Auger electrons and secondary electrons from a sample. Each of these electrons has a specific kinetic energy as it emerges from the sample towards the analyzer. The role of the analyzer is to separate electrons by their kinetic energies and then detect the photoelectron signal. Ultimately, this leads to spectra that give the number of detected electrons as a function of binding or kinetic energy. The units for intensity are counts/second and the binding/kinetic energy is in units of electron volts (eV).

2.2.2.1 Spectrometer

The XPS spectrometer has a main experimental chamber and a preparation chamber, which are separated from each other by an air lock. The preparation chamber is also separated by another airlock from ambient conditions outside the XPS apparatus. Typical operating conditions require the main chamber to be at 10^{-9} Pa and the preparation chamber to be at 10^{-3} Pa. The ultra-high vacuum condition in the main chamber is particularly necessary to prevent the surface contamination of the sample and to ensure that ejected photoelectrons are not attenuated by collisions with gas-phase molecules between the sample and the analyzer.[63] Turbo-molecular and ion pumps are used to facilitate these ultra high vacuum requirements. The preparation chamber is at a lower vacuum setting because it must be regularly brought to atmospheric conditions in order for the user to load and remove samples from the chamber.

The X-ray source, and analyzer are located in the main experimental chamber. The hemispherical analyzer is located at the back of the spectrometer and is characterized by its dome-like shape. Samples are moved throughout the apparatus using both a spring-loaded arm to transfer samples and a movable sample stage, which holds samples during XPS experiments (see Figure 2.2). More detailed descriptions of the various components are described in the following sections.

2.2.2.2 X-Ray Source

The X-ray source generates X-rays via the X-ray fluorescent mechanism. The X-ray source as two components: a switchable anode, and two cathodes made of different materials that generate X-rays when bombarded by electrons. First, one of the two anodes is chosen for its proximity to a particular cathode. The cathode materials will have been chosen for their increased ability to release energy as X-rays via fluorescence rather than through other mechanisms, such as photoelectron or Auger electron processes. Also, the energy at which these X-rays emerge is different for each cathode material chosen. The X-ray source used for this thesis had one anode directed at a Mg cathode and the other is directed at an Al cathode. The potential difference between the cathode and the anode is 20 kV. A current is passed through the selected anode filament, which excites electrons towards the cathode. This results in various electronic transitions within the cathode material, which, in the main, produces Kα radiation. Briggs notes that the energy released from two particular electron transitions (the $2p_{3/2} \rightarrow 1s$ and the $2p_{1/2} \rightarrow 1s$ transitions) in both Al and Mg are the main source of Kα X-ray radiation.[61] The Mg Kα radiation has an energy of 1253.6 eV and the Al Kα radiation has an energy of 1486.6 eV. Of course, the Kα radiation is not the only energy emitted; a continuous distribution of X-ray energies are produced and directed at the sample.[61] This wide energy distribution is typical of non-monochromatic sources, but monochromatic X-ray sources can be purchased that use quartz and the principles of diffraction to limit the energy range of the emitted X-rays.[44, 61]

2.2.2.3 Sample Stage and Sample Loading

The sample stage is located in the centre of the main experimental chamber and the X-ray radiation is directed at its location. The sample stage itself can be moved and tilted within the main chamber. The mechanism allows for rudimentary positioning of the sample in three-dimensions and the stage can be tilted through ~ 90^0. However, tilt angles of 0^0, 45^0 and 60^0 with respect to a horizontal surface are clearly marked for routine use. The sample stage is grounded, which in theory means that the Fermi energy of the spectrometer and the sample should be the same and hence, the work function observed is that of the spectrometer; however, binding energies are referenced to the Fermi Level at 0 eV. The contribution of the spectrometer workfunction must be calibrated as noted above. In many cases, the phenomena of surface charging, where the accumulation of positively charged core-holes due to photoelectron ejection imparts an overall positive surface charge; this charging effect will shift the Fermi Level to another value that can be calibrated using an internal standard. Here we used either the Au $4f_{7/2}$ (84.0 eV) or C1s (285.0 eV).[53, 61]

2.2.2.4 Hemispherical Analyzer

The hemispherical analyzer has three components that, combined, serve to separate and detect photoelectrons based on their kinetic energy. First, ejected photoelectrons must pass through variable (V) electron lenses; second, photoelectrons pass through the hemisphere itself; third, the photoelectron signal passes through an electron multiplier detector. The following description of the Hemispherical Analyzer owes much to four chapters written by Ian Drummond, Masato Kudo, Martin Seah and John Grant, in *Surface Analysis.*[44, 59, 60, 64]

2.2.2.4.1 Resolving Power

The components of a hemispheric analyzer have purposes that are crucial to improving the resolution of the system. At this point, it is important to introduce the equation that describes the resolving power of the analyzer. As Drummond makes clear, "[the] resolving power is the ability of the analyzer to resolve peaks with small energy differences".[44] The equation is listed below, assuming that the analyzer entrance and exit slits are the same size:

$$\frac{\Delta E}{E} = \frac{w + r_0\alpha^2}{2r_0} \qquad (3)$$

where ΔE is the FWHM (full width at half maximum), E is the kinetic energy of the electrons (also known as the pass energy, see section 2.2.2.4), w is the width of the analyzer slits, α is the half-angle of the total spread of electrons (in radians) at the entrance of the analyzer and r_0 is the radius of the semi-circular path through the analyzer that an electron travels. The value $\frac{\Delta E}{E}$ is referred to as the “relative’ resolution, whereas the FWHM maximum value is referred to as the “absolute” resolution of the analyzer. Suggested values of r_0, α, and w are 127 mm, 3^0 and 1 mm respectively.[44] At a pass energy of 20 eV (used in this thesis) then Equation 3 suggests a resolving power of 0.0053 and a ΔE value of 0.106 eV. In reality this value is rarely reached, due to various factors like the detector response, the width of the photon line emitted by the X-ray source (most important), peak fitting software, and the quality of the sample, among other limitations to resolution. However, the manufacturer of the spectrometer used in this thesis suggests a value for ΔE value of 0.25 eV, which gives use a base resolving power of 0.0125 at a pass energy of 20 eV. Other comments about the resolution of the X-ray technique, particularly in a practical sense will be mentioned in subsequent sections as appropriate to the discussion at hand.

2.2.2.4.2 Variable Electron Lenses

The main purpose of the lens system is to focus incoming electrons towards the entrance to the hemispherical analyzer and to retard the electron kinetic energy, and both are necessary to the increase of analyzer resolution. There is a need to focus the broad beam of electrons ejected from the sample, so that the angular spread of the beam is as small as possible ($<6^0$) in order to achieve good resolution and to maximize the number of photoelectrons passing through the analyzer slit.[44] Retardation of the kinetic energies of incoming electrons is necessary to reduce their energies so that resolution is maximized without unreasonably small values of w, α or r_0 in equation 3.

It is clear from equation 3 that unreasonable physical values for these variables would be needed to maintain the requirement that chemical shifts of ~0.1 eV should be detected by commercial spectrometers.[44] A relative resolution of 100 is deemed reasonable for commercial spectrometers[44] and the required chemical shift detection ability for this resolving power is obtained by slowing down the electrons rather than reducing w, α or r_0 to smaller values.

The mechanics of the focusing and retardation processes will be described below. The electrons are focused and retarded using a series of lenses. There are a variety of lenses in use in commercial spectrometers and they often are associated with specific hemispherical analyzers.[44, 64] In general, one set of lenses focuses the incoming beam of electrons from the sample through an aperture. The second set retards the beam of electrons and further focuses the beam through the entrance slit to the analyzer. As previously mentioned, it is necessary to retard the electrons strongly. This is done by placing a potential on the analyzer entrance slit that is sufficient to slow the electrons down to what is called the pass energy (the energy that the electron has when it enters the analyzer). If an electron with kinetic energy of 1253.6 eV is about to enter the analyzer, then to have a pass energy of 20 eV it needs to be retarded with a -1233.6 eV potential.

There are two main modes for scanning various kinetic energies. One is to vary the potential of the retard plate and keep the analyzer electrostatic plate at a constant potential difference (fixed analyzer transmission, or FAT mode used here). The other option is to fix the lenses of the electrostatic plates a constant pass energy and change the potential difference between the hemispherical plates to scan for electrons. This is known as the fixed retard ratio (FRR) mode. As the pass energy, and hence resolution of the spectrometer varies with kinetic energy, this mode is not useful for XPS work where spectral resolution must be held constant to compare peak binding energies.[41] It is useful, however in Auger spectroscopy work, where higher signal intensities are required.

2.2.2.4.3 Electrostatic Hemispherical Analyzer

The hemispherical analyzer is a pair of concentric plates that are separated with enough space to allow electrons to enter and exit the hemisphere following a semi-circular pathway to the analyzer exit slit. Electrons that are properly focused, that have the correct charge, and that have the particular kinetic energy that is being scanned will pass to the exit slit without deviating from a central semi-circular path of radius r_0 (see equation 3). Electrons that are not properly focused, that do not have the correct charge, or do not have the correct kinetic energy will have radii that are too small or too large; those electrons will hit the hemispherical plates and will not exit the analyzer. The voltage on the outer hemisphere plate is:

$$V_1 = V_0\left(3 - 2\frac{r_0}{r_1}\right) \tag{4}$$

and the voltage on the inner hemisphere is:

$$V_2 = V_0\left(3 - 2\frac{r_0}{r_2}\right) \tag{5}$$

where V_1 is the voltage of the first plate, V_2 is the voltage of the second plate, V_0 is the pass energy, r_1 is the radius of the inner hemisphere, r_2 is the radius of the outer hemisphere and r_0 is the radius of an unimpeded, central path in between the two hemispheres leading from the entrance to the exit slit.[44] If the hemispherical analyzer is not operating at constant potential difference, then the scanning of kinetic energies can be accomplished – after prior retardation by the lenses – by varying the potential difference between the hemispherical electrostatic plates.

The two electrostatic plates within the hemispherical analyzer can be changed throughout an XPS experiment to scan for different kinetic energies. From an interpretation of the above two equations, an explanation by Drummond[44], and the assumption that there must be a fixed value for r_0 , two expressions for hemisphere voltages can be written; for the outer hemisphere:

$$V_{outer} = -[(E - V_0) + (V_0(1.33) - V_0)] \qquad (6)$$

and for the inner hemisphere:

$$V_{inner} = -[(E - V_0) - V_0(0.5)] \quad (7)$$

where E is the energy of the incident electron (before retardation) and V_0 is the pass energy. The values for r_0, r_1 , and r_2 in all the above equations are those suggested by Drummond, which are 127 mm, 154.2 mm and 101.6 mm respectively.[44] Thus, to scan for a certain value of E, the scanning mechanism must change the hemispherical electrostatic potential difference. In the case of an electron having kinetic energy of 969.0 eV (C1s) which is retarded to the pass energy of 20 eV, the outer and inner hemispheres have potentials of -982 eV and -998.6 eV respectively. We see from the above treatment that the analyzer itself can apply the voltages necessary for scanning, and by extension retardation, just as is possible with the electron lenses.

2.2.2.4.4 Electron Detector

The purpose of the detector is to increase the S/N ratio of the XPS output and detect the signal intensity at any kinetic energy value. The most common detector is a channel–type electron multiplier. The channel-type multiplier is a semi-conducting, glass, curved tube that has potential difference applied across its length.[44, 64] Electrons that have passed through the analyzer enter the multiplier tube and are accelerated towards the detector plate while hitting the walls of the multiplier ~25 times.[44, 64] At each point of impact, more electrons are released, which amplifies the signal. At the end of the tube, the electrons are usually detected as a current which can be converted to a intensity signal in units of counts per second. While this is a typical XPS detector, there are others that operate in a similar manner and they are described elsewhere.[44] However, the basic principle of increasing the signal without compromising on signal quality is key to any detector system.

2.2.3 Background Correction and Peak Fitting Methods

The proper application of background and peak fitting methods are important in the high quality analysis of collected spectra. The primary reason for correcting for background and lineshape is due to the presence of secondary electron processes and sources of peak broadening, both of which will be discussed in this section. The three most common background subtraction methods in use by surface chemists will be discussed: the linear, Shirley and Tougarrd methods. Each has its merits when fitting XPS and Auger spectra. Finally, the choice of lineshape for curve fitting will be examined in the context of this thesis. Useful reviews and explanations of the various considerations, background corrections and peak fitting methods are given by Tougaard,[65] and Seah.[58]

2.2.3.1 Peak Broadening

In general, there should only be one XPS peak for each unique core-level photoelectron transition that is Lorentzian in shape, which is characteristic of a photoelectron transition.[58] Unfortunately, spectra are rarely described in such a simple manner due to the broadening effects of various physical phenomena and instrumental limitations. This lineshape broadening has the effect of broadening peaks to the extent that they can mask other peaks in the spectrum; the chemical shift between XPS peaks of similar chemical environments can be less than 1.0 eV apart. This introduces the problem of poor resolution in complex XPS spectra. Approximation methods for lineshape and background correction methods attempt to acknowledge broadening effects, but are not a perfect solution to the problem; these methods are discussed in other sections.

It is important to consider the limitations of the XPS technique with respect to peak broadening and resolution. The physical broadening of any one XPS peak is due to three main factors:

1) lifetime broadening of core-level transitions

2) lifetime broadening of X-ray transitions (X-ray linewidth)

3) phonon broadening

4) electron loss processes

Other sources of line broadening include surface charging, instrumental, and software sources.[62] These sources of line broadening can also be categorized into homogeneous and inhomogeneous effects, which have an effect on the choice of peak fitting methodology, as explained later.

It is important to first consider the lifetime broadening of both the photoelectron transition and the X-ray transitions of the excitation source. Theoretically, the linewidth of an ejected electron from a core-level or an X-ray transition should be governed solely by the Uncertainty principle:

$$\Delta p \Delta x \geq h \qquad (8)$$

where p is the momentum, x is the position and h is Planck's constant. In essence, the deviation of an electron from its position will never be smaller than Planck's constant. In the context of XPS analysis, we can record this minimum linewidth as:

$$\Delta E \Delta t \geq h/2 \qquad (9)$$

where E is energy and t is the lifetime of the transition. The narrowest peak (lowest ΔE) is therefore the one with the longest lifetime. This so called, intrinsic lifetime broadening has a distribution that is described by the Lorentzian function and is a homogeneous source of line broadening.[58]

Grant notes that the lifetime of a core-hole depends on the decay mechanisms that can follow the ejection of a photoelectron and those mechanisms include X-ray fluorescence, electrons ejected by the Auger process, and electrons ejected by the Coster-Kronig process (an Auger process involving one or two electrons from the same principal shell as the ejected photoelectron).[59] The lifetime of these core-holes are on the order of $10^{-14} – 10^{15}$ seconds. If these lifetimes are inserted into the Uncertainty principle equation, the it is clear that FWHM values range from 0.21 eV to 2.1 eV. The X-ray excitation is also governed by the Uncertainty principle and typical X-ray linewidths are ~0.7 eV for an Mg Kα X-ray anode, ~0.85 eV for Al Kα sources and ~0.1eV to 0.3 eV for monochromatic X-ray sources[61]; these values are within the expected range of linewidths. These linewidths are also approximately half the contribution to FWHM in the range of 1.5 – 1.7 eV of a photoelectron peak.

Inhomogeneous broadening effects include energy loss processes and phonon broadening and a Gaussian function is accepted as a means to approximate their contribution to peak shape.[58] Energy loss processes are a cause of asymmetry in XPS spectra, particularly at the low kinetic energy side of any photoelectron peak.[61] The major source of this energy loss is inelastic electron scattering and it is seen as large step-like features in an XPS spectra (see Figure 2.4 for a visual around 100 eV). Phonon broadening is caused by the interaction of electrons with various vibrational modes (phonons) in a crystalline solid. A phonon-electron interaction will affect the momentum of the electron and a wave vector of the phonon.[53, 62] Thus, this would change the detected energy of the photoelectron transition and contribute to peak broadening at both the high and low kinetic energy side of the peak; it all depends on the type of phonon-electron interaction. It is likely that other vibrational modes in non-crystalline solids can interact with electrons to cause phonon-like line broadening.

Surface charging, instrumental and software sources of line broadening should also be briefly mentioned. Surface charging can change the kinetic energy of photoelectrons being ejected from a surface. In most cases, an abundance of positive core-holes means that the surface will have an overall positive charge, which would lower the kinetic energy of outgoing electrons from their original energy, thus leading to peak broadening. The response of the XPS analyzer to electrons can also contribute to peak broadening. The efficiency by which electrons can be detected affects the peak intensity at any one kinetic energy. This response is usually calibrated by the manufacturer in the form of the transmission function, and it serves as a means to ensure that XPS quantification data is comparable across different spectrometers.[44] Software sources of line broadening can include the choice of background subtraction methods and curve fitting algorithms. The linear background correction is known to create asymmetry in the peak shape, while the Shirley and Tougaard methods better correct for asymmetry. As well, the choice of lineshape can be a factor: the choice of a Gaussian type peak would better approximate inhomogeneous sources of line broadening, while a Lorentzian peak would better approximate homogeneous sources of line broadening.[62] The effects of the software analysis on peak broadening will be discussed in more detail in subsequent sections.

2.2.3.2 Linear Background Correction

Linear backgrounds exist in spectra of materials that are not strongly affected by energy loss processes due to the high energy thresholds required to induce these processes.[62] Polymeric materials fall into this category, and the linear background method is sufficient to fit certain spectral regions, such as the C1s region.[62] The linear background is determined by drawing a line between two points, close to the peak of interest. As indicated by Seah, one point is at the high kinetic energy side of the peak (E_{max}) and the other is at the low kinetic energy side of the peak (E_{min}).[58] The area under these lines is subtracted from the area above the peak to find the total peak area.

There are a few limitations to this method that must be considered: first, the start and end points chosen are user-defined and may not represent the average value of the background signal; second, this method is inadequate for strongly sloping backgrounds, such as those of metal samples or heterogeneous samples, such as some of the multi-layered surfaces studied in this thesis. The linear background method was only used when the assumptions and parameters of the Shirley background (described below) were automatically rejected by the analysis software; this was particularly the case when a photoelectron peak was adjacent to a second, more intense photoelectron peak, which caused the background to increase from high to low binding energy. This is a situation that does not facilitate the use of the Shirley background.

2.2.3.3 Shirley Background Correction

The Shirley background correction[66] is used when the background rises dramatically within a spectrum. This is most prevalent in metallic samples or, in the case of non-metallic samples, around photoelectron peaks corresponding to metallic elements, such as Au. The Shirley method makes the following assumption: at any given kinetic energy the background is caused by inelastically scattered electrons which result from the scattering of electrons that have a higher kinetic energy; the background at this point is proportional to the number of electrons with higher kinetic energy.[58, 66-68]

Proctor and Sherwood outline an iterative method used to calculate the background and it will be described in this section.[67] This paper describes how a software algorithm might practically calculate the background. In a spectrum of n equally spaced points, of separation h, the background at point x is defined by:

$$B(x) = \frac{(a-b)Q}{(P+Q)} + b \qquad (10)$$

where a is the average background at the starting point, b is the average background at the end point, Q is the background subtracted area from x to k, P is the background subtracted area from point a to x, and Q is the background subtracted area from point x to k, and (P+Q) is the total background subtracted area from a to k. Proctor and Sherwood define Q as:

$$Q = h[(\sum_{i=x}^{k} y_i) - 0.5(y_x + y_k)] \qquad (11)$$

where y is the peak intensity at the associated point. The algorithm starts with a linear background with an average value of b and substitutes this into the $B(x)$ expression. This generates a second background that can be subsequently used as a value for b to generate further backgrounds and so on, in an iterative manner. When (P+Q) converges to a value that remains constant in subsequent iterations, then the background correction is completed. The maximum number of iterations and the limit of convergence are user defined in the Avantage software.

While the Shirley method is considered to be more accurate than the linear method, there are still some limitations to its usage. The choice of starting and ending points for the background line are important: this method is noted to be relatively independent of the point at the high kinetic energy side of the peak, but is affected by the choice of point at the low kinetic energy side of the peak.[58] This is apparent when trying to background correct a series of peaks at subsequently higher background levels, as the Shirley fit will over or underestimate the background.[65] Thus, the Shirley method is most accurate in narrowly defined spectral regions that are on the order of 5 -10 eV, where extreme shifts in the background level are less likely. Also, there is the requirement that background at E_{max} is less than the background at E_{min}. Such a situation could be non-existent when a peak of weak intensity is adjacent to a peak of large intensity. An example is the S 2p peak region: if the presence of an Si 2s photoelectron peak (~153 eV) is particularly intense, then the background around a week S 2p signal (~162 eV) will increase such that E_{max} does not equal E_{min}. When there is a need to correct for background signal over a wider range of kinetic energy values, then the Tougaard method (discussed below) is more useful.

2.2.3.4 Tougaard Background Correction

The Shirley and linear background correction algorithms are not based on any physical parameter of the material being studied. Tougaard proposed an algorithm that would incorporate parameters to account for the physical observation of energy loss processes that are caused by inelastic scattering of electrons.[69, 70] The energy loss after inelastic scattering of electrons depends on the distribution of atoms in a solid, the depth distribution of those atoms and the inelastic scattering cross-sections.[58, 65] The first two processes were incorporated into a general formula,[65] but the inelastic scattering cross-sections vary widely between solids, thus making it difficult to use them in routine XPS analysis. To overcome this, Tougaard introduced the idea of Universal cross-sections: the general probability that an inelastic collision involving an electron of certain kinetic energy will lose energy as it travels through a solid.[71] The Universal cross-section for a material is not the exact cross-section, but instead a value based on user-chosen parameters to estimate this probability.[72] After a decade of experimental evidence, it was found that two formulas of the Universal Cross-section were sufficient to use in a background subtraction algorithm: one was a two-parameter equation, useful for metals and related oxides and alloys; the second was a three-parameter equation that was proved necessary for the spectra of polymers, semi-conductors, and free-electron like solids, such as Al.[65, 72]

The Tougaard method was not used in this thesis due to the fact that most of the spectra obtained did not meet the minimum requirements for the related equation. The Tougaard method requires acquisition of spectral regions that are roughly 30 -50 eV wide and most of the spectra here were about 10-20 eV wide. Another limitation of the

Tougaard method is that, to my knowledge, there are no known Universal cross-section parameters specific to proteins. There are published values for metals, oxides, alloys, and polymers,[72] which could be used, but they may not be good estimates for a protein surface. Also, most of our analysis compares relative peak areas and this type of analysis is most commonly done using the Shirley method, because the method requires spectra that are narrower (less data acquisition time) and has sufficient accuracy for this type of analysis.

2.2.3.5 Peak Shape

There are a number of lineshapes that are used to fit XPS spectra that address the peak broadening effects, and some of them are listed and explained by Fairley.[62] The Avantage software used a peak fitting function that is a product of the Gaussian and Lorentzian functions to fit the curve:

$$f(x) = \frac{peak\ height}{[1 + M(x - x_0)^2/\beta^2] \bullet \exp\{(1 - M)[\ln 2(x - x_0)^2]/\beta^2\}} \qquad (12)$$

where x_0 is the peak centre, M is the mixing parameter that governs the percentage of Gaussian and Lorentzian character of the lineshape (this percentage is displayed in the Avantage software output) and β is the FWHM.[62, 73] If M = 0, then the two functions reduce into the pure Gaussian form and if M = 1, then the two functions reduce to the pure Lorentzian form; it is easy to see the contributions of each function to the final form by making a simple calculation. The variables, x_0 and M can be entered, changed or constrained using the Avantage software. The Avantage software also allows a user to constrain the FWHM. The software program was able to change these variables to make the peak fit converge on the experimental data automatically.

The result of the peak fitting algorithm must be optimized to the spectral signature that one is trying to approximate. This is done by finding the minimum difference (convergence) between the spectral signature and the approximation curve. The Powell method[74] was used by the Avantage software to find this minimum convergence. The method works by first estimating the location of a minimum, then proceeds to change multiple variables at a time, in the direction of greatest change, until the local minima is reached. The combination of the Powell method and the lineshape functions creates an iterative method for finding the best approximate lineshape of a XPS peak. Values for the convergence and the number of iterations are user defined.

There are advantages and limitations to the use of equation 12 to fit XPS curves. The advantage of combining the Lorentzian and Gaussian lineshapes is that one can simultaneously estimate the distribution of homogeneous and inhomogeneous line broadening. The disadvantage of equation 12 is that it does not consider peak asymmetry. This can be addressed by incorporating asymmetrical tail functions.[62] The extent of asymmetry is usually dependent on the choice of background and the Shirley background is known to reduce the extent of asymmetry compared to the linear background subtraction method.[58, 62, 65] The Tougaard background subtraction method is usually used with the Doniach-Sunjic lineshape; discussion about the relationship between these two methods can be described elsewhere.[62, 75, 76] The combination of the Shirley background subtraction and the Gaussian-Lorentzian lineshape provides a good basis for relative peak quantification.[58, 65]

The combined use of the background subtraction and the peak shape algorithms leads to a number of results that can be seen in the Avantage software output. A typical XPS output table displays the following data:

1) Start and end kinetic energy values of the spectral range of interest (eV)
2) Peak kinetic energy (or binding energy) (eV)
3) Peak height (counts/second)
4) Height ratios (in comparison to other peaks in the spectral range)
5) Peak Area
6) Area Ratio (compared to other peaks in the same spectral range)
7) FWHM (eV)
8) Lorentzian/Gaussian %

All of the above parameters can be constrained by the user prior to starting the peak fitting algorithm. Also, these listed parameters have been mentioned elsewhere in this particular section. It should be noted that not all of the above outputs are independent, which means that a user-defined constraint may have a greater affect on peak shape than intended. There are other output results which cannot be constrained, but are shown in the Avantage software output. The most relevant to this thesis include:

1) Normalized Peak Area
2) Atomic Percentage
3) Sensitivity Factors
4) Transmission Function Value

and these values will be explained in detail in the next section, as they are generally related to each other.

2.2.3.6 Peak Areas and Normalized Peak Areas

XPS software programs can calculate the peak area under a fitted peak using simple integration techniques. However, some thought is necessary before comparing peak areas of different samples and elements and the concept of Normalized peak areas needs to be introduced as a means to correct peak areas for the photoelectron cross-section and transmission function of the spectrometer. Before using peak areas as a comparative tool, one needs to consider the sample(s) being compared, the element being compared, and the detected spectrometer background level, which is different for every sample. The spectrometer background level is the signal detected that is below the Fermi Level (< 0 eV); this is usually a relatively stable signal in the range of 0 eV and -20 eV in the "valence band" region (i.e. kinetic energy of 40 eV to -20 eV). Peak area ratios (e.g. C1s/Au4f$_{7/2}$, N1s/C1s) that are calculated using values belonging to the same sample, can be computed without correcting for the spectrometer background signal. The background signal would be cancelled in all cases. These ratios can be compared to the same ratio computed for other samples without difficulty. Peak area ratios that are calculated using values belonging to two different samples (e.g. Au4f$_{7/2\ \mathrm{sample1}}$ / Au4f$_{7/2\ \mathrm{sample2}}$ …) requires that the individual peaks be corrected for the spectrometer background signal. Once this is done, then the ratios are normalized to one another, but this should not be confused with the concept of Normalized Areas.

The term ‘Normalized Area’ refers to the practice of correcting the detected peak areas for the photoelectron cross-section and the transmission function of the spectrometer. The Normalized area is computed using the following formula:

$$Normalized\ Peak\ Area = \frac{I_n}{S_n T} \qquad (13)$$

Where I_n is the non-corrected peak area, S_n is the relative sensitivity factor for the photoelectron, and T is the transmission function of the spectrometer.[53] The last two variables should be explained in more detail. The sensitivity factors are a means of adjusting the peak areas to reflect the different photoelectron cross-sections of each element. The sensitivity factors used in this thesis are those published by Wagner and are relative to the intensity of the F1s signal, which is assigned an arbitrary value of $S_{F1s} = 1.00$.[77] The transmission function, which is also known as the analyzer response function, is unique to each spectrometer and is related to the sensitivity of the detector to emitted photoelectrons.[60] Knowledge of the value of this function is only necessary if data collected on two different spectrometers are compared to one another. This is not the case in this thesis, but for reference, the value of T for the spectrometer used is 2.0.

2.2.4 XPS Experimental Procedure

The XPS experiments were conducted using a Thermo Instruments Microlab 310F surface analysis system (Hastings, UK). The analysis occurred in ultra-high vacuum conditions (10^{-9}–10^{-10} Torr) using a Mg Kα X-ray source (1253.6 eV) at 15kV anode potential and 20 mA emission current. The Fixed Analyzer Transmission mode

(FAT) was used to obtain the photoelectron signal using a pass energy of 20 eV , a surface/detector take-off angle of 75^0, variable number of scans (2 – 50, depending on the signal-to-noise level required), and a dwell time of 60 ms or 120 ms (again, depending on the S/N level required). The choice of FAT mode means that kinetic energies are scanned by adjusting the retard potential within the electron lenses. Every spectrum was calibrated to the bulk C1s line at 285.0 eV, due to the effects of charging on the samples (2 – 10 eV). The XPS spectrometer included the *Advantage* software program, which was used to process the resultant data. The Shirley algorithm was used as the background subtraction method for all peaks, except for the S2p region (167 eV). This particular region requires a Linear background subtraction due to a reverse sloping background (Shirley fit algorithm requires $E_{max}<E_{min}$ to be accurate).[58] The Powell peak-fitting algorithm was used for all peaks and peaks were chosen automatically and then manually for peaks that were not well resolved. No constraints were used to fit the peaks. The underlying substrate for all XPS experiments was epitaxal Au (111) sputter-coated on mica (300 nm) purchased from Georg Albert (PVD-Beschichtungen: Heidelberg Germany).

Chapter 3

Results and Discussion of XPS Data

3.1 XPS Surface Overlayer Thickness

The relative thickness of XPS samples was calculated using the formula:

$$I_s = I_0 e^{-t/\lambda} \qquad (14)$$

where t represents the overlayer thickness, λ the escape depth/electron attenuation length of the photoelectron, α the angle between the ejected photoelectron and the surface normal, I_0 is the peak intensity from some non-attenuated species (In this case, the Au $4f_{7/2}$ peak of the Flame-annealed Au sample, which had no PMMA (Sample J, Appendix A), and I_s is the peak intensity of the species of interest.[56] The chosen non-attenuated species was a flame-annealed Au sample. The values of I_s and I_0 were normalized relative to their own individual spectrometer background signals, as determined by averaging the last 20 energy points of the portion of the valence band spectra which was above the Fermi level energy. The value of λ (2.69 nm) was estimated for PMMA using the NIST Database of Electron Attenuation Lengths.[57] (see Appendix B for more details). This EAL value was used to estimate all the thicknesses of the PMMA samples regardless of the surface modification. Relative thickness values for all samples studied over the course of this thesis are shown in Appendix A, while average values for each surface type are shown in Table 3.1, along with the standard deviations.

In Table 3.1 some general trends in the overlayer thickness of modified samples may be observed. First, the non-flame annealed Au sample, show an attenuation of the Au $4f_{7/2}$ peak consistent with an overlayer thickness of 0.55 nm (± 0.2 nm), which is presumably due to surface contamination. This contamination could be from solvents used in the cleaning processes, adventious carbon compounds, and products of ambient surface reactions or deposition. There is also a general trend towards a thicker overlayers after each subsequent modification to the PMMA substrate. The largest change in thickness occurs when the proteins are added to the substrate. There is an inconsistency in the average phnH values compared to the TmGH1 on PMMA values. The average thickness of phnH was expected to be smaller than that of TmGH1, since the phnH protein has a mass of ~ 23 kDa, while TmGH1 has a mass of ~ 53 kDa. Moreover, the dimensions for phnH are approximately 5.3 nm x 8.7 nm x 7.6 nm,[78] while those for TmGH1 are 9.5 nm x 9.5 nm x 11.4 nm.[47] Notwithstanding the differences in protein solution concentrations, we should have expected phnH to form a thinner overlayer than TmGH1 (compare 'TmGH1 on PMMA' with 'phnH on PMMA' in Table 3.1); this is not the case, even when considering standard deviations. If 'TmGH1 on PMMA' with 'phnH on PMMA' in Table 3.1 are corrected for the thickness of the cross-linker layer, then we obtain thickness values of 3.7 nm (± 0.9 nm) and 9.8 (± 5 nm) respectively. While the phnH thickness value contains that of TmGH1, within standard deviation, it is still large despite the fact that phnH is smaller protein and the sample was exposed to a smaller solution concentration of phnH. It is evident that there is inconsistency in the thickness values of the phnH samples that is probably due to the varying experimental conditions for phnH samples (see Appendix A). Regardless, the overall trend in Table 3.1 show that modification of the surface is leading to greater surface thickness, which is an expectation of the general surface modification scheme proposed in this thesis.

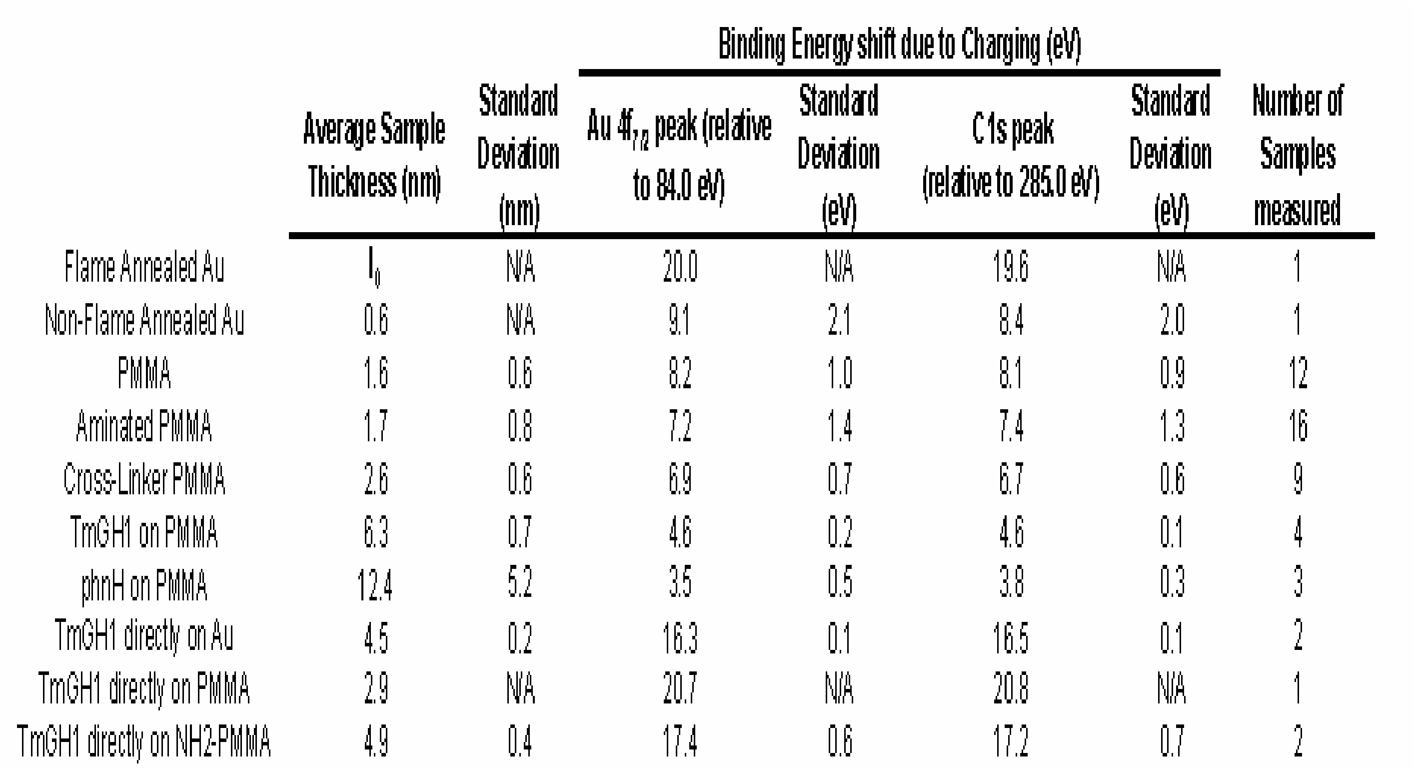

	Average Sample Thickness (nm)	Standard Deviation (nm)	Binding Energy shift due to Charging (eV)				Number of Samples measured
			Au $4f_{7/2}$ peak (relative to 84.0 eV)	Standard Deviation (eV)	C1s peak (relative to 285.0 eV)	Standard Deviation (eV)	
Flame Annealed Au	I_0	N/A	20.0	N/A	19.6	N/A	1
Non-Flame Annealed Au	0.6	N/A	9.1	2.1	8.4	2.0	1
PMMA	1.6	0.6	8.2	1.0	8.1	0.9	12
Aminated PMMA	1.7	0.8	7.2	1.4	7.4	1.3	16
Cross-Linker PMMA	2.6	0.6	6.9	0.7	6.7	0.6	9
TmGH1 on PMMA	6.3	0.7	4.6	0.2	4.6	0.1	4
phnH on PMMA	12.4	5.2	3.5	0.5	3.8	0.3	3
TmGH1 directly on Au	4.5	0.2	16.3	0.1	16.5	0.1	2
TmGH1 directly on PMMA	2.9	N/A	20.7	N/A	20.8	N/A	1
TmGH1 directly on NH2-PMMA	4.9	0.4	17.4	0.6	17.2	0.7	2

Table 3.1: Average sample thickness as calculated using the method of Flitsch, and binding energy shifts due to charging for a series of PMMA and surface-modified PMMA samples. Standard deviations are for measurements from multiple samples. Only those samples whose signal could be background corrected were used to calculate the thickness of samples.

The overall thickness of the various layers is also consistent with the size of the adsorbed species, with the exception of phnH (as noted above). Ethylenediamine is approximately 0.4 – 0.5 nm (based on C-C and C-N lengths of sp^3 C, which are 0.154 and 0.147 nm respectively). The length of the portion of the Sulfo-EMCS cross-linker which remains covalently attached to the surface is approximately 1.4 nm (calculated from the same C-N and C-C sp^3 C bond lengths). The amine and the cross-linker together are approximately 1.9 nm thick, similar to the measured increase in thickness (2.6 – 1.6 = 1.0 nm) to PMMA, within the standard deviation of the error. The dimensions of TmGH1 are on the order of 9.5 nm x 9.5 nm x 11.4 nm.[47] The addition of TmGH1 adds an extra 3.7 (± 0.9 nm) nm in thickness, which is of a similar scale to the protein dimensions, although not within the propagation of errors in the standard deviation. The thickness values should be used as a qualitative rather than a quantitative measure. Overall, the thickness values indicate that surface modifications are producing overlayers on the PMMA surface of the expected dimensions.

3.2 XPS Charging Effects

Ejected photoelectrons leave core orbitals with a positive charge that can be occupied by another electron. However, multiple photoelectron processes occurring on a insulated sample or a sample that is electron-poor, will create more positive charge than there are available electrons to balance that charge. This positive charge retards emitted photoelectrons and decreases their kinetic energy as they emerge from the sample. The apparent binding energy of the entire XPS spectrum of that sample is then higher than expected and has to be calibrated relative to a peak of known binding energy. The difference between the calibration peak and the experimental peak is known as the charging effect or potential (ΔeV). Samples that are grounded properly to the spectrometer or samples analyzed by a spectrometer with an electron flood gun avoid this charging mechanism.[79] There are two choices for calibration peaks for our samples: the bulk carbon C1s peak (285.0 eV) and the Au $4f_{7/2}$ peak (84.0 eV). The peak at 285.0 eV is characteristic of samples exposed to ambient environment, as a thin layer of carbon results from the deposition of organic material on samples. Within a XPS spectrum this appears as a broad, single peak at this particular binding energy. All the substrates had a common and well ordered layer of Au whose XPS spectrum is unaffected by the surface modifications, particularly chemical; the Au acts as an internal standard and a reference peak for calculating the surface thickness. One of these two peaks was chosen as the calibration peak, but a brief analysis is needed to justify the choice of the C1s peak over the Au $4f_{7/2}$ peak.

Despite the fact that the underlying Au signal is expected to change less than the C1s signal from PMMA and subsequent modifications, it was decided that spectra would be calibrated to the C1s peak rather than the Au $4f_{7/2}$ peak. This calibration method was chosen after comparing the charging shift of the C1s peak (285.0 eV) to the Au $4f_{7/2}$ peak (84.0 eV). The average charging values for various classes of samples are shown in Table 3.1 (and values for all samples in Appendix A). It is evident from this Table that the average charging values for the primary C1s peak is similar to the Au $4f_{7/2}$ signal, within standard deviation. Moreover, all the samples also contain a strong carbon signal at 285.0 eV, due to the large number of C-C bonds in organic compounds, while the Au $4f_{7/2}$ signal is strongly attenuated in some cases.

It was thought that the use of Au as an underlying substrate for samples would minimize the effects of surface charging. However, the samples where Au was near the surface, such as flame-annealed Au, the charging values were the highest. The Au on these samples is supported by mica, which is an insulator known to have large charging effects. As the flame-annealed Au surface is exposed to modification, binding energies shift to lower values, with the lowest belonging to the modified-PMMA protein samples. Moreover, it seems that at least exposure to ambient conditions or the addition of PMMA is necessary to reduce the charging effect of samples. Protein attached directly onto Au (see 'TmGH1 directly on Au', Table 3.1) does not reduce charging as much as a layer of PMMA or organic contamination. Presumably most PMMA surface modification procedures increase the conductivity of the surface.

Ionizable groups, such as COO^- and NH_3^+, form part of the structure of our organic overlayers and they allow some ionic conduction to occur. We can demonstrate this by comparing the charging values for the protein-terminated PMMA samples to those for the protein-terminated Au samples. There is an increase in surface charge relative to other samples containing modified-PMMA layers. Since there is no layer of modified-PMMA between the Au and the proteins, there are fewer ionic groups on the surface to promote conduction, thus some conductivity is lost. Another reason could be that certain samples simply had better electrical contact with the sample stage than others. This is likely not the main reason due to the number of samples that showed the surface conduction-charging relationship and because the experimental sample stage set-up within the XPS chamber is fairly uniform. A final reason for observing higher charging on the flame-annealed Au is that it has a thinner layer of Au than other samples, which further reduces conductivity at the surface. This is supported by an increased Si signal and decreased Au signal for this sample, as will be demonstrated in the next section.

3.3 XPS Survey Scan

A XPS survey scan of all samples was taken to confirm the presence of Au, C, N, O, and S on the surfaces, as well as to determine if any other elements and their associated Auger electron peaks were present. Figure 2.4 shows the survey scans obtained for non-flame annealed Au and unmodified PMMA. A comparison of the Au 4f peak intensities show that these peaks are less intense for the unmodified-PMMA samples, but this is expected as the PMMA overlayer attenuates the Au signal. In contrast, the C1s and O1s regions of the unmodified PMMA samples are more intense than the other two Au samples because characteristic carbon and oxygen moieties of PMMA contribute additional C1s and O1s signal to these regions. This Figure also shows the contamination present on the blank Au surfaces, which is still present despite copious cleaning with ddH_2O and MeOH. The C1s and O1s signal could be reduced by flame annealing the substrate. However, this increased the Si 2p (~152 eV) signal (from the underlying mica) which can limit the ability to observe changes in the nearby S2p (~162-168 eV) region. It is important to see the S2p signal, because this transition is necessary to confirm the orientation of attached proteins to a modified-PMMA surface. The evidence supports the assertion it is not necessary to flame anneal the Au substrate, since the spin-coating of PMMA will create a thin and flat surface (confirmed by AFM roughness analysis, see Chapter 4) which will attenuate the signal from any contamination below the surface.

3.4 XPS C1s Spectra

The C1s region is crucial to the understanding of the surface chemistry of the samples studied here. An overlay of C1s XPS spectra of representative samples can be seen in Figure 3.1; peak binding energy and FWHM can be seen in Tables 3.2 and 3.3, while the elemental ratios can be found in Table 3.4; the relative contribution of various C1s peak types is shown in Table 3.5. The deconvoluted peaks are shown below each spectrum in Figure 3.1 and they correspond to the different chemical environments.

The PMMA C1s spectra obtained may be generally interpreted using the literature. [28] The resolution of the unmodified PMMA spectra suggested a 3 peak deconvolution scheme shown in Figure 3.1 for all samples: bulk carbon (C-C, 285.0 eV; peak 1); carbon adjacent to an electronegative group (C-O / C-N / C-NH_2, 286.2 - 287 eV; peak 2); and carbonyl-type carbon (C=O / NC=O, 288.5 - 289 eV; peak 3). All spectra discussed below will be interpreted using this peak assignment scheme.

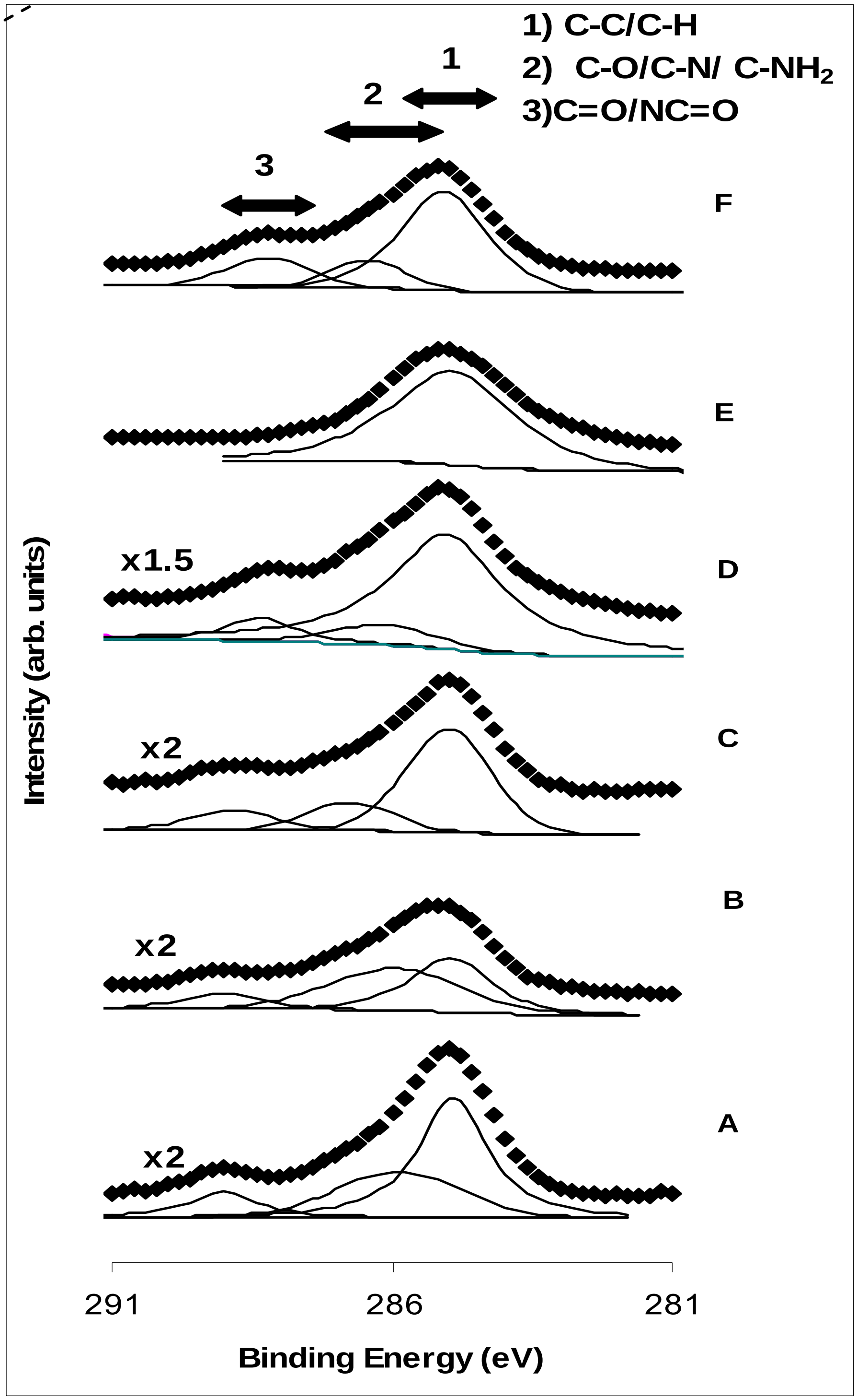

Figure 3.1: C1s XPS spectra of samples representative of various surface modifications. The surfaces studied are as follows: PMMA (A) Aminated PMMA (B) 1mM Sulfo-EMCS (C) TmGH1 on Sulfo-EMCS modified PMMA (D) phnH on Sulfo-EMCS modified PMMA (E) TmGH1 directy on Au (F)

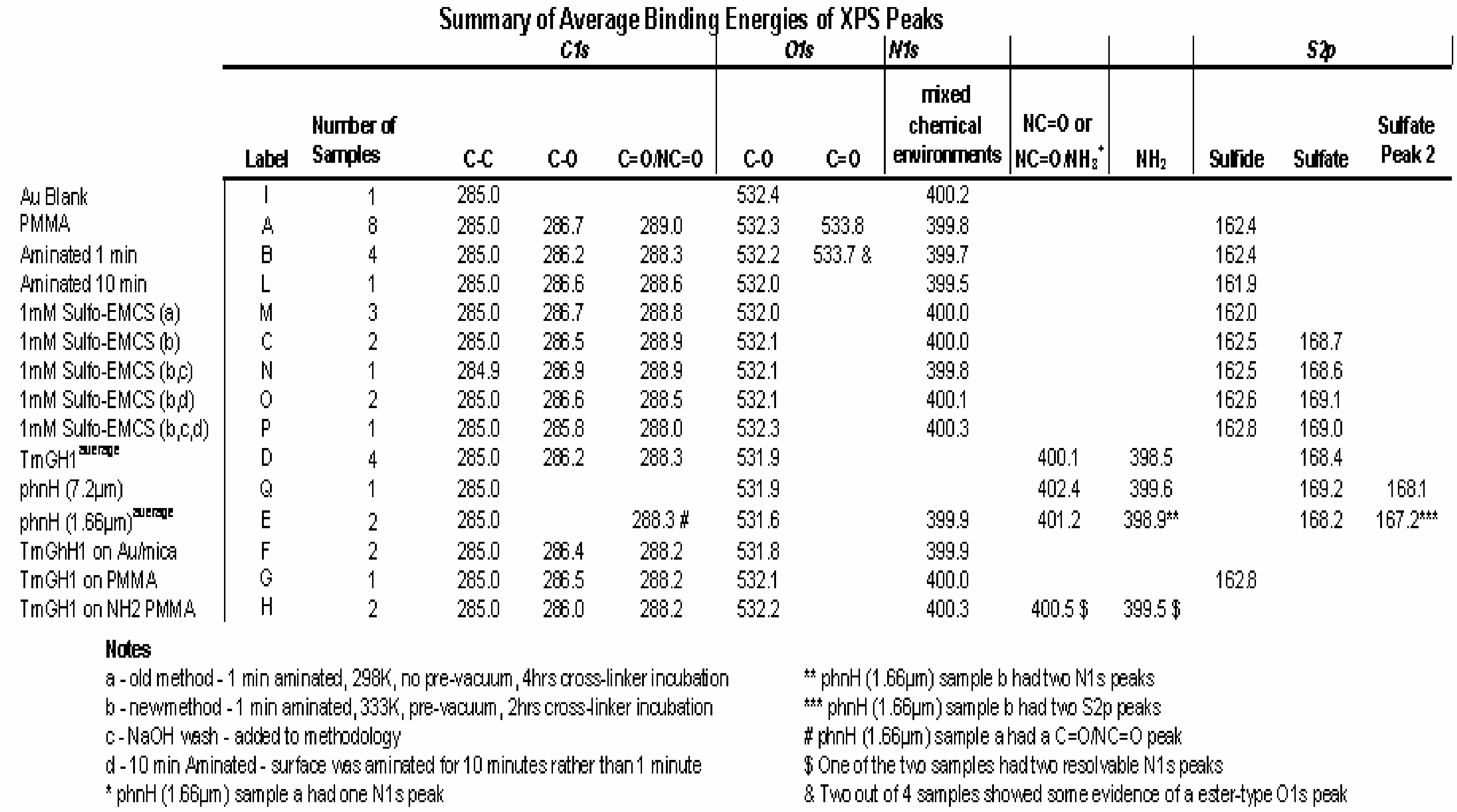

Summary of Average Binding Energies of XPS Peaks

			C1s			*O1s*		*N1s*			*S2p*		
	Label	Number of Samples	C-C	C-O	C=O/NC=O	C-O	C=O	mixed chemical environments	NC=O or NC=O/NH$_3^+$	NH$_2$	Sulfide	Sulfate	Sulfate Peak 2
Au Blank	I	1	285.0			532.4		400.2					
PMMA	A	8	285.0	286.7	289.0	532.3	533.8	399.8			162.4		
Aminated 1 min	B	4	285.0	286.2	288.3	532.2	533.7 &	399.7			162.4		
Aminated 10 min	L	1	285.0	286.6	288.6	532.0		399.5			161.9		
1mM Sulfo-EMCS (a)	M	3	285.0	286.7	288.8	532.0		400.0			162.0		
1mM Sulfo-EMCS (b)	C	2	285.0	286.5	288.9	532.1		400.0			162.5	168.7	
1mM Sulfo-EMCS (b,c)	N	1	284.9	286.9	288.9	532.1		399.8			162.5	168.6	
1mM Sulfo-EMCS (b,d)	O	2	285.0	286.6	288.5	532.1		400.1			162.6	169.1	
1mM Sulfo-EMCS (b,c,d)	P	1	285.0	285.8	288.0	532.3		400.3			162.8	169.0	
TmGH1^{average}	D	4	285.0	286.2	288.3	531.9			400.1	398.5		168.4	
phnH (7.2µm)	Q	1	285.0			531.9			402.4	399.6		169.2	168.1
phnH (1.66µm)^{average}	E	2	285.0		288.3 #	531.6		399.9	401.2	398.9**		168.2	167.2***
TmGhH1 on Au/mica	F	2	285.0	286.4	288.2	531.8		399.9					
TmGH1 on PMMA	G	1	285.0	286.5	288.2	532.1		400.0			162.8		
TmGH1 on NH2 PMMA	H	2	285.0	286.0	288.2	532.2		400.3	400.5 $	399.5 $			

Notes

a - old method - 1 min aminated, 298K, no pre-vacuum, 4hrs cross-linker incubation
b - newmethod - 1 min aminated, 333K, pre-vacuum, 2hrs cross-linker incubation
c - NaOH wash - added to methodology
d - 10 min Aminated - surface was aminated for 10 minutes rather than 1 minute
* phnH (1.66µm) sample a had one N1s peak

** phnH (1.66µm) sample b had two N1s peaks
*** phnH (1.66µm) sample b had two S2p peaks
# phnH (1.66µm) sample a had a C=O/NC=O peak
$ One of the two samples had two resolvable N1s peaks
& Two out of 4 samples showed some evidence of a ester-type O1s peak

Table 3.2: This table summarizes the collected binding energies (eV) of the XPS spectral peaks. The error associated with these values is ± 0.2 eV.

Summary of Average FWHM of XPS Peaks

			C1s			*O1s*		*N1s*			*S2p*		
	Label	Number of Samples	C-C	C-O	C=O/NC=O	C-O	C=O	mixed chemical environments	NC=O or NC=O NH$_3^+$	NH$_2$	Sulfide	Sulfate	Sulfate Peak 2
Au Blank	I	1	1.60			2.13		2.02					
PMMA	A	8	1.95	1.88	1.45	2.18	1.56	2.62			2.91		
Aminated 1 min	B	4	1.80	1.84	1.89	2.54	1.33 &	2.65			2.34		
Aminated 10 min	L	1	1.93	1.81	2.51	1.14		1.18			2.04		
1mM Sulfo-EMCS (a)	M	3	2.17	2.05	1.47	2.47		3.15			2.37		
1mM Sulfo-EMCS (b)	C	2	1.72	1.94	1.81	2.76		2.79			2.40	1.90	
1mM Sulfo-EMCS (b,c)	N	1	1.91	1.93	1.87	2.63		2.72			1.15	1.18	
1mM Sulfo-EMCS (b,d)	O	2	1.90	1.73	2.19	2.47		2.67			2.12	2.67	
1mM Sulfo-EMCS (b,c,d)	P	1	1.29	1.44	3.16	2.45		2.56			2.12	2.26	
TmGH1^{average}	D	4	2.14	2.15	1.51	2.48			1.83	2.30		2.45	
phnH (7.2μm)	Q	1	1.69			2.34			1.92	2.15		1.43	1.52
phnH (1.66μm)^{average}	E	2	2.31		1.65 #	2.49			2.00	2.04*		2.03	1.54***
TmGhH1 on Au/mica	F	2	1.92	1.55	1.81	2.41		2.15					
TmGH1 on PMMA	G	1	2.09	1.42	1.96	2.45		2.06			4.51		
TmGH1 on NH2 PMMA	H	2	1.80	2.08	2.01	5.01			1.36 $	1.89 $			

Notes

a - old method - 1 min aminated, 298K, no pre-vacuum, 4hrs cross-linker incubation

b - newmethod - 1 min aminated, 338K, pre-vacuum, 2hrs cross-linker incubation

c - NaOH wash - added to methodology

d - 10 min Aminated - surface was aminated for 10 minutes rather than 1 minute

* phnH (1.66μm) sample a had one N1s peak

** phnH (1.66μm) sample b had two N1s peaks

*** phnH (1.66μm) sample b had two S2p peaks

phnH (1.66μm) sample a had a C=O/NC=O peak

$ One of the two samples had two resolvable N1s peaks

& Two out of 4 samples showed some evidence of a ester-type O1s peak

Table 3.3: This table summarizes the FWHM (eV) of the fitted XPS spectral peaks. The error associated with these values is ± 0.2 eV.

	Average of Elemental Ratios for Various Sample Types (Normalized Data)							
Type	**Label**	**No. of Samples**	**N/S**	**O/S**	**C/S**	**O/N**	**O/C**	**C/N**
Au Blank	I	1				4.19	0.21	19.99
PMMA$^{\#}$	A	8	3.39	trace	trace	15.12	0.44	trace
Aminated 1 min	B	4	4.21	48.75	85.55	12.11	0.52	22.57
Aminated 10 min	L	1	8.38	22.89	27.89	2.73	0.82	3.33
1mM Sulfo-EMCS (a)	M	3	3.77	56.84	58.10	12.98	0.72	16.89
1mM Sulfo-EMCS (b)	C	2	12.51	125.71	164.24	11.22	0.78	14.08
1mM Sulfo-EMCS (b,c)	N	1	8.42	84.96	61.19	10.09	1.39	7.27
1mM Sulfo-EMCS (b,d)	O	2	23.15	98.57	166.92	3.79	0.53	7.09
1mM Sulfo-EMCS (b,c,d)	P	1	15.74	166.06	140.94	10.55	1.18	8.96
TmGH1^{average}	D	4	56.10	133.56	245.67	2.51	0.57	4.41
phnH (7.2μm)	Q	1	2.47	19.90	57.66	8.06	0.35	23.36
phnH (1.66μm)^{average}	E	2	7.59	19.08	61.75	2.74	0.45	6.88
phnH (1.66μm)^{average}	E1	1	12.32	29.30	109.58	2.38	0.27	8.89
phnH (1.66μm)^{average}	E2	1	2.86	8.87	13.92	3.11	0.64	4.86
TmGH1 on Au	F	2	no S 2p	no S 2p	no S 2p	1.32	0.35	3.73
TmGH1 on PMMA	G	1	31.56	58.95	143.54	1.87	0.41	4.55
TmGH1 on NH2 PMMA	H	2	10.34	30.54	48.58	3.09	0.66	4.67
TmGH1 on NH2 PMMA Multi C1s peaks	H1	1				2.88	0.63	4.57
TmGH1 on NH2 PMMA Single Set of C1s peaks	H2	1				3.29	0.69	4.77

Notes

a - old method - 1 min aminated, 298K, no pre-vacuum, 4hrs cross-linker incubation
b - new method - 1 min aminated, 333K, pre-vacuum, 2hrs cross-linker incubation
c - NaOH wash - added to methodology
d - 10 min Aminated - surface was aminated for 10 minutes rather than 1 minute
- The N/S, O/S, C/S and C/N ratios are based on collected spectra for 2 out of 8 samples

Table 3.4: This is the average of those elemental ratios calculated by using the normalized data (corrected for sensitivity factors and transmission function) for the area under the peaks. The total area for each element was used in each calculation. The error for these values is approximately 10-15%. (Briggs and Grant, 2003)

	Label	No. of Samples	C1s Area			Standard Deviation (eV)		
			C-C	C-O	C=O/NC=O	C-C	C-O	C=O/NC=O
Au Blank	I	1	100%					
PMMA Blank Control	A	6	76%	13%	12%	0.04	0.02	0.01
PMMA Blank	K	2	71%	19%	10%	0.07	0.14	0.02
Aminated 1 min	B	4	66%	23%	11%	0.23	0.20	0.06
Aminated 10 min	L	1	69%	21%	10%			
1mM Sulfo-EMCS (a)	M	3	71%	19%	10%	0.02	0.08	0.01
1mM Sulfo-EMCS (b)	C	2	65%	22%	12%	0.05	0.06	0.01
1mM Sulfo-EMCS (b,c)	N	1	71%	19%	11%			
1mM Sulfo-EMCS (b,d)	O	2	69%	17%	15%	0.02	0.02	0.00
1mM Sulfo-EMCS (b,c,d)	P	1	57%	21%	22%			
TmGH1	D	4	78%	13%	10%	0.02	0.04	0.01
phnH 1.5 mL	Q	1	100%					
phnH 1.2 mL	E	2	98%		3%	0.12		0.02
TmGH1 on Au	F	2	69%	15%	17%	0.03	0.00	0.01
TmGH1 on PMMA	G	1	68%	16%	16%			
TmGH1 on NH2 - PMMA	H	2	68%	15%	16%	0.20	0.18	0.02
					Average	*0.08*	*0.08*	*0.02*

a - old method - 1 min aminated, 298K, no pre-vacuum, 4hrs cross-linker incubation
b - new method - 1 min aminated, 338K, pre-vacuum, 2hrs cross-linker incubation
c - NaOH wash - added to methodology
d - 10 min Aminated - surface was aminated for 10 minutes rather than 1 minute

Table 3.5: This table shows the percent composition of the C1s peaks for each sample, as defined by:

$$\%\ \text{Peak Area} = \frac{\text{Normalized Peak Area}}{\text{Sum of Normalized C1s Area}}$$

For modifications that were repeated, the standard deviation of the C1s peak areas has been computed. An average of all the standard deviations for each C1s peak is shown in the bottom right corner of the Table. The average values are either below or within the range of 5 - 15%, depending on the spectrometer used. (Briggs and Grant, 2003)

The resolution of the C1s spectra of the modified surfaces did not suggest deconvoluting spectra by a 4-peak scheme as reported by others.[20, 24, 28] A 4-peak deconvolution scheme is not representative of obtained spectra and the adoption of the 3-peak scheme is sufficient for discussion of the surface chemistry as demonstrated by Bai *et al*..[4] Changes to the peak locations, FWHM and intensity were monitored, in order to elucidate the surface chemistry after substrate modification.

3.4.1 PMMA

We can first analyze the peak assignment for unmodified PMMA using Figure 3.1 (sample A) and Tables 3.2 and 3.3. Three peaks can be seen and they have the following assignments: peak 1 (C-C, 285.0 eV); peak 2 (C-O, 286.7 eV); and peak 3 (C=O, 289.0 eV). These are consistent with the monomer structure of PMMA shown in Figure 1.1 and the peaks are characteristic of PMMA studied elsewhere.[24, 43] The binding energy shifts of peak 2 and 3 from the bulk carbon signal of peak 1 can be explained by considering the proximity of carbon to electronegative elements or functional groups. These groups attract electron density from an adjacent carbon atom, which translates to a C1s transition that has a higher binding energy. The carbonyl chemical environment is more electronegative than a ether-type environment, thus explaining the ~ 4 eV chemical shift of peak 3 compared to the ~1.7 eV shift of peak 2 for sample A. It is also particularly noteworthy that the PMMA spectra produces a distinctive three-peak envelope compared to the single peak of a Au sample, such as that reported for sample I in Table 3.2. The elemental ratios and the FWHM data are also characteristic of a PMMA surface.

In Table 3.4, the average value of the O/C, C/S and C/N peak area ratios are reported for sample set A and K, the PMMA samples. The values of the O/C ratio for sample set A is 0.44, which is consistent with the theoretical O/C ratio for an infinitely thick surface of PMMA, which should have a value of 0.4 (see Figure 1.1). Only trace amounts of N or S2p signal is observed, consistent with negligible N or S being present in these samples.

The FWHM data in Table 3.3 helps to establish some reference values for analyzing the variety of chemical environments under any one peak assignment; they can only be used in a relative sense. As previously discussed, a FWHM value between 1.5 – 1.7 is considered to be a good indication that any given peak represents a species in a single chemical environment. Any increase in the FWHM value suggests that there are different chemical environments represented by one peak that too close to one another to be resolved. For sample A we see that the FWHM values are 2.08 eV (± 0.2 eV), 1.61 eV(± 0.2 eV), and 1.46 eV (± 0.2 eV) for the bulk carbon, C-O and C=O peak assignments. These values are within the 1.5-2.0 range, within experimental error, which suggests that the surface composition is relatively homogeneous. However, it will be most instructive to compare the FWHM values in tandem with binding energy shifts for subsequent samples as a measure of types of chemical environments present at the surface between samples.

3.4.2 NH_2-terminated PMMA

The reported average binding energies for the peaks in the NH_2-terminated PMMA samples (1 minute exposure) in Figure 3.1 (sample B) are 285.0 eV (± 0.2 eV), 286.2 eV (±0.2 eV), and 288.3 eV (±0.2 eV) for peaks 1, 2 and 3 respectively (see Table 3.2). Peaks 2 and 3 are shifted as compared to their corresponding peaks in sample set A. There is a 0.7 eV shift for the carbonyl carbon (peak 3) to lower binding energies to that of PMMA. The C1s signal for this carbonyl carbon is at 289.0 eV (± 0.2 eV) for PMMA (sample A, Fig. 8), which is in the expected range binding energies (288.6 eV – 289.03 eV).[42] The carbonyl peak's binding energy after 1 minute exposure to ethylenediamine is below this range. This evidence supports the idea that some methoxy groups have been replaced by amide linkages. The electronegativity of nitrogen is lower than that of oxygen, thus a NC=O linkage would withdraw less electron density from C than an OC=O configuration. This leads to an expectation of lower binding energies for the carbonyl peak of a NH_2-termianted PMMA C1s spectrum, as we see in the results in Table 3.3.

We also see evidence of a chemical shift for the peak representing the C-O type of chemical environment and it is further evidence for the loss of methoxy groups from the surface. There is ~0.5 eV chemical shift to lower binding energy from samples A to B (peak 2, Table 3.3). For polymers containing a C-N bond, such as polyamide, the peak at a binding energy of 286 eV has been characterized as belonging to a C-N bond,[80] and for ethylamine (on metals) the C-N bond signal is located within a range of 286.1eV – 286.7 eV [42, 81]; Briggs also suggests a chemical shift of ~1.2 eV for the C-N bond.[41] In the case of PMMA, the C-O C1s signal should be in the range of 286.4 eV to

286.7 eV. The above literature values show that the C-N type peak should have a lower minimum binding energy than the C-O type peak. A shift to lower binding energy with the removal of methoxy groups from the surface is expected theoretically and is seen in the experimental data presented here.

The carbonyl peak for sample B (Figure 3.1) combines a contribution from both types of carbonyl signal (NC=O and OC=O), since no surface is 100% converted after chemical modification from one type to another. In Table 3.3 we can see for sample set A that the FWHM value for the PMMA carbonyl peak is 1.45 (± 0.2 eV). We see that these values increase to 1.89 (± 0.2 eV) for the 1 minute NH_2-terminated PMMA sample set (B). This increase of approximately +0.4 eV in the FWHM value between sets A and B is evidence for a broader range of carbonyl environments within sample B. This observation is further supported by an increase of the same FWHM value to 2.51 (± 0.2 eV), when the PMMA substrate is exposed to the ethylenediamine solution for 10 minutes. Comparisions between the other FWHM values for sample sets A and B/L in Table 3.3 do not lead to conclusive discussion, since the values remain the same, within experimental error, between samples.

An analysis of the C1s spectral intensity and a comparison of the elemental ratios also provides us with clues to support successful surface modification from PMMA to NH_2-terminated PMMA. A visual comparison of the spectra of sample A and sample B in Figure 3.1 shows that the overall carbon intensity is decreased, the envelope of peak 1 is broader, and the peak height is reduced. Such visual clues are quantified in Table 3.4 by comparing the C1s related elemental ratios of each sample type. The O/C ratio has increased between PMMA (sample sets A) and NH_2-terminated PMMA (sample sets B [1 minute] and L [10 minutes]) from 0.44 (± 12%) to 0.52 (± 12%) (1 minute) and then 0.82 (± 12%) (10 minutes). The C/N ratio for sample B is 22.57 (1 minute exposure) and for sample L is 3.33 (10 minute exposure). While the large value for sample B represents a negligible amount of N on the surface, it still represents more N on the surface than sample A (PMMA); this trend is confirmed by the value for sample L which was the result of exposing the sample to ethylenediamine for a longer time period. The C/N trend is consistent with the removal of a methoxy group and the introduction of an amide linkage and primary amines to the surface. The O/C ratio should decrease, as O is removed, if the entire sample consisted of amine-terminated groups. However, this does not take into account the attenuation effect. The ethylenediamine layer, which is relatively carbon-poor, may attenuate the C1s signal from the carbon-rich underlying layer of PMMA. This is further supported by the evidence that the NH_2-terminated PMMA is thicker than PMMA in Table 3.1. In general, the trends in the elemental ratios, particularly the O/N ratios and C/N ratios, between PMMA and NH_2-terminated PMMA samples suggests that successful modification of PMMA has been completed.

3.4.3 Sulfo-EMCS-terminated PMMA

To my knowledge there are no other studies of Sulfo-EMCS terminated surfaces by XPS. The data will be interpreted in the same manner as the other spectra in this thesis. The data from the C1s region of the Sulfo-EMCS terminated PMMA (sample C, Figure 3.1) will now be compared to previous sample. Sulfo-EMCS is a hetero-bifunctional cross-linker where one end of the molecule reacts with primary amines on a substrate through an aminolysis reaction to create a covalent amide bond (see C, in

Figure 2.1). The resultant surface has a variety of carbon environments, including C-N bond, C-C bonds, and NC=O bonds, along with the ester-type groups belonging to the unreacted PMMA that is a constituent of the underlying NH_2-terminated PMMA suface. These environments are represented by 3 peaks in the C1s spectrum. The collected data demonstrates evidence of a chemical change to the NH_2-terminated surface after exposure to the Sulfo-EMCS/buffer solution. Most of the discussion below will involve sample set C in the Tables and Figures, since is represents the optimized methodology for creating the protein-terminated surfaces. Section 3.10 discusses the optimized procedure as it applies to these samples.

The binding energy data shows that there are some chemical shifts of the C1s peaks for this sample compared to the data for the NH_2-terminated samples. On average, the chemical shift for peaks 2 and 3 are +0.3 eV and +0.6eV respectively, when comparing sample set C (Sulfo-EMCS terminated) to B (NH_2-terminated) in Table 3.2. Both shifts are consistent with an increase in the density of amide functional groups on the surface. The terminal amine groups have converted to amide bonds through aminolysis, as well the new surface is terminated by a maleimide, which has an imide as a sub-component. The C1s binding energy chemical shifts between the PMMA, NH_2-terminated and Sulfo-EMCS-terminated surfaces are consistent with expectations for this series of chemical modifications.

The FWHM data corresponding to the typical NH_2-terminated and Sulfo-EMCS-terminated surfaces are shown as sample set B and sample set C in Table 3.3. A direct comparison of the surface composition based on the FWHM values for these two sample sets is not possible, because the values are within experimental error. However we can compare the Sulfo-EMCS-terminated surface to the preceding PMMA surface (sample set A and K, Table 3.3) in much the same way that was done in the previous section, but with a particular focus on the carbonyl peak values. It is expected that a surface that has more carbonyl-type environments would have a larger FWHM for a fitted peak generally constrained to the same binding energy region. The introduction of imide groups and another amide bond from the addition of Sulfo-EMCS are expected to contribute to C1s photoelectron signal at approximately 289 eV.[41] A comparison of the FWHM for sample set A and sample set C (Table 3.3) shows an increase in the FWHM value by 0.35 eV (± 0.2 eV). Moreover, the average FWHM for the carbonyl peaks of the PMMA sample sets (A, K; Table 3.3) and the Sulfo-EMCS sample sets (M, C, N, O, P; Table 3.3) result in values of 2.09 eV (standard deviation ± 0.6 eV) and 1.45 eV (standard deviation ± 0.02 eV). These results demonstrate that in general the modifications leading to a Sulfo-EMCS terminated surface produce surfaces that contain a wider variety of carbonyl groups than the original PMMA substrates.

The overall intensity of the Sulfo-EMCS terminated C1s signal is marginally higher than that of the NH_2-terminated surfaces, and this can be seen visually in Figure 3.1 by comparing sample B with sample C. Trends in the intensity ratios in Table 3.4 show evidence for surface modification. A comparison of the O/C ratio between sample set B and sample set C shows an increase from 0.52 (± 12%) to 0.78 (± 12%). The average O/C ratio for similar samples sets for the NH_2-terminated surfaces is 0.67 (± 12%) (B and L, Table 3.4) and for the Sulfo-EMCS group is 0.92 (± 12%) (M, C, N, O, P, Table 3.4). An increasing trend between these two sample types is consistent with the addition of oxygen to the surface. However, more carbon than oxygen has been added to the surface as well, which should have contributed to a decrease in this ratio, compared to PMMA (C:O of 3:1 compared to 5:2). This inconsistency is most likely due to the attenuation of the C1s signal from underlying layers, thus increasing the O/C ratio.

In the case of the C/N ratios, there was the curious result of a decreasing trend between samples, when an increasing trend is expected. If one compares samples in Table 3.4 in the same manner as the O/C ratios were, then the C/N values obtained are: 22.57 (± 12%)(sample set B), 14.08 (± 12%)(sample set C), 12.95 (± 12%) (average of B and L), and 10.86 (± 12%) (average of M, C, N, O, P) The theoretical C/N values for a surface consisting entirely of -NH_2 groups and one of Sulfo-EMCS are ~0.66 and 4.5 respectively. These values can be interpreted using the notion of relatively carbon-rich and carbon-poor layers above the surface, which was introduced in section 3.4.2. Relative to the NH_2-terminated surfaces, the Sulfo-EMCS section of the surface is carbon-poor. Also, this carbon-poor layer would attenuate signal from the relatively carbon-rich layer underneath. According to the thickness calculations (section 3.1) the addition of Sulfo-EMCS increases the surface thickness by approximately 1 nm. An additional 1 nm of travel distance of C1s photoelectrons through PMMA from the underlying NH_2-terminated surface would reduce the C1s signal to ~69% of its previous value (using equation 14 and λ for PMMA, as an approximation). While this happens to be the approximate reduction in the C/N ratio from sample set B to C (~62%), one should only view the attenuation effect as one explanation for the decrease in the C/N ratio. This is clear when comparing aggregate values, such as the above average C/N ratios; the Sulfo-EMCS surface causes the signal to drop to ~39% of the NH_2-terminated value. A combination of an attenuation effect and the introduction of another carbon-poor overlayer contribute to a decreasing trend in the C/N ratio; the O1s and the N1s signal as they relate to the O/C and C/N ratios will be compared later. Also, it is more beneficial to discuss the C/S results in the later section regarding the S2p XPS spectra.

3.4.4 TmGH1-terminated PMMA Surfaces

To my knowledge there are no other studies of TmGH1 – terminated surfaces by XPS, but analysis will be similar to previous samples. In section 3.9, TmGH1 XPS data will be compared to XPS data obtained using other protein samples. The relevant C1s data comparing the TmGH1 surfaces to the previous Sulfo-EMCS terminated surface(s) will be used as evidence to show that TmGH1 is present on the modified surfaces as shown schematically in Fig. 4 (surface D). Comparision of the data for the TmGH1-terminated PMMA surfaces and those surfaces which involved direct exposure of TmGH1 to individual substrates (i.e. Au, PMMA, NH_2-terminated surfaces – see sample sets F, G, H1 and H2 in Table 3.3) will be discussed in section 3.9. There are a number of obvious features common to TmGH1 XPS spectra (Figure 3.1, D), that signal a newly modified surface. The overall C1s signal intensity is ~30% more intense than the previously modified surfaces. Peaks 1 and 2 are less resolved in these spectra and peak 3 seems more prominent in spectra D when compared to the amine or Sulfo-EMCS modified samples. This visual evidence is consistent with the addition of carbon-dense proteins and more carbonyl functional groups onto the modified PMMA surface. The subsequent paragraphs will quantify these brief visual observations and cite specific evidence to support the hypothesis.

Both peaks 2 (C-O/C-N/C-NH_2) and 3 (C=O/N-C=O) undergo chemical shifts to lower binding energies. The average binding energies of peak 2 should be compared between the optimized Sulfo-EMCS surface (sample set C, Table 3.2) and the TmGH1 suface (sample D, Table 3.2); the respective averages are 286.5 eV (± 0.2 eV) and 288.2 eV (± 0.2 eV), representing a – 0.3 eV difference in average binding energy. This is consistent with a C1s chemical environment representing carbons adjacent to less electronegative species. In proteins carbons are often found beside oxygen, nitrogen and sulfur atoms (i.e. methoionine), and in this case it is most likely that there is an increase in C-N bonds relative to C-O bonds (consistent with the large number of peptide bonds in proteins). This would lead to a lower average binding energy for peak 2, since nitrogen is less electronegative than oxygen. As further evidence for this hypothesis, the average binding energy for sample set D is certainly lower than PMMA (sample sets A and K) and Sulfo-EMCS terminated surfaces (sample sets M, C, N, O, P, with their surface of imide groups), and it is within the lower range of the binding energy values of NH_2-terminated surfaces (sample sets B and L); it is this last comparison which is the strongest evidence towards supporting a surface richer in C-N bonds than C-O bonds.

The carbonyl-peak chemical shift of the TmGH1-terminated surfaces suggests that there are more carbonyl groups adjacent to nitrogens (i.e. amides, imides and peptides) than those adjacent to oxygen (i.e. esters). The average binding energy of peak 3 (C1s, Table 3.2) for the TmGH1 surfaces is 288.3 eV (± 0.2 eV), which is 0.6 eV (± 0.3 eV) lower than the corresponding value for the optimized Sulfo-EMCS surface, representing one relatively rich with ester and imide groups, along with some amide groups (sample set C, 288.9 eV (± 0.2 eV); also see surfaces B and C in Figure 2.1). As well, this reported value of 288.3 eV (± 0.2 eV) is the same value, within error, of that for NH_2 -terminated surfaces that are also relatively rich in amide functionalities (sample sets B and L, Table 3.2; surface B in Figure 2.1). This large chemical shift to lower binding energies is not only caused by an increase in the concentration of C and N containing carbonyl moieties, but it is also caused by the attenuation of the C1s photoelectrons from the ester-type groups of the underlying PMMA structure. The thickness of a TmGH1 on PMMA surface, according to Table 3.1 (see section 3.1 for further explanation) is 6.32 nm (± 0.73; literature TmGH1 length from C to N terminus is ~ 5.5 nm[47]). A photoelectron escaping the underlying PMMA substrate would have to travel ~4.7 nm to escape from the surface and in doing so would be attenuated to ~17% of its original value (see section 3.1). The binding energy results for the carbonyl peak of the TmGH1-terminated PMMA samples suggests a surface rich in carbonyl groups containing nitrogen and poor in ester-type carbonyl groups; both observations are consistent with proteins that have many peptide bonds between constituent amino acid units.

The previous comparisons of the C1s FWHM values between samples was considered to be instructive, but limited in scope. In this section, the FWHM comparison between the TmGH1-terminated surface on PMMA (sample set D, Table 3.3) and the Sulfo-EMCS samples (M, C, N, O, P, Table 3.3), particularly the optimized sample set C is clearer and serves as strong evidence for a surface terminated with a protein. The C1s FWHM values for sample set D are 2.14 eV (± 0.2 eV) for peak 1, 2.15 eV (± 0.2 eV) for peak 2, and 1.51 eV (± 0.2 eV) for peak 3. The values for the optimized Sulfo-EMCS surface (sample set C, Table 3.3) are 1.72 eV (± 0.2 eV) , 1.94 eV (± 0.2 eV) and 1.84 eV (± 0.2 eV) for the same set of C1s peaks. The FWHM values for the first two peaks for sample set D are not only larger than those for sample set C, but also represent among the highest values of average FWHM across all samples in Table 3.3. This suggests that there is a greater variety of C1s signal coming from photoelectrons with kinetic energies close to those belonging to bulk carbon (~285 eV) and C-N (~286.3 eV). This is consistent with a protein with carbons adjacent or within a large variety of functional groups (i.e. C-O, C-N, C-S, related groups…). The FWHM for peak 3 for sample set D is both lower than the corresponding value for sample set C and among the lowest values for the width of the carbonyl peak. In addition, the average FWHM value for this sample set is approximately the same as that the corresponding peak for PMMA samples, representing only the ester-type carbonyl functional group. Despite the many types of carbonyl groups in TmGH1, this FWHM value suggests that the C1s signal here predominately arises from carbonyl carbon from one functional group, which are amides, as indicated in the previous paragraph.

The elemental ratios for the TmGH1 samples in Table 3.4 (sample set D) further confirms the trends mentioned previous, particularly that the C1s peak intensity is characteristic of a large protein on the surface. The C/N ratio has continued its downward trend, for the optimized methodology, from the unmodified PMMA through to the TmGH1-terminated PMMA surfaces (sample sets K→B→C→D), with the C/N ratio value for sample set D being the lowest at 4.41 (± 12%). Intuitively, this trend is not associated with surfaces having larger carbon components; instead it indicates surfaces that have an increasing nitrogen component and this will be discussed in the section regarding the N1s XPS spectra (section 3.6.4). The reported O/C ratio for the TmGH1-terminated PMMA samples is 0.57 (± 12%), which is a decrease from the value for sample set C (0.78 (± 12%)). This is opposite to the previous trend of an increasing O/C ratio and it suggests that the C1s signal has increased relative to the O1s signal, which indicates a rise in carbon within the surface composition. This is expected after the deposition of a large protein. Furthermore, it is consistent with a carbon-rich layer at the surface, which is certainly true for proteins, like TmGH1. The C/S ratio of 245.67 (± 12%) is consistent with an extremely high C1s signal relative to the S2p signal and the interpretation of this ratio is best explained in sections 3.7 and 3.9. What we can say is that it is the highest C/S ratio of all the previous modifications (sample sets K→B→C→D), which is expected for a final modification that adds the most amount of carbon onto the surface. More important uses of the C/S ratio to characterize the surfaces and methodology are explained in sections 3.7 and 3.9. This analysis of the C/N, O/C and C/S ratios indicate that the TmGH1-terminated PMMA surface is carbon-rich

3.4.5 phnH-terminated PMMA Surfaces

To my knowledge there are no other studies of phnH-terminated surfaces by XPS, but analysis will be similar to previous samples. In section 3.9, phnH surface XPS data will be compared to XPS data obtained using other protein samples. The phnH-terminated PMMA XPS results are in some ways problematic and in other ways indicative of surface modification. The analysis is limited by both the number of samples studied and by the poor reproducibility of the results. The purpose of conducting a XPS study of phnH to a Sulfo-EMCS terminated surface was to try and confirm the orientation of the terminal cysteine group of the TmGH1-terminated PMMA surface. The protein phnH has two terminal cysteine groups, so if one is pointed towards the substrate and one towards the surface, then an increased S2p signal should be detected, as will be discussed later. While some results are promising, one should be careful when considering the phnH-terminated PMMA results based on the C1s analysis presented here.

There were three phnH samples studied: one made from a 7.2 μM phnH/buffer solution and two made from a 1.66 μM phnH/buffer solution, which are labeled sample Q, E1 and E2 in Tables 3.2, 3.4 and 3.3. Spectrum E2 in Figure 3.1 is representative of the C1s spectra of both Q and E2; the spectrum of E1 will be discussed later. This spectrum is characterized by a single broad peak at 285.0 eV and the FWHM is ~2 eV. This spectrum is inconsistent with the obtained spectrum for a TmGH1-terminated PMMA (spectrum D) due to the lack of expected carbonyl peak at ~288 - 289 eV. A more consistent spectrum was obtained for sample E1, which does have a carbonyl peak at 288.3 eV (± 0.2 eV) with a FWHM of 1.65 eV (± 0.2 eV). As determined for TmGH1 samples, the presence of a carbonyl peak should be expected for samples containing many amide bonds within the structure (i.e. peptide bonds connecting amino acid units). There may be a few reasons for the poor reproducibility of the C1s spectra: first, the carbonyl peak may not be resolvable in some samples due to the increase in signal from many C1s chemical environments with similar binding energies; second, the addition of a large amount of carbon to the surface may be attenuating carbonyl C1s signal from the protein itself or underlying layers of the surface; third, the absorbed protein may have been denatured in samples E2 and Q. This could be caused by heat, poor pH control of the buffer solution (disrupt ionic bonding), exposure to methanol or ethanol (disrupt hydrogen bonding). However, protein denaturation is not known to disrupt primary structure (peptide bonds linking amino acids), so a carbonyl signal would still be expected. The lack of reproducible carbonyl signal is indicative of a problematic sample or methodology. Discussion of the various ratios will be made in subsequent sections as applicable to this sample type, with much of it focused on the S2p signal, which is necessary to confirm the presence of a covalent bond between TmGH1 and the terminal maleimide of the Sulfo-EMCS terminated surface.

3.5 XPS O1s Spectra

The O1s region offers some insight into the surface chemistry of the samples, but the data is not as firm as the C1s or the N1s regions. O1s XPS Spectra of representative is shown in Figure 3.2. The binding energy data and FWHM data are shown in Tables 3.2 and 3.3 respectively. The elemental ratios of peak intensity are shown in Table 3.4. The spectra can be generally interpreted using XPS data from literature examples of PMMA and other modified PMMA surfaces.[28, 43, 82] The observed signal arises from O1s photoelectron signal from a wide variety of oxygen containing functional groups that should be expected on the modified surfaces, including hydroxyl, carbonyl, ether-type bonds, ester-type bonds, and ketone groups. Particular peak assignments will be discussed in the subsequent sections. A brief note needs to made regarding resolution and signal deconvolution. As mentioned before (section 2.2.3), a XPS spectrum ideally can be deconvoluted using an individual peak for each O1s chemical environment that is present on the surface. However, in the case of O1s, the binding energies of the various O1s chemical environments are similar enough that deconvolution beyond two O1s chemical environments generally does not yield statistically significant results.

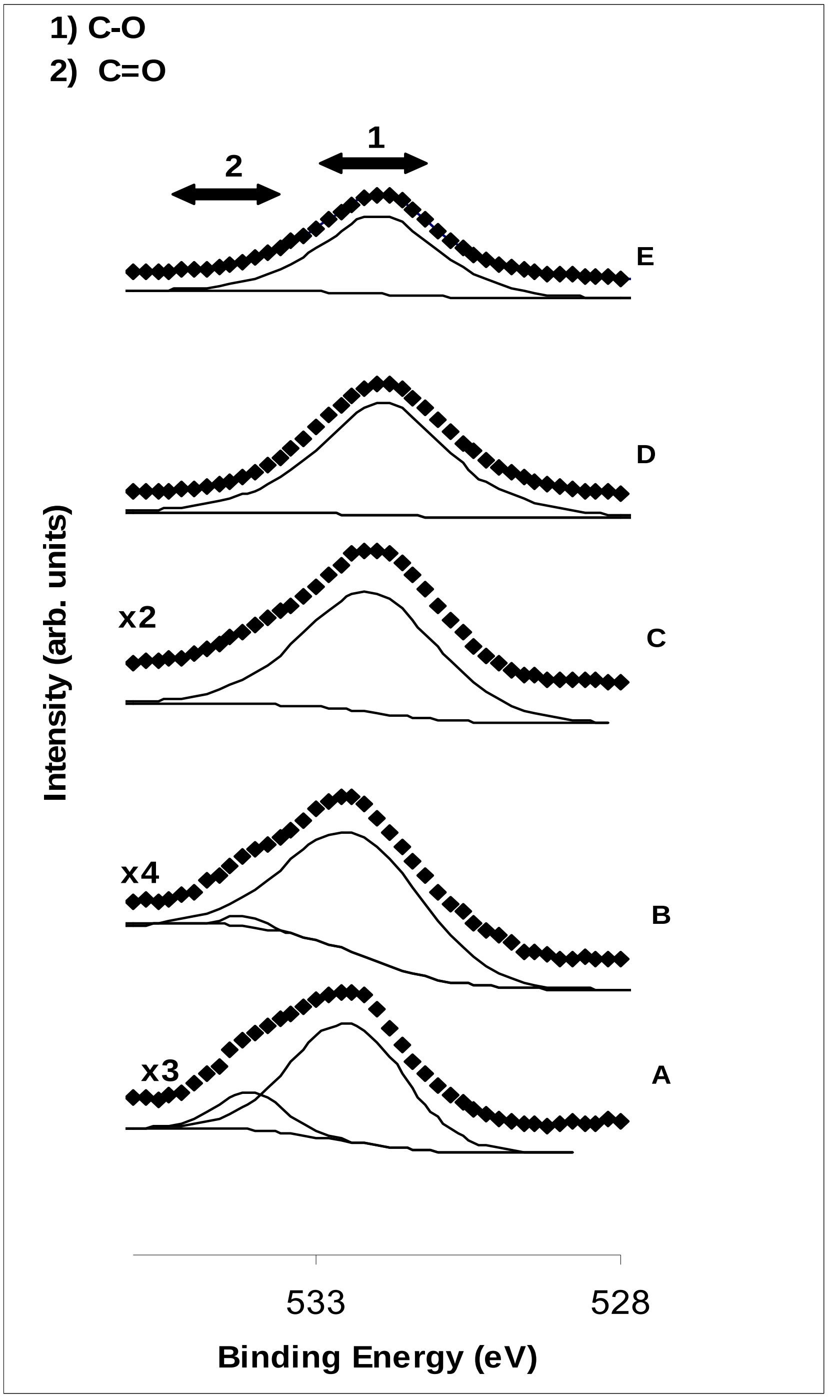

Figure 3.2: O1s XPS spectra of samples representative of various surface modifications. The surfaces studied are as follows: PMMA (A) Aminated PMMA (B) 1mM Sulfo-EMCS (C) TmGH1 on Sulfo-EMCS modified PMMA (D) TmGH1 directy on Au (F)

3.5.1 PMMA

A spectrum of a representative unmodified PMMA sample is shown in Figure 3.2 (sample A). There were two resolvable peaks at a binding energy of 532.3 eV (± 0.2 eV) (peak 1) and 534.0 eV (± 0.2 eV) (peak 2) (see Table 3.2, sample set A) that were respectively assigned to ether-type (C-O) and carbonyl-type oxygen chemical environments of the terminal PMMA surface as shown in Figure 2.1 (surface A). The carbonyl type O1s signal arises at a higher binding energy due to a higher electronegativity and pi-system that cause electron density to be retained more than the ether-type chemical environment. The binding energy values in Table 3.2 for sample set K, which is also unmodified PMMA, is within error of those values of sample set A. The average FWHM values for these peaks as reported for sample A (Table 3.3) are 2.05 (± 0.2 eV) (peak 1, Fig. 8) and 1.50 (± 0.2eV) (peak 2, Fig. 8), which are comparable to those of sample set K. The higher FWHM value for peak 2 is most likely due to other oxygen groups of similar binding energy, such those groups that would be present due to surface oxidation.

In Table 3.4 there are three oxygen related ratios reported for unmodified PMMA samples (sample set A): O/S, O/N, and O/C. The O/C ratio has been discussed previously. The values for the O/S and O/N ratio for this sample set indicated that only trace amounts of N or S were observed on these samples.

3.5.2 NH_2-terminated PMMA

The spectra labeled B in Figure 3.2 is representative of the signal from samples that had been exposed to ethylenediamine/DMSO solution for 1 minute to form terminal primary amine groups. In general the observed spectrum is similar to literature examples of XPS spectra were PMMA had been exposed to N_2 plasma.[28] The literature is an aid to the interpretation of the data presented here, since there is no previously published XPS data for the NH_2-terminated PMMA samples made for this thesis. One main peak and a shoulder have been identified in the signal envelope as arising from ether-type O1s photoelectrons (peak 1) and ester-type photoelectrons (peak 2) using the same rationale presented in the previous section. Other than their relative ratios, these peaks are not significantly different from those observed for PMMA in section 3.4. The inability to truly differentiate peaks 1 and 2 may be due to a low signal to noise ratio, along with the other limitations of the XPS technique (i.e. resolution etc.)

In Figure 3.1, we can observe that the overall intensity of the O1s region has decreased in spectrum B compared to spectrum A (from 3x to 4x). This suggests that there is less oxygen on the NH_2-terminated surfaces, which is consistent with the removal of methoxy-group oxygen. This observation can be further quantified by observing the trends in the elemental ratios shown in Table 3.3 between the PMMA (K) and the NH_2-terminated PMMA of sample set B. There is a decrease in the O/N ratio value from 15.12 (± 12%) to 12.11 (±12%) as unmodified PMMA is exposed to ethylenediamine. This is consistent with the removal of oxygen units, as expected for the conversion of ester-groups to amide groups through aminolysis.

There is a difference between the O/N ratios of the PMMA surfaces exposed to ethylenediamine for 1 minute and 10 minute, respectively labeled as sample sets B and L in Table 3.4. There is a dramatic decrease in the O/N ratio when PMMA is exposed for 10 minutes 15.12 (± 12%) to 2.73 (± 12%). This decrease is certainly consistent with a reduced surface composition of oxygen compared to the 1 minute samples. This suggests that a longer exposure to ethylenediamine produces a surface with more terminal primary amines. We could not use the 10 minute sample in the optimized procedure because sample quality deteriorated for exposures greater than 1 or 2 minutes. This was most likely caused by DMSO solvating or swelling the PMMA layers.

The O/C ratio increases from A→B (0.44 (± 12%) to 0.52 (± 12%), which is an unexpected result. Expectations suggest that this ratio should decrease: first, the theoretical trend is a downward trend from 0.4 to 0.33 (2/5 to 1/3); second, the O1s signal should be attenuated more than carbon due to the surface orientation of ester and amide functional groups; third, the attenuation length of an O1s photoelectron of an NH_2-terminated surface is less (2.00 nm, see Appendix B) than a C1s photoelectron (2.57 nm, see Appendix B) from the same surface, which would mean that O1s signal is attenuated more than C1s signal. All of the above three observations would contribute to a decreasing overall O1s intensity relative to the total C1s intensity. It must be surmised that the effect on the O/C ratio of the C1s signal from the carbon-poor layer of the terminal amine structure (compared to the underlying carbon-rich PMMA) is greater than the effect of the decreasing O1s photoelectron signal due to removal of the methoxy-group and other reasons. In hindsight, this makes sense, considering that the carbon density is larger than that of oxygen, and thus any major effect to the C1s signal would have a more pronounced affect on related ratios.

3.5.3 Sulfo-EMCS terminated PMMA

The O1s spectrum for the Sulfo-EMCS terminated PMMA sample is shown as C in Figure 3.2. The major difference between this spectrum and the previous two (A and B) is that only one peak was resolved and deconvoluted from the O1s signal of spectrum C. The binding energy for this single O1s peak is reported as 532.1 eV (± 0.2 eV) for sample set C in Table 3.2. This value remains relatively constant (within experimental error) for all the Sulfo-EMCS terminated surfaces. This peak has a binding energy that is lower than those reported for the ether-type peak assignment for sample sets K, B and L; however, this is not indicative of a change, since a difference of 0.1 eV -0.2 eV is within experimental error. On the other hand, the reported FWHM values for the Sulfo-EMCS terminated PMMA samples are, on average higher than the values belonging to previously modified samples. The reported value for the optimized Sulfo-EMCS terminated surface is 2.76 eV (± 0.2 eV), which is certainly higher than the reported values for sample sets A, K, B and L. Also, the average FWHM value across all Sulfo-EMCS terminated samples is 2.6 eV (± 0.2 eV), which is higher than the associated average FWHM for the PMMA (A and K) and NH_2-terminated PMMA sample sets (B and L). While multiple peaks cannot be deconvoluted, we can say that there is a greater variety of O1s chemical environments on the surface. This is consistent with multiple O1s signals that would result from a Sulfo-EMCS terminated PMMA surface: the imide, amide, ester, ether-type O1s photoelectron signal.

There are trends in the O1s related elemental ratios of the Sulfo-EMCS terminated PMMA surfaces compared to the previous modifications. The O/S ratio for this sample type will be discussed in the section on the S2p XPS spectra, while the O/C ratio has been previously discussed in Section 3.4.3. The reported O/N ratio for the optimized Sulfo-EMCS surface is 11.22 (± 12%). The O/N ratio is a decrease from the value of 12.11 sample set B (1 min NH_2-terminated PMMA), and it continues a downward trend from A→B→C for the ratio in same Table. This trend is not consistent with a surface that is relatively rich in oxygen from the PMMA layers and the additional carbonyl groups after the addition of Sulfo-EMCS. One reason for this trend is the increased N1s signal intensity, since each modification to PMMA layer adds an increased nitrogen component, such as the amines and amides within the NH_2-terminated PMMA surface and the amides and imides of the Sulfo-EMCS terminated PMMA surface. This would increase the N1s signal relative to the O1s signal and reduce the O/N ratio as seen here. The second reason is that O1s signal from the oxygen-rich PMMA layer will be attenuated by ~ 35 – 40% (assuming an O1s EAL of 2.0 nm) as it travels from a depth of 1.71 nm within the surface to the top of the surface at 2.62 nm, as presented in Table 3.1.

3.5.4 TmGH1-terminated PMMA

The O1s spectra of a representative TmGH1-terminated PMMA surface is shown in Figure 3.2 (spectra D) and the related data is part of sample set D in Tables 3.2, 3.3 and 3.4. The spectra shows a single O1s peak with an average binding energy of 531.9

eV (± 0.2 eV) and an average FWHM of 2.48 eV (± 0.2 eV), as respectively reported in Table 3.2 and 4.

Compared to sample set C, there is a chemical shift of 0.2 eV to lower binding energy for the sample set representing TmGH1 samples (D) in Table 3.2. This shift is within experimental error. However, it should be noted that there was a chemical shift of similar magnitude for the O1s peak 1 when comparing samples sets B→C. It was stated then that a small shift to lower binding energy of peak 1 was not indicative of surface modification. In this case, we see a continuing trend of decreasing binding energy from A→B→C, which suggests that the addition of more complex molecules has a non-random effect on the observed O1s spectra. When Sulfo-EMCS, and particularly a protein like TmGH1 is added to the surface, one introduces a greater variety of O1s chemical environments. In the case of modifying PMMA surfaces, the prominence of ester-type O1s signal decreases, since the majority of carbonyl groups in a protein are amide linkages; amides O1s photoelectrons have a lower binding energy than ester O1s photoelectrons. Also, the binding energy could be depressed by the presence of ionic oxygen within carboxylic acid groups (i.e. $R\text{-}COO^-$), where photoelectrons would be ejected with greater kinetic energy due to electrostatic repulsion and higher energy core states. After considering these influences, it seems natural to expect a lower binding energy for surfaces that not only attenuate the underlying ester O1s signal, but also on account of the variety of chemical environments that exist after modification with a protein, such as TmGH1.

Confirmation of a greater variety of O1s chemical environments could be made by observing the trends in the FWHM data in Table 3.3. The average FWHM value for sample set D for TmGH1-terminated surfaces is 2.48 eV (± 0.2 eV). This value is not significantly different from the average FWHM of the Sulfo-EMCS terminated surfaces (2.56 eV (± 0.2 eV) from sample sets M,C,N,O,P). However, the above value is among the higher FWHM values and is certainly larger than the average FWHM of sample sets A/K (PMMA) and the average of sets B and L (NH_2-terminated surfaces) in Table 3.3. This larger FWHM value for sample set D is indicative of a wider variety of oxygen oxidation states on the surface as evidenced by the binding energy data.

The O/N ratio for the TmGH1-terminated PMMA samples are shown in Table 3.4 as sample set D. The O/S ratio will be discussed in Section 3.7, while the O/C ratio has been discussed previously (Section 3.5.4). The reported O/N ratio is 2.51 (± 0.2 eV), which is among the lower values observed, and certainly the lowest for the optimized surface modification progression K→B→C→D. This O/N ratio is also consistent with those reported for other proteins absorbed onto substrates.[83] The trend for the above mentioned progression is that of a decreasing O/N value. This is consistent with a surface that is increasing its nitrogen content relative to its oxygen content as discussed further in section 3.6.4 (N1s spectra). In terms of the O1s signal, it is believed that the results are partially caused by an attenuation of the O1s signal from the underlying PMMA and other layers due to the addition of a relatively thick layer of proteins (see section 3.1 for thickness details).

3.5.5 phnH-terminated PMMA

As previously mentioned in Section 3.4.5, the phnH XPS results were harder to interpret. Spectrum E in Figure 3.2 is representative of all the phnH-terminated PMMA samples. A single broad peak with an average binding energy 531.8 eV (± 0.2 eV)and having an average FWHM of ~2.4 eV when considering both sample sets Q and E in Tables 3.2 and 3.3. The binding energy value is among the lowest observed and it is comparable to the O1s binding energy of TmGH1 samples (sample set D). The wide variety of O1s chemical environments within proteins or related surfaces (as indicated by the large FWHM value) and the attenuation of underlying O1s signal due to an overlayer would decrease the binding energy relative to other samples, especially those relatively rich in ester functionalities (i.e. PMMA). The overall shape and position of the spectra is consistent with expectation for this type of sample.

The O/N and O/C ratios for the phnH-terminated sample indicate that the phnH surfaces, regardless of their actual condition are more similar to TmGH1-terminated surfaces than other examples studied here. The reported O/N ratios for sample sets Q and E are within the range of O/N values occupied by the protein samples (sets D, Q, E, F, G, H1, H2). As well, the trend of decreasing O/N ratio for the samples representative of the optimized procedure (K→B→C→E) is similar to that described for the TmGH1-terminated proteins. A sequential addition of nitrogen added to the surface and an attenuation of ester O1s signal due to a protein-like overlayer would contribute to a decreasing O/N ratio.

The overall O/C ratio averages in Table 3.4 are not consistent with the expected protein layer formed. The O/C ratio for sample sets Q and E are 0.35 (± 12%) and 0.45 (± 12%) respectively (sample sets Q and E, in Table 3.4). The O/C trend between the two samples is consistent with one being exposed to a higher protein concentration than the other (i.e. Q < E) since a higher concentration solution would deposit more carbon bulk that one with a lower concentration. However, the O/C ratio for both sample sets is lower than the reported value for TmGH1-terminated PMMA samples (0.57 (± 12%), sample set D), which is not consistent with the fact that phnH is twice as small as TmGH1. There is limited evidence for a proper phnH-terminated surface based on the analysis of the O1s spectral data.

3.6 XPS N1s Spectra

The N1s spectral region is helpful to the characterization of the modified-PMMA surfaces. Aside from unmodified-PMMA or Au, all the samples contain nitrogen and in varying amounts, which can be quantified. Representative N1s spectra of samples are shown in Figure 3.3 and the related binding energy and FWHM values can be found in 3 and 4. The values of the O/N and C/N ratios will be discussed in terms of the N1s signal and they are found in Table 3.4. The spectra in Figure 3.3 can generally be interpreted using data from XPS studies of PMMA surfaces modified by N_2 plasma.[28]

3.6.1 PMMA

There is no nitrogen within the monomer unit of PMMA. There is a very small N1s signal is recorded for the PMMA samples belonging to sample set A in Figure 3.3 (spectrum A). This spectrum has been deconvoluted by a single broad peak with binding energy of 399.8 eV (± 0.2 eV) and FWHM of 2.62 eV (± 0.2 eV). The binding energy value is certainly in the region of ~400 eV, which is expected for a peak representing bulk nitrogen. This bulk nitrogen could not have arised from the thin-layer of PMMA on the samples, but instead must be the result of surface contamination. There is also an N1s spectra recorded for unmodified-Au, which is tabulated in Table 3.2 (sample set I) and it has a binding energy of 400.2 eV (± 0.2 eV). It is likely that the N1s peak recorded for the PMMA samples arises due to contamination of the underlying Au layer.

The O/N and C/N ratios for sample set A in Table 3.4 will be analyzed to isolate the origin and magnitude of the N1s signal for PMMA. The N/S ratio will be analyzed in the section on the S2p XPS spectra. The O/N and C/N ratios are respectively 15.12 (± 12%) and 32.46 (± 12%) for sample set A and 4.19 (± 12%) and 19.99 (± 12%) for sample set I (unmodified Au). A priori, the O/N and C/N ratios for sample set K are the highest of all the sample types. Also, the O/N ratio from I → K increases and the C/N ratio increases from I → K. What this suggests is that the amount of nitrogen on the surface of PMMA samples is negligible and in fact seems to be less nitrogen than even the unmodified-Au samples. Not only is no nitrogen added to the surface of Au during the PMMA spin-coating process, but the N1s signal is attenuated by the PMMA overlayer. This result establishes that the N1s signal from Au contamination will not significantly affect the N1s components of the other ratios.

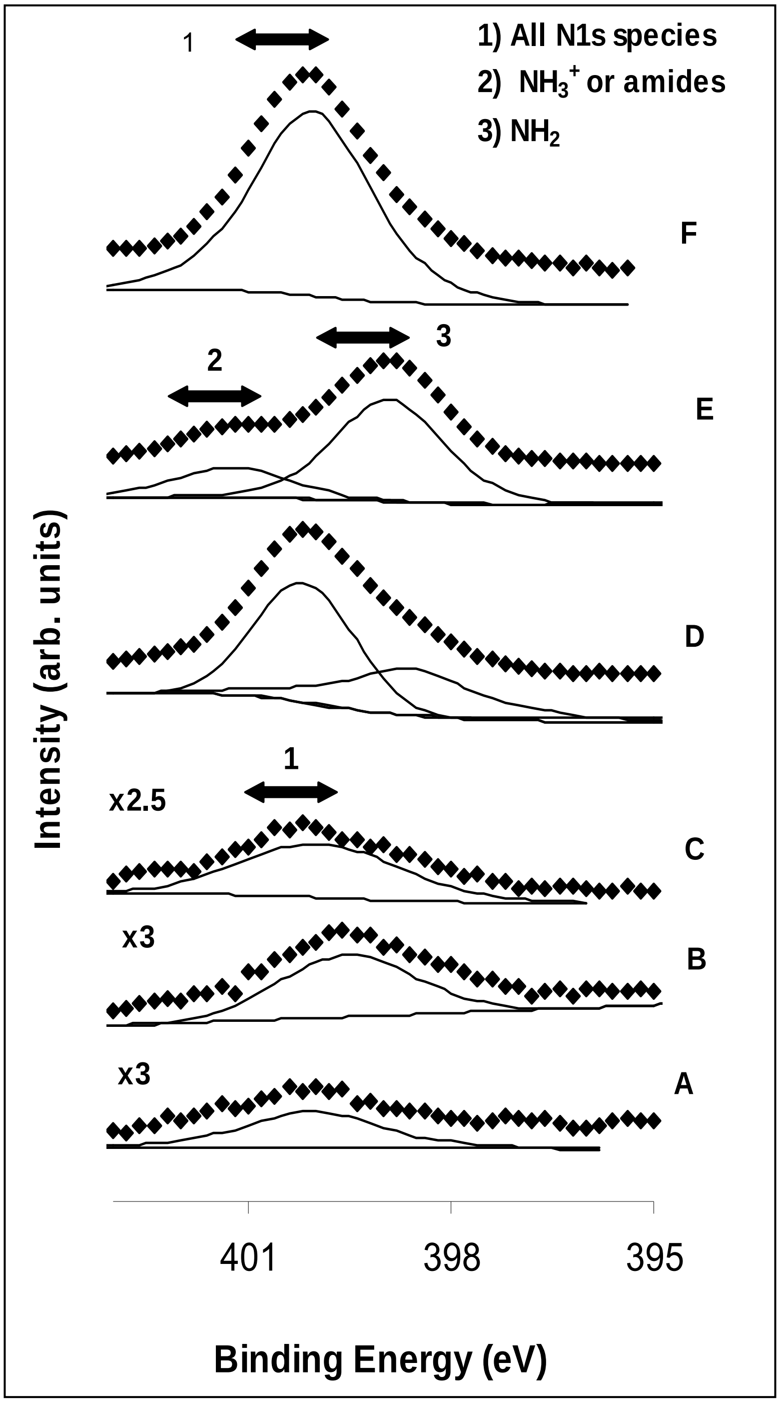
1
1) All N1s species
2) NH_3^+ or amides
3) NH_2
F
2
3
E
D
1
x2.5
C
x3
B
x3
A
Intensity (arb. units)
401
398
395
Binding Energy (eV)

Figure 3.3: N1s XPS spectra of samples representative of various surface modifications. The surfaces studied are as follows: PMMA (A) Aminated PMMA (B) 1mM Sulfo-EMCS (C) TmGH1 on Sulfo-EMCS modified PMMA (D) phnH on Sulfo-EMCS modified PMMA (E) TmGH1 directy on Au (F)

3.6.2 NH_2-terminated PMMA

The first modification to PMMA was exposure to ethylenediamine to create a surface of primary amines as shown schematically in Figure 2.1 (B). Two nitrogen atoms are added to the surface following the removal of the methoxy-group, thus creating an amide bond to the underlying PMMA and primary amine units at the surface. The addition of nitrogen to the surface changes the nature of the N1s spectra in a characteristic manner. In Figure 3.3, spectrum B represents a typical N1s signal for an NH_2-terminated PMMA surface. A single broad peak was resolved from the signal at an average binding energy of 399.8 eV (± 0.2 eV) for sample set B, which represents a 1 minute exposure to ethylenediamine. The binding energy of the N1s peak for sample set L (10 minute exposure) is within error of the binding energy reported for sample set B. These binding energies are consistent with other literature examples of PMMA terminated with primary amines and other N chemical environments (~400 eV).[24, 28]

In principle, there are two chemical environments for nitrogen on the aminated PMMA sample, as shown schematically in Figure 2.1 (B) - an amide and an amine group, but only one peak was resolved. Published values for the amine are 398.3 – 398.6 eV [27, 42] and for the amide 400.1 eV.[27, 42] As the amide lies at a lower energy level, it is likely that the signal from the amide is attenuated compared to the amine, and the two are not well resolved. The observed signal at 399.8 eV is midway between these two values. The resultant signal seems to have some contribution from both of the N1s oxidation states.

Protonated amine groups ($-NH_3^+$) at ~402 eV binding energy have also been reported in the literature. The observed average FWHM for the single N1s peak for this sample type of 2.65 eV (± 0.2 eV) and relatively higher binding energy suggests that this peak may contain contribution from the protonated amine N1s signal, along with the amide and amine contributions. In general the FWHM values for all the sample sets in Table 3.3 are larger than the 1.5 – 2.0 eV range presumably because they contain signal from all the above N1s chemical environments. Deconvolution of the spectra however was no found to be statistically significant. In any case, the main objective in acquiring the N1s spectra is to find the peak intensity of the entire region, not the intensities individual chemical environments, as was the case for the C1s spectrum.

The O/N and C/N ratios are most relevant to the above discussion. The addition of nitrogen to the surface should decrease both the O/N and C/N ratios compared to those for the PMMA samples. In Table 3.4 we indeed see evidence of this expectation: the O/N ratio has decreased from 15.12 (± 12%) to 12.11 (± 12%) and the C/N ratio has decreased from 32.46 (± 12%) to 22.57 (± 12%) when comparing sample sets K → B. Regardless of the dynamics of the O1s and C1s intensities, the simple fact that more nitrogen is added to the surface is reflected in these trends. This is indicative of a change from an ester-terminated surface to an amine-terminated surface.

Part of the goal of this thesis was to find an optimal method of making the protein terminated surfaces. One option was to increase the number of absorption sites for Sulfo-EMCS on an aminated surface by increasing the time that PMMA was exposed to the ethylenediamine solution. Data for a 10 minute exposure is shown for sample L in Tables 3.3, 3.2 and 3.4. The main change after this exposure was that the FWHM of the N1s peak was reduced to 1.18 eV (± 0.2 eV), which is smaller than the value previously stated for sample set B. Moreover, when you contrast sample set B with sample L in Table 3.4, the trends between all the ratios (N/S, O/N and C/N) are indicative of an increased nitrogen component at the surface. These results demonstrated that a longer exposure should be tried, but there was evidence of increased charging and visual degradation of the sample; the former most likely due to protonated amine groups and the latter due to sample/solvent effects.

3.6.3 Sulfo-EMCS terminated PMMA

The N1s region of the XPS spectrum is particularly useful for characterizing a chemical change from an NH_2-terminated surface to a Sulfo-EMCS terminated surface. Spectrum C in Figure 3.3 is representative of a typical result belonging to sample set C in Tables 3.2, 3.3 and 3.4. Sample set C represents the optimized methodology to create the Sulfo-EMCS samples. The single peak in spectrum C has an average binding energy of 400.0 eV (± 0.2 eV). This represents a chemical shift to higher binding energies compared to the NH_2-terminated surfaces (B→C, ~ 0.3 eV). While this is within experimental error, this chemical shift was a clear feature of many of the different Sulfo-EMCS terminated samples as seen by comparing B → M, C, N, O, and P in Table 3.2. A shift to higher binding energies suggests that surface nitrogen is now in a higher oxidation state. The terminal maleimide group on the surface contains an imide functional group and the portion of the structure attached to the surface is an amide group. The nitrogen atoms within both of these functional groups are adjacent to electronegative carbonyl groups, which reduce the kinetic energy of ejected N1s photoelectrons. Thus a chemical shift to higher binding energies is a clear sign of successful chemical modification from an NH_2-terminated surface to a Sulfo-EMCS terminated surface.

Further evidence for this modification can be seen from the FWHM values. A comparison of the average FWHM between the NH_2-terminated surfaces (B and L) and the average of all the Sulfo-EMCS terminates surface (M, C, N, O, and P) demonstrate an increase of ~ 0.9 eV in the FWHM value. This suggests that a wider range of N1s chemical environments are present on Sulfo-EMCS terminated surfaces, as would be expected for a new surface that has a combination of amines, amides, imides and protonated amines present.

A successful modification from NH_2-terminated to Sulfo-EMCS terminated surfaces should result in a decrease in both the O/N and C/N ratios if one were to ignore any dynamic effects of the O1s and C1s signal. The reported O/N ratio for sample set C (Table 3.4) is 11.22 (± 12%) and for the C/N ratio is 14.08 (± 12%). Both of these values are lower than the preceding optimized surface modification (sample set B). This evidence, along with the binding energy shift and differences in the FWHM value further demonstrate that there has been a successful modification from NH_2-terminated surfaces to those terminated by Sulfo-EMCS.

3.6.4 TmGH1-terminated PMMA

A successful modification from a Sulfo-EMCS terminated surface to that terminated by TmGH1 would be expected to demonstrate an increased intensity of the C1s spectrum as well as demonstrate evidence of chemical environments that are typical of proteins (i.e. signal from amide bonds that are part of peptide units connecting protein amino acids). Initial observation of spectrum D in Figure 3.2 shows that the overall intensity of the N1s signal has increased dramatically from the representative signal of a Sulfo-EMCS terminated surface (spectrum C). This change of intensity will be quantified later when examining the O/N and C/N ratios. Two peaks are resolvable in spectrum D, which is also a change from previous spectra. The binding energy of the peak assigned to N1s signal from higher oxidation states is 400.1 eV (± 0.2 eV) (D, peak 2, Table 3.3). These oxidation states include amide, imide, N-O and NH_3^+, N1s photoelectron signal. The binding energy of the lower intensity peak assigned to N1s signal from lower oxidation states, particularly amine nitrogen, is 398.5 eV (± 0.2 eV).

It should be noted that this deconvolution scheme is consistent with the earlier suggestions that amides and amines contribute to the overall signal of spectrum A, B or C. The binding energies of the single peaks for these samples lie roughly between the binding energies of the two deconvoluted peaks that have been identified in this section. As well, the FWHM values for the two deconvoluted peaks (sample set D, Table 3.3) are clearly lower than those reported for the broad single peak of sample sets K, B, and C, for example. This too indicates that the earlier assignments are a combination of the obvious deconvolution scheme presented here.

A TmGH1 terminated surface is expected to contain the largest amount of nitrogen of all the surface modifications discussed thus far; this would be evidenced by large decreases in the O/N and C/N ratios. We can see in Table 3.4 that the transition between C→D lowers the O/N ratio from 11.22 (± 12%) to 2.51 (± 12%) and for the C/N lowers the ratio from 14.08 (± 12%) to 4.41 (± 12%). First, the expected decreasing trend is seen, which supports the large deposition of nitrogen, which is an important constituent of the amino acids within TmGH1. These changes in the O/N and C/N ratio are also the largest changes of all the modifications thus far. Unfortunately, the N1s XPS data are limited in that they cannot provide evidence for a covalent bond between TmGH1 and the maleimide group of Sulfo-EMCS terminated surfaces, only that the protein is adsorbed on the surface.

3.6.5 phnH-terminated PMMA

The N1s region of the spectrum of phnH-terminated PMMA is different from the TmGH1-terminated PMMA surface. The N1s spectra of the other two samples, E2 and Q are represented in Figure 3.3 as spectrum E. At first glance, it is clear that the intensity of the 3 in spectrum E is higher than that of the same peak in the spectrum representing TmGH1 (D). The N1s signal from amine-type chemical environments is higher for the phnH-terminated samples than the TmGH1-terminated samples. Also, the peak intensity for the amide-type peak (2, Figure 3.3) is lower than that for spectrum D; in essence, it seems that the spectral signal has ‘reversed’ when comparing spectra D to E. The deconvolution scheme for spectrum E does not seem to represent a protein-type environment with strong signal from the amide linkages between amino-acids. This is the strongest evidence presented for the denaturing of the phnH protein on the surface of PMMA and it would further explain the lack of reproducibility among the phnH sample data. The evidence for protein denaturing is not as strong for sample E1 (from sample set E), which is characterized by a broad single peak and other spectral regions, such as the previously mentioned C1s region and the S2p region, do not show strong evidence for total protein denaturing. Regardless, it seems that protein-terminated surfaces are being damaged or denatured either by preparation methods or by the X-ray source; the latter is a particular problem for known organic substrates.[84]

3.7 XPS S2p Spectra

The S2p region was analyzed, due to its importance in determining the level of solvent (DMSO) and chemical contamination (residue from the Sulfo-EMCS aminolysis reaction) on the surface. It also gives evidence of the orientation of the proteins on the surface and suggests whether there is a covalent bond between the protein and the cross-linker. An overlay of S2p XPS spectra of representative samples can be seen in Figure 3.4; peak binding energy and FWHM can be seen in Tables 3.2 and 3.3; elemental ratios can be found in Table 3.4.

In Figure 3.4, we can see that there are two S2p peak assignments: sulfide (~162.2 eV) and sulfate (~167-169 eV), both of which are consistent with known literature values.[41] The sulfide signal in the spectra of PMMA and NH_2-terminated PMMA presumably arise from sulfur contamination within the underlying gold substrate. The solvent used to help chemisorb ethylenediamine onto the surface was DMSO. It is possible that a contribution from the sulfur in DMSO also contributes to the peak intensity, although the sulfur in DMSO is primarily in a sulfate-like environment ($CH_3OSO_2OCH_3$). At least the lack of evidence of a sulfate peak in the S2p region of the Aminated PMMA spectra suggests that the cleaning regime and placement in a vacuum oven was sufficient to reduce DMSO contamination of the samples. The introduction of a sulfate peak in the spectra of Sulfo-EMCS terminated PMMA (spectrum C) arises from unreacted Sulfo-EMCS or the SO_3^- leaving group that helps facilitate the aminolysis reaction that binds Sulfo-EMCS to an amine group on the previously modified surface. The sulfate S2p peak was expected to be minimized or even eliminated after a number of sample cleansing steps (using buffers), an overnight vacuum oven treatment, the XPS chamber vacuum conditions, or through attenuation after the addition of proteins onto the surface. Instead, the sulfate peak is still present, and at an increased intensity, in the spectra of the protein-terminated PMMA samples (D and E) – particularly phnH (E). The continued existence of the sulfate peak is attributed to the oxidation of various sulfur containing groups present within any protein, such as those of the cysteine and methionine amino acid units. Also, the strong S2p signal of phnH (spectrum E) is indicative of the protein orientation on the surface, which will be discussed later.

The covalent bond created from the maleimide group on Sulfo-EMCS and a thiol-terminated protein was expected to be evident as a sulfide signal in the TmGH1 terminated PMMA and phnH-terminated PMMA S2p spectra in Figure 3.4 (D and E). Instead, no evidence for sulfide is present in the S2p spectra of these protein coated surfaces. This result can be explained by first considering that the escape depth of a photoelectron of sulfur is 3.3 nm (for alkanethiols) and that the dimensions of TmGH1, or related proteins, is on the order of 7.0 nm by 4.7 nm by 2.0 nm.[101]; the dimensions of phnH are roughly twice the abovementioned values.[78] Regardless of protein orientation, the S2p signal from sulfide buried within or under these proteins should be attenuated to 0.13 of the initial value ($e^{-2} = 0.13$) This is most evident when comparing the sulfur

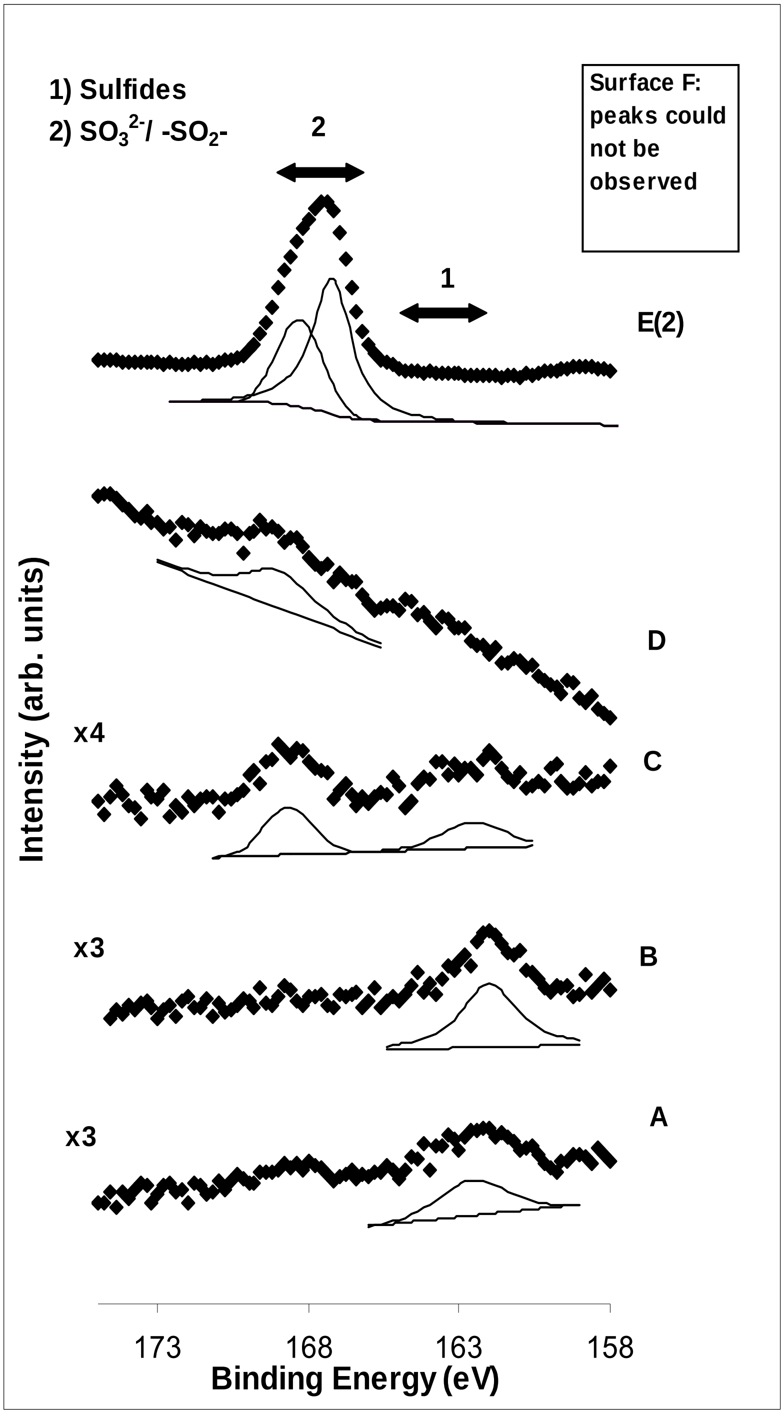

Figure 3.4: S2p XPS spectra of samples representative of various surface modifications. The surfaces studied are as follows: PMMA (A) Aminated PMMA (B) 1mM Sulfo-EMCS (C) TmGH1 on Sulfo-EMCS modified PMMA (D) phnH on Sulfo-EMCS modified PMMA (E) TmGH1 directy on Au (F)

related ratios between sample sets D and E in Table 3.4. TmGH1 has one terminal cysteine group, while phnH has two terminal cysteine groups.

If sulfur is present at the surface, then a lower x/S ratio (E) would be expected, since the sulfur is not attenuated under the bulk of the protein. The protein, phnH, does show a higher overall S2p signal, consistent with at least one of its two cysteine groups being oriented towards the surface. The strong and well resolved S2p signal at 168 eV for phnH (spectrum E, Figure 3.4) supports the above explanation. This peak is considered to be the result of either sulfate, sulfonate or sulfinate signal, but it is probably the first two since the binding energy of the S2p peak is consistent with a +6 oxidation state. This peak is deconvoluted into two peaks: one from the S2p$_{1/2}$ signal; the other from the S2p$_{3/2}$ signal, as expected for high intensity resolved sulfur S2p spectra.[42, 85] The fact that the intensity of this peak is at least four times larger than the corresponding peak from the TmGH1-terminated PMMA spectrum (D) suggests that this peak represents a surface oxidation (sulfide → sulfate or sulfonate) of the terminal cysteine group after removal from the buffer conditions of the initial reaction and exposure to air for a small length of time. At the same time, the lack of sulfide signal in the S2p spectra of both proteins is indirect evidence for a terminal sulfur to be oriented towards the substrate. The analysis of the S2p signal of the proteins must be combined with other evidence in order to fully elucidate the nature of the chemical bond between TmGH1 and the surface. These XPS results only confirm the orientation of the proteins on the surface, with one of the cysteine groups pointed towards the surface.

Previous discussion regarding the other XPS regions served as evidence for protein denaturing occurring for at least two of three phnH-related samples. This might be used as an argument to question the above discussion of the S2p spectra. However, there is at least one phnH-related sample, that certainly confirms the discussion above without being labeled as a denatured sample – this sample is E1 from sample set E. The spectrum of E1 has a single S2p peak at 168.1 eV (±0.2 eV) that cannot be reasonably deconvoluted into two distinct S2p peaks. This is consistent with the TmGH1 S2p spectra presented above. Also, the C/S, N/S, and O/S values are in between those of a denatured sample (E2) and TmGH1-terminated samples (compare E1 to E2 – E1 to D). We could consider the 'denatured' samples to have a higher concentration of sulfur on the surface due to random orientation of the terminal cysteine groups on the surface due to chemisorption. In the case of sample E1, the values of the sulfur related ratios are stronger evidence for a more ordered arrangement of protein on the surface. The ratios are smaller than TmGH1-terminated surfaces due to the smaller size of the phnH protein and because there is more, non-attenuated S2p signal from a surface-oriented cysteine group. In addition, the fact that the sulfur ratios are larger for E1 than E2 could mean that some of the S2p signal is attenuated due to at least on of the cysteine groups being oriented towards the surface, as explained above.

3.8 Carbon Composition of Surfaces

Table 3.5 shows the percent composition of the C1s spectra for a variety of samples, where the percentages are defined by:

$$\% \, C1s \; peak \, area = \frac{Normalized \; Peak \; Area}{Sum \, of \; Normalized \; C1s \; Peak \; Areas} \qquad (15)$$

The values are reported as averages in most cases with the associated standard deviations. These percentage values give a rough indication of surface composition and carbon chemical environments within each modified surface. Analysis of this data will further confirm successful modification for the optimized procedure.

PMMA (sample set A) shows an average distribution of C1s environments of 74% (± 8%) for bulk carbon, 16% (± 8%) for ether-type carbons, and 11% (± 2%) for ester-type carbons. This seems consistent with surface with roughly equal numbers of carbonyl and methoxy-carbon chemical environments and of course, the carbon skeleton of PMMA comprises the bulk of the C1s signal in this region. After exposure to ethylenediamine solution for 1 or 10 minutes, the bulk carbon percentage is reduced by ~ 8% (± 8%) in the former case and ~ 5 % (± 8%) in the latter. There is a corresponding increase in the peak two C1s signal of ~7% (± 8%) after 1 minute exposure and 5%(± 8%) after 10 minute exposure to the ethylenediamine solution. This is consistent with the removal of methoxy groups and the attenuation of underlying C1s signal. There is no statistically significant change in the percentage of peak 3, representing amide and ester carbon environments, between PMMA samples and amine-terminated samples. This is expected since the PMMA ester groups have converted to amide groups, which does not result in the loss of carbonyl functional groups.

In general, the exposure of aminated samples to Sulfo-EMCS/buffer solution does not dramatically change the percent composition of the bulk C1s peak or even that of peak 2 (C-O/C-N). However, there is a slight increase (3-4% on average for M, C, N, O, and P) in the amount of carbonyl signal in the C1s region, which could be attributed to the C1s signal from the surface-oriented imide groups of the Sulfo-EMCS terminated samples. More interesting trends can be found within the set of tabulated samples that represent Sulfo-EMCS terminated surfaces (M, C, N, O, and P) in Table 3.5. Sulfo-EMCS terminated PMMA surfaces made from samples that were exposed to ethylenediamine/DMSO solutions for 10 minutes (sample sets O and P) resulted in higher carbonyl signal. The values of 15% (± 2%) (sample O) and 22% (± 2%) (sample P) reported for the carbonyl peak contribution to the C1s signal is also higher than those for the corresponding peak of the aminated samples (B and L). This means that this higher signal is indicative of a higher surface density of terminal maleimide groups, rather than from underlying amide moieties. Maximizing the number of terminal maleimide groups is ideal, but it has been mentioned that increased exposure time to the ethylenediamine solution degrades the samples, thus it was not used in the optimized procedure discussed in this thesis. The optimized procedure for making Sulfo-EMCS terminated PMMA samples was determined to be that of sample C. While the method to make C did not increase the carbonyl signal significantly (only an additional 1 - 2% compared to B and L), it did increase the C-N signal (peak 2) to a level comparable to sample set P. Moreover, the bulk carbon signal for sample set C is closer to the value for sample set P than any of the other Sulfo-EMCS terminated PMMA samples. Washing the aminated surfaces with 1 M NaOH did not change the distribution of C1s signal in a substantial manner, as evident by comparing sample set C with N in Table 3.5.

The exposure of the Sulfo-EMCS terminated PMMA samples to TmGH1/buffer solution further changes the distribution of the C1s signal. The bulk carbon signal increases by an average of 11% when compared to samples M, C, N, O and P and this is consistent with the addition of a large, carbon-rich protein to the surfaces. The C-N/C-O peak signal decreases by an average of 7% and the carbonyl contribution to the C1s signal decreases by an average of 4%, when compared to the C1s signal of the Sulfo-EMCS terminated samples. These trends are consistent with a change from a surface containing a relatively high proportion of imide, amide and ester signal, to a surface with a wider variety of carbon chemical environments. A vast majority of the signal would be expected to arise from the carbon backbone of a protein on the surface. The data in Table 3.5 shows that the surfaces are being modified in the expected manner and they also support some of the choices made for optimizing the procedure.

3.9 Evidence for a Covalent Bond between TmGH1 and modified-PMMA

One of the goals of this thesis is to characterize TmGH1-terminated surfaces that have a covalent bond between the modified PMMA surface and TmGH1 itself. Most of the evidence presented in previous sections supports the assertion that TmGH1 is being absorbed onto modified-PMMA surfaces. The S2p region provided evidence for the orientation of the cysteine group of TmGH1 towards the modified-PMMA surface, which would be expected if it were covalently attached. Hotchkiss *et al.* recommended a procedure for determining whether a biological molecule was actually covalently attached to a surface.[12] He suggested that the all surfaces that lead to an optimized and modified surface for the attachment of proteins should be exposed to the protein. This experiment should provide some evidence to distinguish a chemisorbed protein surface from that in which the protein has physisorbed to the surface. It should be noted that the concentration of the TmGH1 solutions for samples F, G, and H in Table 3.4 are currently unknown, but that they are higher than 3.73 μM, which was used to form the samples in set D. At the end of this section a comment will be made about errors associated with this discussion.

Unmodified Au was the first surface that was exposed to TmGH1. A terminal cysteine group would have a free thiol group that should covalently bond with Au, as reported elsewhere for *L*-cysteine.[86] Spectrum F in Figure 3.1 is similar to spectrum D, representing TmGH1-terminated PMMA, but with some differences. The deconvoluted peaks in spectrum F have smaller FWHM in Table 3.3 when compared to TmGH1-terminated PMMA (compare sample set D to F), thus spectrum F is better resolved. The higher resolution represents the difference between Au surfaces exposed to TmGH1 versus a surface where TmGH1 has been deposited on top of modified layers containing organic compounds. The N1s spectrum for TmGH1-terminated Au is shown as spectrum F in Figure 3.3. Only one peak could be resolved from this spectrum, but the binding energy of this peak and the general signal envelope is more consistent with spectrum D (TmGH1-terminated PMMA) than spectrum E (‘denatured’ phnH-terminated PMMA). The S2p peaks for the TmGH1-terminated Au sample could not be resolved. This result is consistent with the terminal cysteine oriented towards the surface and possibly covalently attached to substrate as discussed in the previous section. The peak area ratios (O/N, O/C, C/N) for the TmGH1-terminated Au samples are shown in Table 3.4 (sample set F). The values for sample set F are on the order of those for sample set D, which represents TmGH1-terminated PMMA. The values are lower for sample set F, when compared to D, which is attributed to the lack of underlying organic layers in the former sample. While the Au surface may be covered with TmGH1, it does not seem that it is covered to the same extent as the TmGH1-terminated PMMA samples. In Table 3.1, the average thickness of an Au sample exposed to TmGH1 is reported to be 4.54 nm (± 0.2 nm), which is lower than that reported for a TmGH1-terminated PMMA sample. However this value is consistent with the addition of TmGH1, which was expected to add ~3.7 nm to the surface (6.32 nm – 2.62 nm = 3.7 nm). There is no evidence of S2p signal, which indicates that the terminal cysteine group of TmGH1 is oriented towards the surface. The above evidence suggests that covalently bonded TmGH1 surfaces are possible with Au and the evidence supports the arguments for a TmGH1-terminated PMMA surface as presented elsewhere in this thesis.

The PMMA surfaces were exposed to TmGH1 as well and the evidence suggests that the surface is not well covered with TmGH1 protein. The thickness of this particular substrate, which is reported to be 2.89 nm (1 sample only) is the lowest of all the TmGH1 related surfaces ("TmGH1 directly on PMMA", Table 3.1), despite the higher concentration of TmGH1/buffer solution used. The addition of TmGH1 in this case only increased sample thickness by ~1.2 nm (2.89 nm -1.61 nm = 1.28 nm) and not the ~3.7 nm expected, as explained previously. It is also notable that the TmGH1 on PMMA sample has one of the highest charging shifts for the Au $4f_{7/2}$ and C1s peaks. Moreover, this charging effect is also higher than the TmGH1 on Au sample, which indicates that the protein surface concentration has been reduced. The O/N, O/C, and C/N ratios for sample set G in Table 3.4 are among the lowest values of all the samples, which suggests that TmGH1 on PMMA has more protein character than PMMA character; TmGH1 is adsorbing onto PMMA. The S2p related ratios in Table 3.4 is higher than that for sample set F and lower than that for sample set D. In this case, a lower sulfur signal indicates that more S2p signal is reaching the detector; this could be indicative of TmGH1 cysteine groups oriented away from the surface. It is difficult to quantify the amount of TmGH1 on the surface based on these ratios, but using a unique element, such as selenium on the proteins would help solve this XPS issue. TmGH1 is certainly adsorbed on PMMA, but not with the same characteristics or quantities as on Au or Sulfo-EMCS terminated samples.

TmGH1 was also exposed to a NH_2-terminated sample to determine the extent to which it adsorbed. The thickness of this new sample was observed to be 4.95 nm (± 0.36), which represents ~3.2 nm increase in surface thickness when compared to the average thickness of NH_2-terminated samples. An approximately 3.7 nm increase was expected (as explained above), so this suggests that there is an increase of TmGH1 attached to the surface; this is especially true when comparing TmGH1 on NH_2-terminated samples with those that have TmGH1 directly on PMMA. This is supported by evidence in Table 3.4, where there is an increasing trend for the O/N, O/C and C/N ratios for samples F→G→H. TmGH1 is attracted to amine terminated surfaces.

The nature of this attachment is important, since TmGH1 cannot bind to an NH_2 terminated surface through a sulfide bond. This is evidenced by lower sulfur related ratios in Table 3.4, which indicate higher surface S2p signal and a general orientation of that terminal thiol away from the surface compared to 'TmGH1 on PMMA'. One potential model could be aminolysis reactions between the amine surface groups and carboxylic acids within the protein. However, the low temperatures, the buffer conditions and the poor leaving group ability of water does not make this a favorable reaction. An alternative model is one where a hydrophilic protein interacts with a charged surface; in this case, a surface of NH_3^+ molecules in a buffer of ~pH 7.2. Adoption of the second model means that counter ions would be needed in solution to mitigate this surface charging effect on both the protein and the surface in order to isolate the presence of a covalent bond between protein and the surface. TmGH1 reacts differently to a NH_2-terminated surface than to a Sulfo-EMCS terminated surface.

The evidence presented in this section supports the notion that terminal cysteine-groups covalently bond to the maleimide group of the Sulfo-EMCS terminated surfaces. It was shown that TmGH1 reacts with Au, PMMA and NH_2-terminated PMMA samples in a different manner. There was protein adsorption onto all three samples, but Au and NH_2-terminated PMMA had a greater concentration of TmGH1 after exposure. While chemisorption of TmGH1 on all three surfaces is certainly a possibility, there was evidence for physisorption. In the Au case, the evidence supports a TmGH1 orientation where the terminal cysteine groups are close to the surface. The thiol end-groups of cysteine are known to bond well to Au and it is this reaction that facilitates much of protein/Au chemistry (i.e. AFM studies etc.).[86] In the case of NH_2-terminated surfaces, it seems that TmGH1 does not react through the cysteine group, but rather it seems that TmGH1 interacts with the positive surface charge of protonated amines.

Readers should be aware that there is another source of sulfur within the TmGH1 structure and that is the sulfur within a methionine amino acid group. At time of publication, the location of the methionine amino acids within the TmGH1 are not available, but it is sufficient to say that these amino acids would make a contribution to the signal of the S2p spectra. The extent of that contribution would be dependent on the attenuation of the S2p signal of these sulfur species; methionine units near the surface of TmGH1 would have a higher S2p signal than those located deeper within the protein.

This discussion does not outright prove a covalent bond between Sulfo-EMCS-terminated surfaces and TmGH1, but it certainly aids in the understanding of protein-substrate adsorption. The notion that there is a sulfide bond between maleimide and cysteine groups of TmGH1 has not been ruled out based on this evidence.

3.10 The Optimized Methodology

Before the optimized method was chosen, a number of different modifications to the general methodology to create the Sulfo-EMCS terminated surface were studied. Most of the discussion above focused on those samples that were part of the optimized procedure. There were also some explanations for the choices made throughout the above discussion. Here these choices and rationale will be summarized. The key goal of the methodology leading to TmGH1-terminated PMMA samples was to covalently attach TmGH1 to a modified PMMA substrate and to do so with a high enough concentration of TmGH1 to facilitate AFM studies. However, while the chemistry may be possible for many of the modifications, one has to consider the quality of the XPS spectra and the physical quality of the samples themselves.

The addition of PMMA to Au was unproblematic. The exposure of the PMMA samples to ethylenediamine presented a set of problems. First, DMSO is known to cause polymer swelling and it was observed that prolonged exposure to DMSO caused visible damage to the samples. Moreover, the XPS spectra of the aminated samples that were exposed for long times to the ethylenediamine/DMSO samples were harder to interpret than other spectra due to spurious XPS peaks. Both short and long exposure times to this solution caused clear changes to the surface composition of PMMA (see Section 3.4.2). The effects of changing exposure time to this solution can also be seen by comparing sample set N to P in Table 3.4; the higher values of the sulfur related ratios and the higher C/N ratio suggest that more Sulfo-EMCS has reacted with primary amines in the case of sample P. In addition, a higher surface composition of carbonyl groups is seen in Table 3.5 for sample P than N. Unfortunately, the spurious XPS peaks in the spectra of samples that were exposed for 10 minutes and physical degradation meant that this time frame was not chosen. As explained earlier, a 1 minute exposure to ethylenediamine causes PMMA to be successfully modified to later react with Sulfo-EMCS.

The solvent could have been changed to ethanol, but the reported SN_2 promoting effects of DMSO to an aminolysis reaction would be lost.[87] The reaction temperature was increased to 333K to promote an increased density of primary amines on NH_2-terminated surfaces. Also, surface contamination needed to be minimized in the S2p region of the XPS spectra of samples because it was thought that a weak sulfide signal would be indicative of a covalent bond between the cysteine groups of the proteins and the maleimide group. Sources of contamination include DMSO residues and sulfate contamination from Sulfo-EMCS after it reacts with the surfaces through aminolysis or hydrolysis. Such contamination was thought to be reduced by reducing the exposure time to Sulfo-EMCS from 4 hours to 2 hours (minimize chance of hydrolysis) and to ensure that samples were exposed to vacuum conditions at 333K. Not only would this promote aminolysis reactions (more amine to Sulfo EMCS reactions), but it would also help remove DMSO and sulfate contamination through evaporation or sublimation. Unfortunately, the change in temperature and the change in vacuum oven exposure were not tested independently. However, when comparing the peak area ratios between sample sets M and C in Table 3.4 we observe higher sulfur-related ratios (i.e. less sulfur) in the latter than the former. Also, we observe comparable values for the O/N, O/C and C/N ratios, despite the longer exposure time to Sulfo-EMCS/buffer solution in the case of sample set M. In Figure 3.4 we see that that spectrum C, representing a Sulfo-ECMS terminated PMMA sample, has the lowest S2p signal of all the spectra in that figure. The elevated temperatures for preparing the NH_2-terminated samples seem to have maintained the amount of deposited Sulfo-EMCS despite the reduced exposure time to that compound. The use of the vacuum oven and the decreased time of exposure to Sulfo-EMCS reduced the intensity of the S2p signal as expected.

Some of the NH_2-terminated samples were washed with 1M NaOH, in order to reduce the amount of NH_3^+ groups on the surface, thus increasing the number of primary amines available to react with Sulfo-EMCS. However, a comparison of sample set O and P in Table 3.4 suggests that washing by NaOH decreased the density of maleimide groups on Sulfo-EMCS terminated PMMA surfaces. The O/N, O/C and C/N ratios are all higher for sample set P than O; this is indicative of less additional nitrogen and carbon on the former surface, when it was expected to have more of both. The actual effects of the NaOH step can be explained by examining the results for sample set P and O in Table 3.5. It is clear from this table that the additional wash with NaOH changes the C1s distribution such that peak 2 (C-O/C-N) and peak 3 (C=O) have increased contribution to the total C1s signal. While NaOH could depronate NH_3^+ groups, it could also facilitate ester and amide hydrolysis. The exposure of a NH_2-terminated surface to NaOH could convert the amides attaching PMMA to ethylenediamine to carboxylic acids, which would be opposite to the intent of the surface modification scheme. To avoid this possibility that NaOH was not used. Regardless, the 1 minute exposure to ethylenediamine/DMSO solution should have minimized the number of NH_3^+ groups formed on the surfaces. The evidence discussed here explains Figure 2.1 in more detail, and it is important for understanding the rationale for the modifications presented in this thesis. The optimized procedure to form a TmGH1-terminated PMMA surface is represented by following the modifications from A→B→C→D in Table 3.4, as previously discussed.

Chapter 4
AFM Experimental and Theory

In this Chapter, the experimental procedure and theory involved with the two Scanning Probe Microscopy techniques used to obtain data for this thesis will be described. The atomic force microscopy and chemical force microscopy techniques will be the focus of this discussion, with a particular emphasis on their utility in collecting surface images and in protein unfolding experiments.

4.1 Atomic Force Microscopy

The atomic force microscopy was first developed in 1986 by Binning, Quante and Gerber.[88] It was invented to address the need to probe non-conducting surfaces, since this was not possible using the previously invented scanning tunneling microscopy (STM) technique. The AFM technique measures the deflection of a micrometer-scale cantilever tip caused by repulsive forces between the tip and the sample; this deflection is a direct measure of the forces involved in the experiment.

A schematic of an AFM apparatus is shown in Figure 4.1 and it has a number of key components: a micro-cantilever mounted tip, a piezoelectric motor, a photodiode detector, and a electric feedback mechanism for positioning the tip above the sample.[89] The sample stage and the vibration dampening box are not included in the figure, but are also important components of an AFM experiment. The micro-cantilever is made from Si or Si_3N_4 and it is pyramidal is shape with an ideal, mono-atomic end point directed towards a sample. There are different tips for contact-mode and tapping-mode experiments and as well there are tips that can be chemically modified; these will be described throughout the chapter. A reflective-coating is placed on the back of the tips to direct the laser light to the photo-diode so that deflection can be detected.

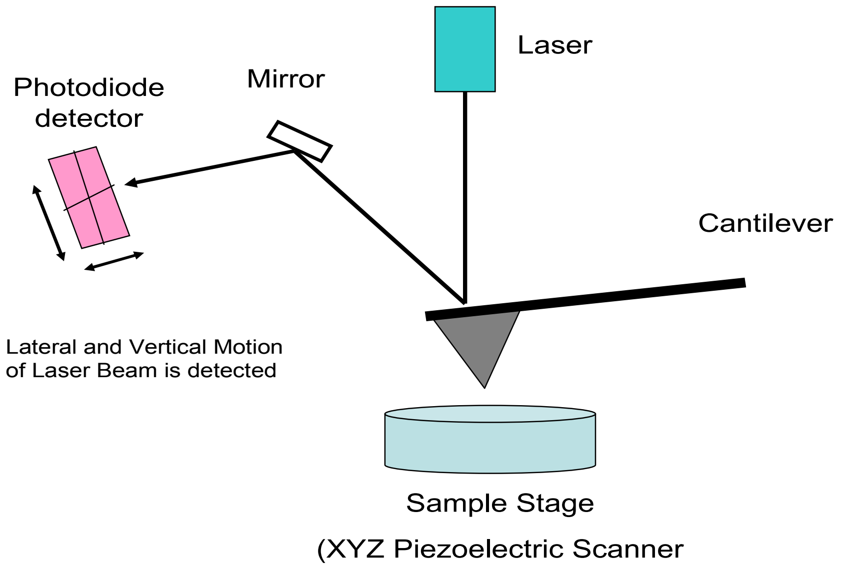

Figure 4.1: A diagram of an atomic force microscope.[89]

The basic operation of the AFM involves mounting the micro-cantilever tip and then shining a laser beam directly on the centre of the back of the tip. The laser light is then reflected towards the photodiode detector. The detector has four quadrants and it is positioned so that the reflection from the tip (signal) is both maximized and centered in the middle of the photodiode. Any change in the z direction represents a vertical movement of the tip and any change in the x-y direction represents a lateral movement of the tip. The deflection of the tip is then converted into a force by employing Hooke's Law. The force constant for most silicon-based cantilevers is about 0.01-100 N/m.[89] The AFM is sensitive to deflections that are ~ 0.01 nm, which means that forces on the order of $10^{-13} – 10^{-8}$ N can be detected at the limit of the AFM capabilities.

4.1.1 AFM: Modes of Operation

4.1.1.1 Contact Mode

In this mode of operation, the cantilever is brought into direct physical contact with the attractive forces at the surface. As the tip moves across the surface, the deflection of the tip towards or away from the surface relates to the changes in the topography. This can be converted into images of surface height and two-dimensional surface profiles. Contact-mode can also be used to perform force-distance microscopy on points of interest on the surface, to perform "pulling" experiments (force required to pull a surface feature is measured), or to perform a nano-indentation. The forces involved in contact-mode are too large for routine investigation of force-sensitive samples, such as biological or polymeric samples. In these cases, intermittent-mode (also , known as ‘tapping mode’) is a better method to use. In this thesis, contact mode AFM operation in liquid was used to obtain force-distance curves in order to measure the forces required to unfold the protein TmGH1.

4.1.1.2 Non Contact Mode

Non-contact AFM modes are used in situation where soft or intermittent contact with the surface is required, which is the case with most biological and polymeric samples. In this mode, the cantilever is oscillated at its resonance frequency (~50 to ~120 kHz) and is brought into intermittent contact with the surface. During the brief moment of contact, the vibrational amplitude of the oscillating tip is lowered; the magnitude of this change is a measure of the topography of the surface and it is used as part of the feedback mechanism of the apparatus.[89] The tip-sample interactions in this operation mode are reduced compared to the contact-mode AFM and its use prevents irreversible damage or physical changes to the surface morphology. The most useful set of images are those showing the ‘height’ of the surface, which is the change in the z-direction required for the piezoelectric motor to maintain a constant amplitude as the tip is scanned across the surface. While the results are not presented in this thesis, the phase-shift images were still useful in confirming the nature of scanned surfaces as the experiment was being conducted. The ‘phase-shift’ image is a record of the difference in phase angle of the source driving the oscillation motion of the tip and the tip response.[89] There are regions of the surface that have different mechanical properties and so the ‘phase-shift’ is a means of distinguishing these areas of the surface. An ‘amplitude’ image shows the amplitude changes as a tip is moved across a surface, and like the phase-shift image, it is a measure of mechanical tip-sample interactions. A feedback mechanism is used to collect data in a constant height or constant amplitude mode.

There are two methods used to drive the oscillation of the cantilever at its resonance frequency. The acoustic AC (AAC) mode of non-contact AFM uses an piezoelectric transducer to generate acoustical vibrations that oscillate the attached cantilever. The MAC mode uses an alternating current to change a magnetic field produced by a solenoid that is underneath the cantilever, which is coated with a magnetic layer.[89] While both methods are employed in non-contact AFM experiments, the MAC mode has a key advantage over the AAC mode. In the MAC mode, only the tip is magnetized, which consequently means that it is the only component that oscillates. The acoustical vibrations of the AAC mode can affect the movement of the rest of the AFM apparatus, as well as the sample. Since the tip is the only oscillation within the MAC mode background signal from AFM apparatus, sample or experimental medium (air or liquid) is reduced.

4.1.2 AFM Force Curves

The utility of the AFM is not limited to imaging only, but it is also used to probe the nature of tip-sample interactions. The measurement of forces between the tip and the sample can be used to characterize different surfaces and surface regions. As well, visualization of these forces as ‘force-distance curves’ can highlight the type, and the number, of tip-sample interactions. In the case of protein unfolding experiments, one is looking for specific tip-sample interactions of a particular magnitude, which shows more than one tip-sample deflection regime. All of this information can be obtained through careful analysis of the force-distance curves (see section 5.2)

There are many different types of forces that cause a deflection of the cantilever tip and they exert an influence on this deflection depending on the tip-sample distance. Long range forces, such as electrostatic attraction and repulsion, electrical double layers, and Van der Waals forces occur in the region of 10 -100 nm away from the surface.[89] Short range forces include hydrogen bonding, contact forces and induced solvent ordering, and these forces occur in the region of 5 – 0.1 nm away from the surface. As well, there are specific and non-specific force interactions: a non-specific tip-sample interaction has the shape of a broad force curve and it is the result of multiple tip-sample interactions (different molecules and different force types); a specific tip-sample interaction is apparent when the force curve has a single or multiple sharp features within its shape, which are characteristic of interactions with single molecules or single force types.[34]

Most AFM analysis is conducted using force – distance curves like those shown in Figure 4.2. In order to create these curves, the initial data (deflection – distance curves) must be converted into force data. This is done by using the following equation:

$$F = k_{cl}\Delta D \qquad (16)$$

where F is the measured force, k_{cl} is the spring constant of the free cantilever and ΔD is the deflection of the cantilever from its rest position.[89] The approach and retraction curves are shown in Figure 4.2. and they have been separated to aid in the explanation of the various tip-sample contact regimes throughout a single approach and retract cycle.

At first, the tip is in a non-contact regime at the start of an approach-retract cycle and the forces between the tip and the sample at this point are negligible (inset 1, Figure 4.2). As the tip approaches the sample, long range forces start to bend the tip away from a nearly horizontal position towards (attractive forces, shown) or away (repulsive forces) from the surface (inset 2). When the force gradient exceeds the spring constant of the cantilever, then the tip ‘snaps’ into contact with the sample. This is called the “snap-to-contact” point and it is represented by inset 3. The tip is further pushed into the sample and an increase in the magnitude of repulsive forces bends the tip away from the sample. The direction of the piezoelectric motors are then reversed and the tip is pulled away from the sample. During the initial retraction, the tip remains in the contact regime, as explained above in the case of inset 4. At some point the tip “jumps” out of contact with the surface because the spring constant of the tip is larger than the adhesive forces of the surface (‘just after’ inset 5). The tip then returns to its initial non-contact deflection at a distance where the force is negligible (inset 1).

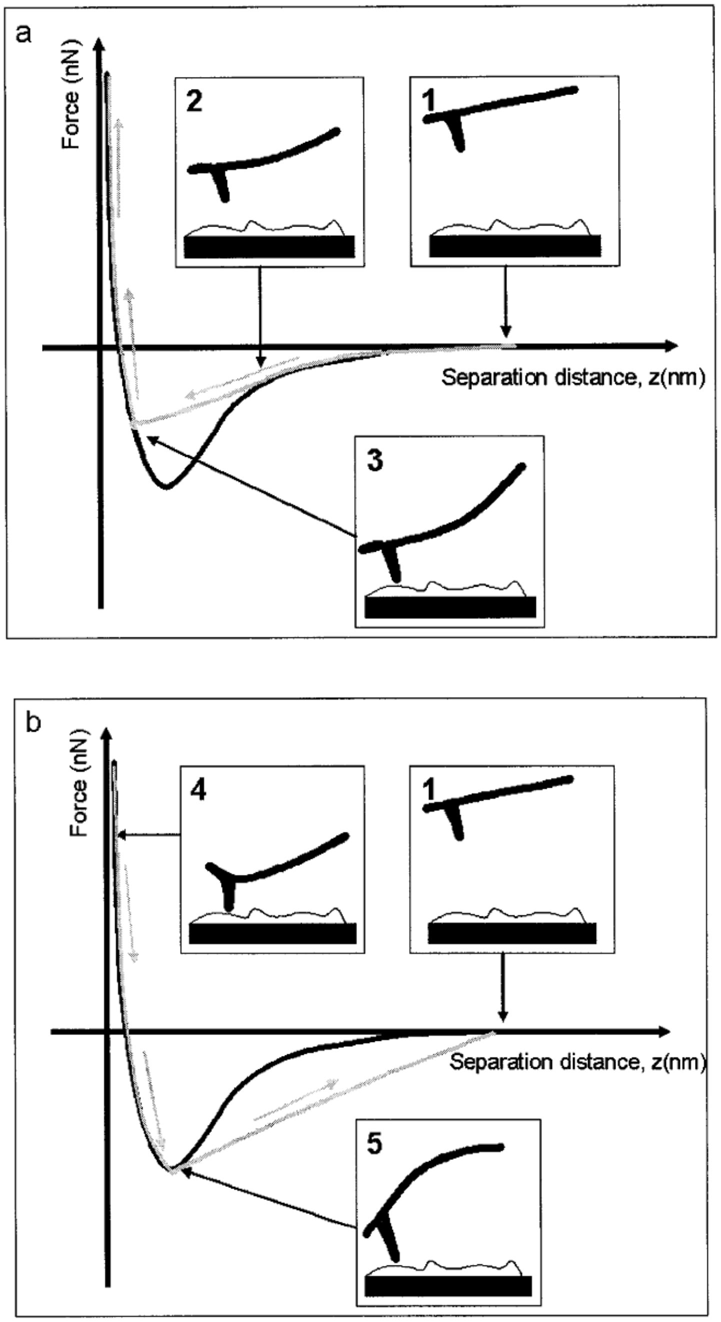

Figure 4.2: Retraction (a) and repulsion (b) AFM force curves for a generic tip-sample interaction.[89]

4.2 Chemical Force Microscopy

The AFM technique described above utilizes cantilever tips that are unmodified and such tips are sufficient for imaging, investigating physical and mechanical characteristics, and for obtaining a surface profile. However, it does not provide any specific chemical information, since tips of unmodified Si, Si_3N_4, and Au are only covered by oxides of silicon or general ambient contamination. Chemical force microscopy (CFM) adds chemical specificity to the AFM method by using tips that have been modified by chemicals to probe surfaces. CFM also includes the modification of samples in order to achieve specific tip-sample interactions.[90]

There are two popular methods to modify AFM tips. The first involves coating silicon based tips with organosilane layers. Clean silicon tips are exposed to reactive silane solutions (e.g. $RSiCl_3$) and the silanes attach to the surface through covalent Si-O-Si bonds. The other useful method is to use tips that have been coated with Au (~100 nm, by Au deposition) which provides a reactive surface for the covalent attachment of organic molecules terminated by thiols. Self-assembled layers of organo-thiols are thus formed on the surface of the tip through S-Au bonds. The choice of terminal functional groups on the tip and the sample must be appropriate to the experiment at hand.

CFM can be used to explore a number of chemical phenomena, including acid-base reactions (e.g. determining pKa), titrations, hydrogen bonding, and chemical mapping, among other experiments.[90] CFM can also be used to promote a certain type of tip-sample interaction which would enhance a particular experimental result. A majority of AFM protein experiments use unmodified silicon based tips or unmodified Au tips (to interact with thiol terminated protein surfaces). The use of these tips seems to promote specific tip-protein interactions that are sufficient to comment about the unfolding mechanisms of the proteins. However, this method requires extremely stable experimental conditions in order to maximize tip-sample interaction strength. CFM could be used to improve tip-protein interactions by terminating the tip with polar and/or non-polar functional groups. This is thought to have the advantage of increasing the probability of tip-protein interactions, which would increase the probability of protein unfolding events. The possible disadvantages of this method include an increase in non-specific tip-sample interactions and the possibility that non-terminal protein functional groups will interact with the tip; the latter situation would not lead to the full extension of the protein upon tip retraction. The utility of a protein-CFM experiment is investigated in this thesis. The widespread use of CFM to investigate protein-terminated surfaces has the possibility of providing both mechanical and chemical information about those proteins.

4.3 Protein AFM Experiments

Atomic force microscopy has been conducted by many to obtain information about protein unfolding mechanics and kinetics.[11, 31, 36] The results of these experiments have improved our understanding of protein structure. The interpretation of force curves obtained in the AFM-protein experiments has been done by others, but it will be explained here in terms of unmodified AFM tips. CFM experiments conducted on proteins are not well established, but the same AFM approach to a protein unfolding experiment can be taken in the CFM case.

Figure 4.3 shows the force curve of a specific tip-protein interaction. The key feature of these force curves are the “saw-tooth” pattern of tip deflection that occurs during tip retraction. During the contact regime (inset 1), the tip has ideally made contact with the terminal end of a protein. As the tip retracts, the protein stretches (inset 2) until the stretching force exceeds that holding the domain together. The domain then breaks and the tip snaps to a nearly equilibrium position (inset 3). The tip continues to retract away from the surface and continues to break multiple folding regimes (if any) until the maximum force is reached, which represents a fully extended protein (inset 4). After this point, the tip jumps off the surface and the tip-sample interaction is negligible (insert 5).

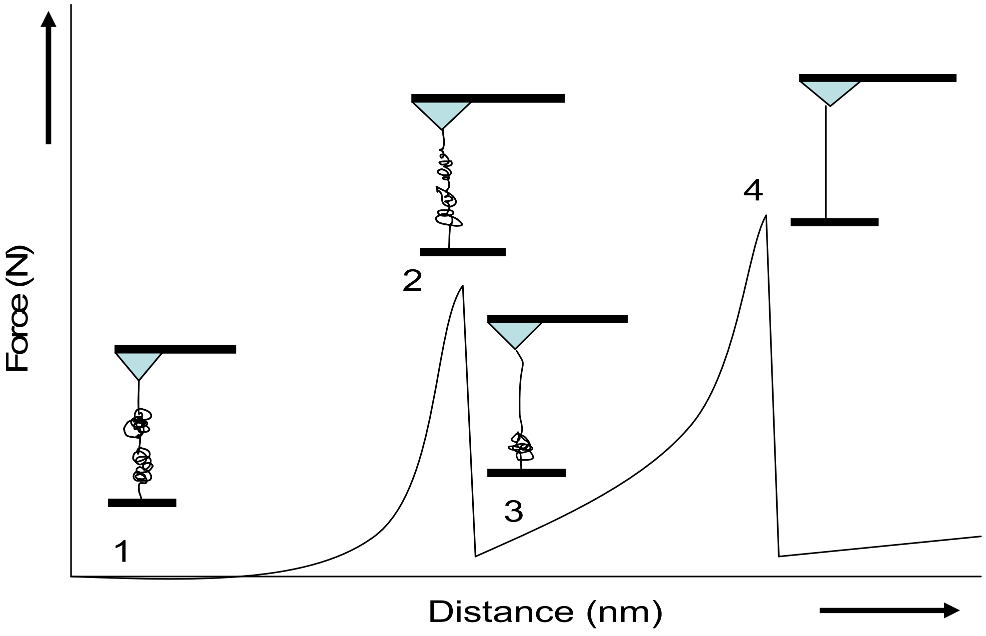

Figure 4.3: A schematic of a protein pulling experiment.

4.4 Tip Calibration

Calibration of AFM and CFM tips are important to ensure that force curve data is analyzed with high quality. The two most common calibration methods are the theoretical/dimensional method of Sader *et al*., [91] the 'added mass' method of Cleveland *et al*., [92] and the 'thermal noise' method (also known as the Thermal Noise Calibration).[93] The thermal noise method was chosen for its ease of use, the lack of information regarding tip dimensions (e.g. thickness etc.; requires the use of Scanning Electron Microscopy), and its non-destructive methodology.

To create their calibration method, Hutter and Bechhoefer first assumed that the cantilever acts like an ideal spring oscillating in one direction (z-direction). This assumption allowed them to use the equipartition theorem, which considers that the thermal energy in a one co-ordinate, quadratic system is generally equal to k_bT, where k_b is the Boltzmann constant and T is the temperature. This leads to the useful formula:

$$k = \frac{k_B T}{P} \qquad (17)$$

where k is the spring constant of the cantilever (N/m) and P is the area of the power spectrum of the thermal noise collected around the resonance frequency.

4.5 Surface Roughness

Surfaces can be characterized by their root-mean squared (RMS) roughness values, which is a measure of the variance of collected from the mean. In the case of this thesis, the RMS roughness values were calculated for the AFM images for various surface modifications. The formula employed is defined as follows:

$$x_{RMS} = \sqrt{\frac{1}{n}\sum_{i=1}^{n} x_i^2} \qquad (18)$$

where n is the total number of datapoints in a series of datapoints, such that it includes the following values: $\{x_1, x_2, x_3 \ldots x_n\}$. RMS roughness values have been used in past AFM studies to characterize the extent of sequential surface modification.[89]

4.6 Sample Preparation and AFM Measurements

The surfaces that were investigated were PMMA, NH_2-terminated PMMA, Sulfo-EMCS-terminated, and TmGH1-terminated PMMA. The underlying substrate in all cases was mica (V-4 Grade, SPI Supplies), however TmGH1 could also be placed on Au substrates. These surfaces were prepared using the same method described in Section

2.1 and general scheme shown in Figure 2.1. All glassware was rinsed and cleansed with MeOH and ddH_2O during the preparation of these samples.

Imaging of the samples was conducted using acoustic AC (AAC) mode for samples in air and contact mode for samples under liquid. The PMMA and NH_2-terminated PMMA samples were imaged in air, while the TmGH1-terminated samples were imaged in their respective buffer solutions. The AAC experiments were conducted using silicon micro-cantilevers (TESP, L=125 μm, F_0=283-308 kHz). Height, Amplitude and Phase images were all acquired using an Agilent AFM system (AFM Controller, Model No. N9605A; system 1). Surface Roughness was determined for all samples using the included PicoScan (version 5) software program provided with the apparatus. The Contact mode images were collected using a dodecanethiol-terminated Au tip (see next paragraph for details). The images were collected using the same AFM controller as above, but with a Molecular Imaging Scanner (Model No. MS300, Nanoscope; system 2). The spring constant of the dodecanthiol-terminated tip was determined to be 24.2 N/m using a the aforementioned scanner with a second AFM controller (Nanoscope E, Molecular Imaging, Model No. NSE; system 3).

Contact mode AFM was conducted using the system 1 set-up on TmGH1-terminated PMMA surfaces. Three types of tips were used: contact mode silicon cantilevers (Ultrasharp, CSC 12/50) and Au coated silicon cantilevers (MikroMasch, CSC38/Cr-Au) terminated either with dodecanethiol (Sigma Aldrich) or 11-mercaptododecanoic acid (Sigma Aldrich). The chemically modified tips were prepared by exposing the Au coated silicon cantilevers to a 1 M solution of dodecanthiol in anhydrous ethanol or an 86 mmol solution of 11-mercapto-dodecanoic acid in anhydrous ethanol. In each case the tip-solution exposure time was greater than 24 hours. The tips were washed twice, for 5 minutes, using anhydrous ethanol and then were placed in an oven for 1 hour to dry at 50 ºC. The tips were then placed in a sealed vial to cool for approximately 15-30 minutes. The tips were then mounted in preparation for the contact-mode experiments.

The contact mode experiments took place in a vibrational dampening box using system 2 and the PicoScan 5 software package. Force Curves were collected from at least 8 different positions on each surface. An approach-retraction sweep time of 0.2 seconds was used to obtain force curves for the Sulfo-EMCS terminated surfaces. In the case of the TmGH1-terminated surfaces, sweep times of 0.2 , 0.5, 1, 2.5 and 5 seconds were used. For the first three sweep settings, approximately 250 force-retraction curves were obtained. However, at the higher sweep time settings only 100 force-retraction curves were obtained to make efficient use of experimental time. Each force-retraction curve contained 1000 datapoints. Before each data collection, the tip and sample were kept in contact for a number of seconds to increase protein adsorption onto the tip and to minimize any spurious results caused by hysterisis of the piezoelectric motor. Data analysis required at least 30 force curves showing specific protein unfolding events and these force curves were chosen and analyzed by the user without a software aid.

Chapter 5

AFM Results and Discussion

In this chapter, the AFM results will be presented and discussed. Readers should be reminded that the results of Section 5.2 contains some data which should be viewed as preliminary, but promising results. The data for those sections was collected from a single TmGH1-terminated sample, using a dodecanethiol-terminated Au Tip (non-traditional tip-protein interaction), and there was only one successful experimental run. Other attempts at obtaining TmGH1 force curves using the same tip-sample interaction and other derivatives proved unsuccessful as of the publication of this thesis.

5.1 Images and Surface Roughness Analysis

Non-contact and contact images of the various unmodified and modified surfaces discussed in this thesis are shown in Figure5.1 and Figure 5.2. RMS calculations have been performed on selected images and the results are shown in Table 5.1. The PMMA and NH_2-terminated PMMA surfaces were imaged using non-contact AFM, while the

TmGH1-terminated surfaces were imaged using contact AFM. It should be noted that contact-mode imaging is not ideal for biological structures due to the potential for surface damage, but that it was an imaging mode available at the time of experimentation. The images in Figure 5.2 should be viewed with this constraint in mind. At the time of publication, non-contact images of the surface were not obtained.

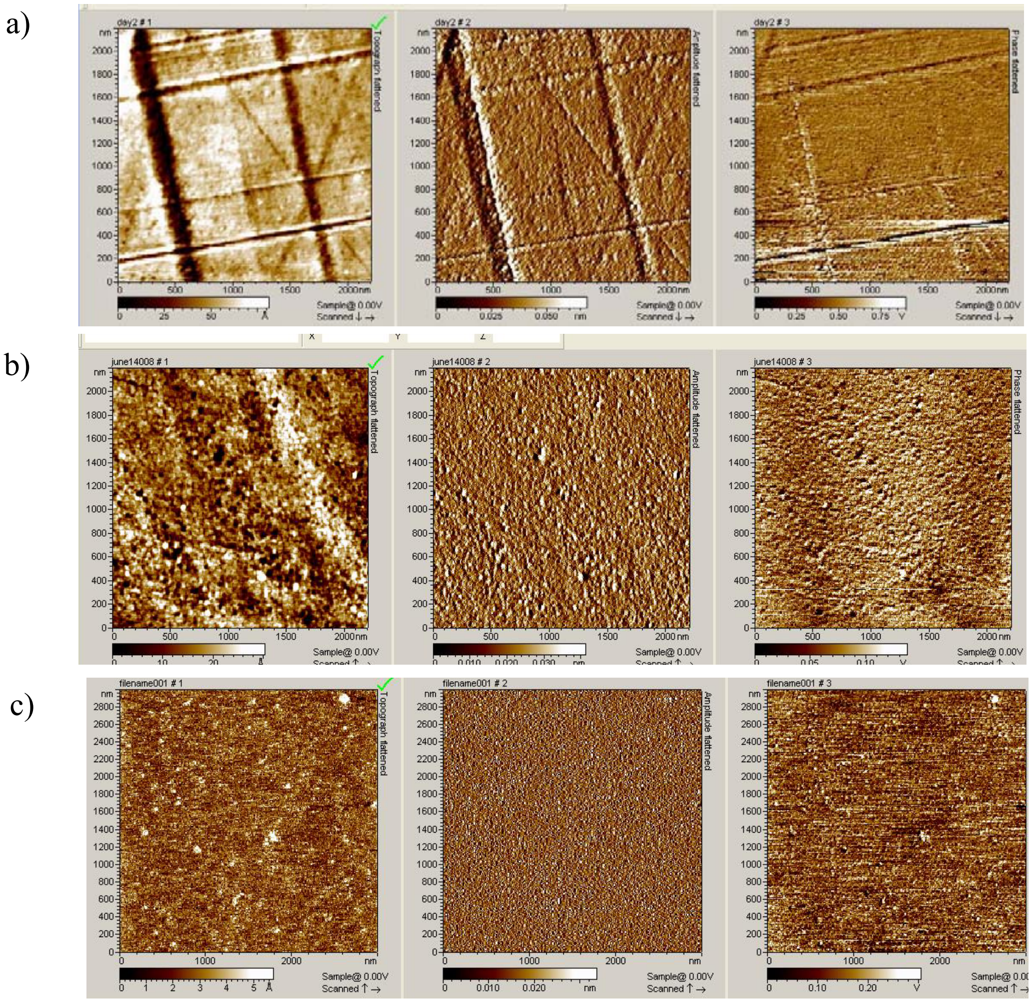

Figure 5.1: Representative AFM Images (Tapping Mode) of three sample types: a) Bulk PMMA (2 um) b) Bulk PMMA - Aminated (2um) c) PMMA spin-coated on mica (3 um). Each set of images is grouped into three separate images: from left to right within each set is i) topographical image ii) amplitude image iii) phase image

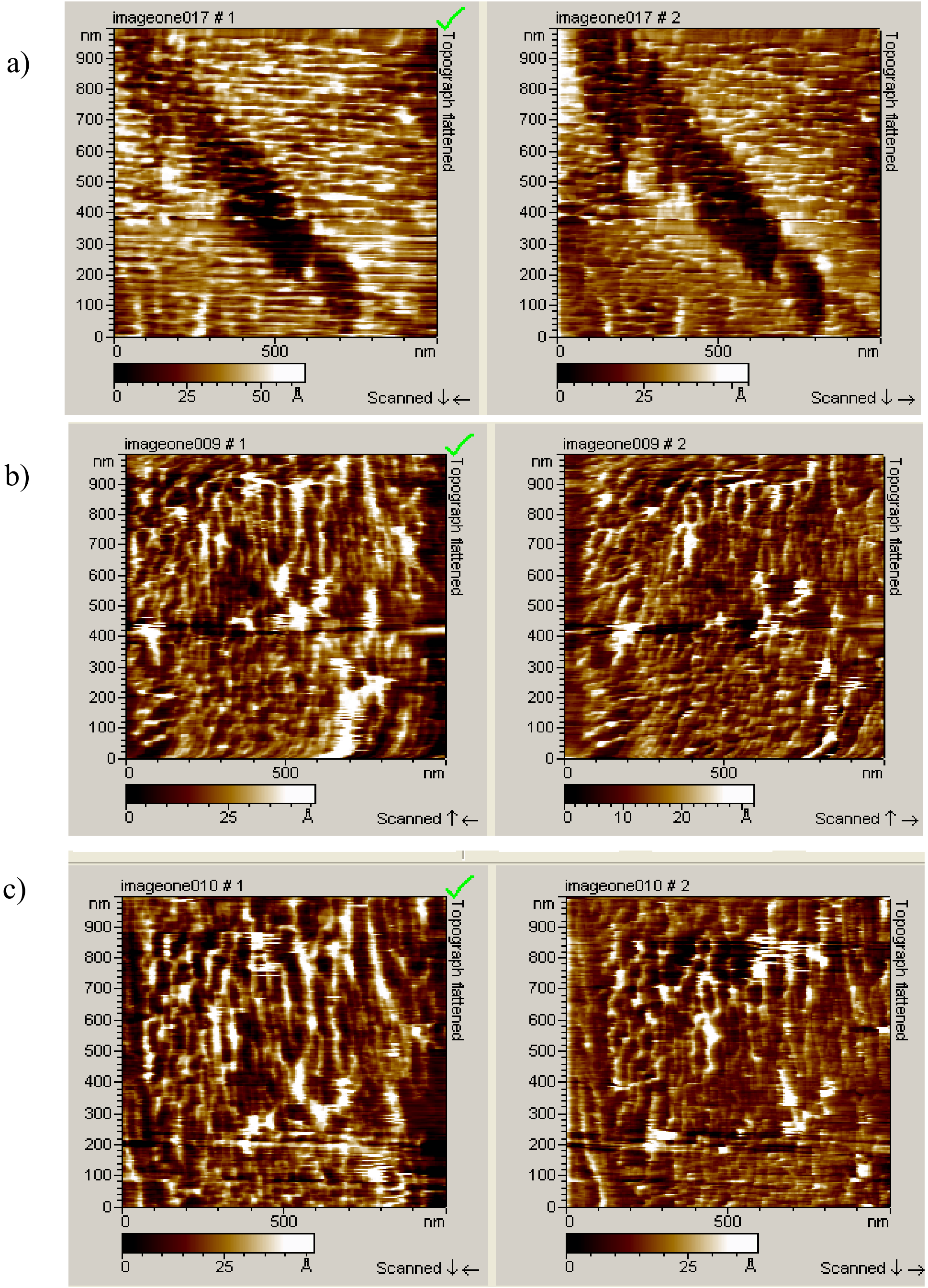

Figure 5.2: Representative AFM Images (Contact Mode) of the probed TmGH1-terminated surface in three separate randomly chosen positions. Each of the images was taken at a scan size of 1 µm by 1µm, with a scan speed of 2 Hz. The images on the

left are for the left to right scan and the images on the right are for the right to left scan of the surface.

Topographical RMS Roughness Data		
Sample	Scan Size	RMS Roughness (nm)
Bulk PMMA	1 µm	28
Bulk PMMA	2 µm	188
Bulk PMMA	450 nm	8
Bulk PMMA NH2	2 µm	12
Bulk PMMA NH2	500 nm	27
Bulk PMMA NH2	1 µm	100
Bulk PMMA NH2	751 nm	51
Mica PMMA NH2	1.5 µm	8
Mica PMMA NH2	3 µm	86
Mica PMMA NH2	660 nm	52
TmGH1 (average of a, b, c)	1 µm	127

Table 5.1: These are the root-mean squared roughness values in nanometers for the AFM images that were studied. The entry for TmGH1 is the average RMS value for the topography (left most) images a, b, c in Figure 5.1 with a standard deviation of ±0.6 nm.

Notwithstanding the different AFM modes used to obtain images, these images show topology changes that occur after modification. One goal was to ensure that PMMA had been successfully modified by ethylenediamine to create NH_2-terminated surfaces. An initial comparison between the ‘bulk’ PMMA (Figure 5.1a) and ‘bulk’ NH_2-terminated PMMA images (Figure 5.1b) seems to show that an initially smooth surface is now pitted. This is confirmed in a limited way by a comparison of the RMS roughness values in Table 5.1. The RMS values for a 1 µm and ~500 nm scan of both surfaces show an increasing trend, where the NH_2-terminated surface is the roughest; this is consistent with expectation. However, the trend between the RMS values of the 1 µm scans of these two surfaces show a large decreasing trend. This inconsistency is most likely due to deep surface ‘cuts’ that were prevalent in the ‘bulk’ samples and these deep surface features can be seen in Figure 5.1a and b. These features are probably the result of scratching of the PMMA surface during the initial creation of the PMMA sheets by the manufacturer. These images are indicative of a change of morphology that is attributed to the modification of PMMA by ethylenediamine to produce NH_2-terminated PMMA surfaces.

Another goal was to produce flat substrates for the adhesion of TmGH1 and the initial step towards achieving that goal was to modify surfaces of spin-coated PMMA. Figure 5.1c shows surface images of spin-coated PMMA after modification by ethylenediamine. The surface seems to be flatter than the ‘bulk’ NH_2-terminated surfaces, but a similar pattern of ‘pits’ on both surfaces can be seen. A comparison of the RMS roughness values of surfaces represented by Figure 5.1b and c, are not as easy to make since the scan sizes are all different. The RMS roughness value for spin-coated NH_2-terminated surfaces is 8 nm (± 0.5 nm, scan size: 1.5 μm), which is a lower than the ‘bulk’ versions of similarly sized images, which have values of 12 nm (± 0.5 nm, 2 μm) or 100 nm (± 0.5 nm,1 μm). While the above results suggest a flatter surface, the other RMS values for the spin-coated NH_2-terminated surfaces do not show evidence of reduced roughness compared to the ‘bulk’ surfaces of similar size. It is possible that spin-coated surfaces of PMMA actually increase surface roughness after modification due to an increased density of NH_2 groups (assuming that ethylenediamine has greater access to PMMA ester groups on spin-coated surfaces). The initial image comparison and the roughness values discussed are evidence for spin-coating producing fairly flat surfaces; at the very least spin-coated surfaces do not exhibit signs of deep scratching or other forms of surface inhomogeneity.

The TmGH1-terminated surfaces were expected to produce the roughest surfaces with the most prominent surface features. Proteins are known to deposit on surfaces and form patterns, channels or globular features in AFM images (mostly non-contact).[51] The images in Figure 5.2 are contact-mode images of TmGH1-terminated surfaces, so the comparisons to the literature are not direct and most likely include evidence of surface damage and noise. However, the images of Figure 5.2 are still, in general, quite different from those in Figure 5.1; there seems to be an elongated ‘honeycomb’-type network on these protein-terminates surfaces, as exhibited in Figure 5.2b and c (taken at different positions on the surface). At another position, the surface seems to have a topology that includes some deep surface features and deposits on the surface. It is possible that different underlying surfaces cause different protein deposition (i.e. an exposed area of PMMA vs. a completely Sulfo-EMCS terminated area). The three TmGH1 images shown in Figure 5.2 have very similar RMS roughness values and the average is 127 nm (± 0.6 nm), despite their apparent visual differences. This value can be considered to be the highest of the RMS values associated with images that are 1 – 1.5 μm in size. This was an expected result, since it is consistent with the addition of large proteins onto a flat surface.

A key note about images in Figure 5.1, particularly b and c, is that the deposition of the proteins seem to be fairly homogeneous and they seem to be connecting to one another. Ideally, the TmGH1 proteins should be dense enough to facilitate AFM force experiments, but also be far apart to minimize non-single protein force curves. These images suggest that a substantial number of the AFM force curves discussed later may be representative of multiple protein-tip interactions (non-specific) rather than just a specific protein-tip interaction. If need be, then the visible protein interactions can be further minimized by changing the protein solution concentrations or varying the exposure time of the modified PMMA surfaces to the protein solutions.

5.2 Force Curves

5.2.1 Tips Used in Experiments

There were three tips used in attempts to obtained specific force curves that are indicative of protein unfolding: Si, Au, and dodecanethiol-terminated tips. The tips were immersed in the protein (phosphate) buffer and brought into contact with TmGH1-terminated samples. The silicon tips were attempted first, but there was no evidence of specific or non-specific events, despite experiments at different pulling speeds. This was not expected, since there are a number of papers that indicate that silicon based cantilevers do facilitate protein unfolding. The silicon tips were also not able to produce force curves on PMMA, NH_2-terminated and Sulfo-EMCS terminated surfaces, but this was an expected result for unmodified Si tips.

Gold tips are not used in protein pulling experiments, but their introduction into this project was useful to determine if there was a difference in the tip-sample interaction between unmodified and modified Au tips. I was unable to obtain any force curves using unmodified Au tips to probe TmGH1-terminated surfaces. Gold tips were then modified with dodecanethiol and 11-mercapto-dodecanoic acid and brought into contact with the surface. The use of dodecanethiol modified tips did lead to observations of force curves for one out of three attempted experiments. The results of this successful experiment are presented here. After this successful attempt, it was thought that the tips could be modified with a thiol that was terminated with a polar head group and a carboxylic acid based thiol was obtained: 11-mercapto-dodecanoic acid. Unfortunately, the use of these modified tips did not lead to any obtainable force curves in two experimental attempts.

There are a myriad of reasons why most of the experimental attempts were unsuccessful despite literature examples and diligent attempts to reproduce the success of one of the dodecanethiol modified tips. Some possible explanations include: improper sample handling, broken tips, protein denaturation on the surface, too much ambient vibrations. The probability of finding individual protein unfolding events is about 5-10% of all samples, so one can imagine that a tip or sample problem would lead to a severe reduction in observable force curves.

5.2.2 Data Classification

The AFM data collected by the force curve measurements were classified into various groups depending on their spectral features. The groups were as follows:

- No discernable force events (Figure 5.3a)
- Non-specific force events (Figure 5.3 b)
- Specific force events (Figure 5.3 c, d, e, f)

Non-discernable force events were eliminated and only reasonable values for Non-specific and Specific force events were chosen, as explained in section 5.2.2. As well, these force curves were obtained with different pulling speeds, and this will be a consideration for future analysis.

Figure 5.3a shows an example of a valid Non-specific force event in the form of the PicoScan output. Figure 5.3b shows an example of a Specific force event in the same format. As expected, a non-specific interaction is characterized by a single force curve well, whereas the force curves with non-specific events (Figure 5.3, c,d,e,f) show evidence of the 'saw-tooth' pattern to various extents.[11, 36] A total of 191 'non-specific' and 419 'specific force' curves were classified from the initial dataset. These 'non-specific' and 'specific' curves were deemed to be 'reasonable', since they had both a positive force value and a positive extension value. If even one event within a force-retraction curve had a negative force or extension value (or both negative), then it was deemed to be an 'unreasonable' result. If an event was unreasonable, then the entire et of events from that force-retraction curve was eliminated. These situations are occurring due to the relative position of the datapoints with respect to either the baseline (zero force) or the intersection of the baseline with the tip sensitivity line. Histograms of these reasonable non-specific and specific events (Figure 5.4a and b) for force and extension values show a normal distribution of data, but with the possibility of multiple peaks in Figure 5.4a.

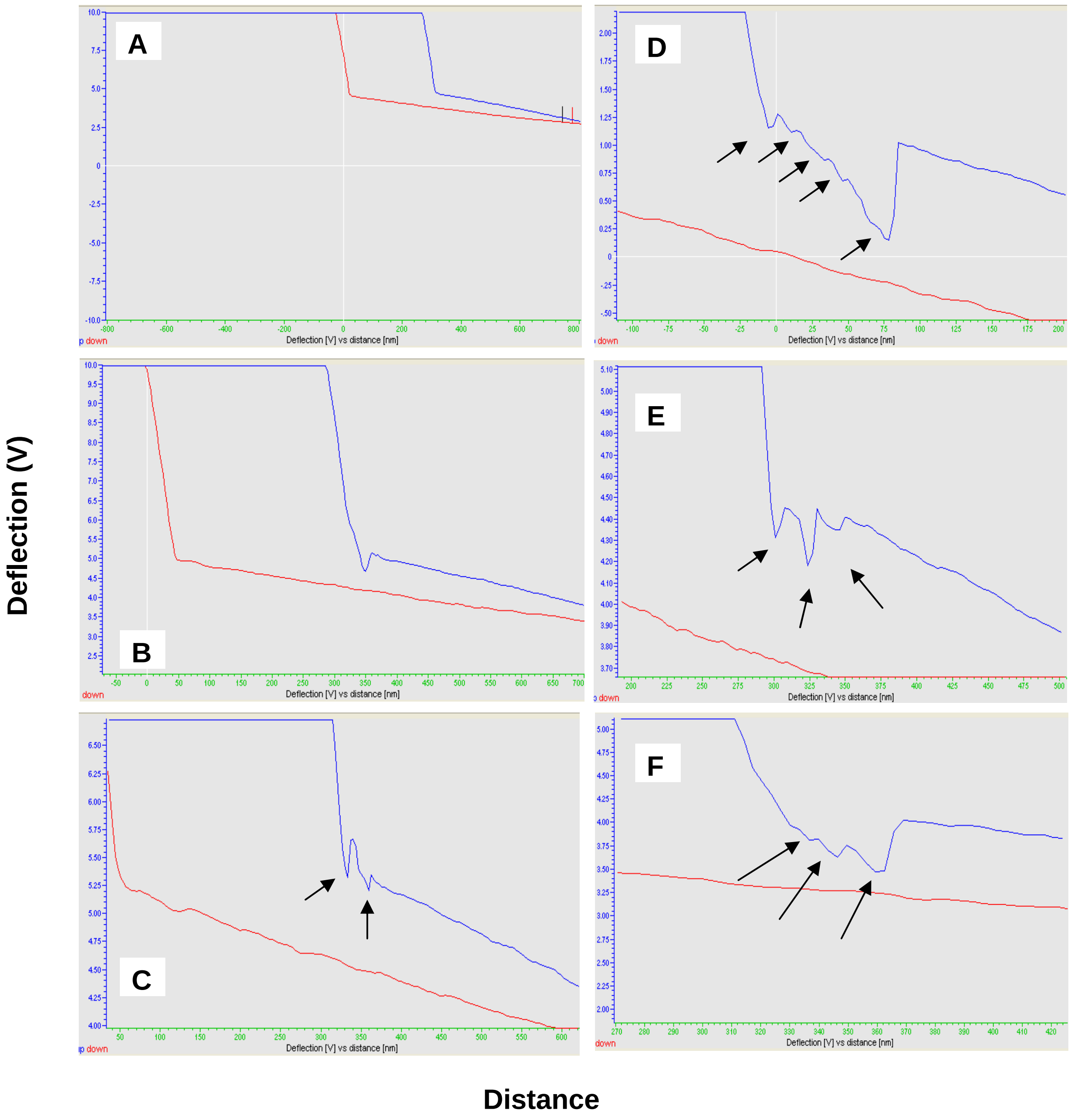

Figure 5.3: Representative Deflection [V] vs. distance [nm] plots resulting from contact between a dodecanthiol modified Au tip and a TmGH1-terminated surface. Force curves a, b, c, and have sweep times of 2.5 seconds; e and f have sweep times of 5 seconds. (a) a contact regime that does not show any specific or non-specific interactions (b) non-specific event (c) two events: i) specific or non-specific ii) specific (d) specific tip-protein interactions (5 events) (e) specific tip-protein interactions (3 events) (f) specific tip-protein interactions (3 events).

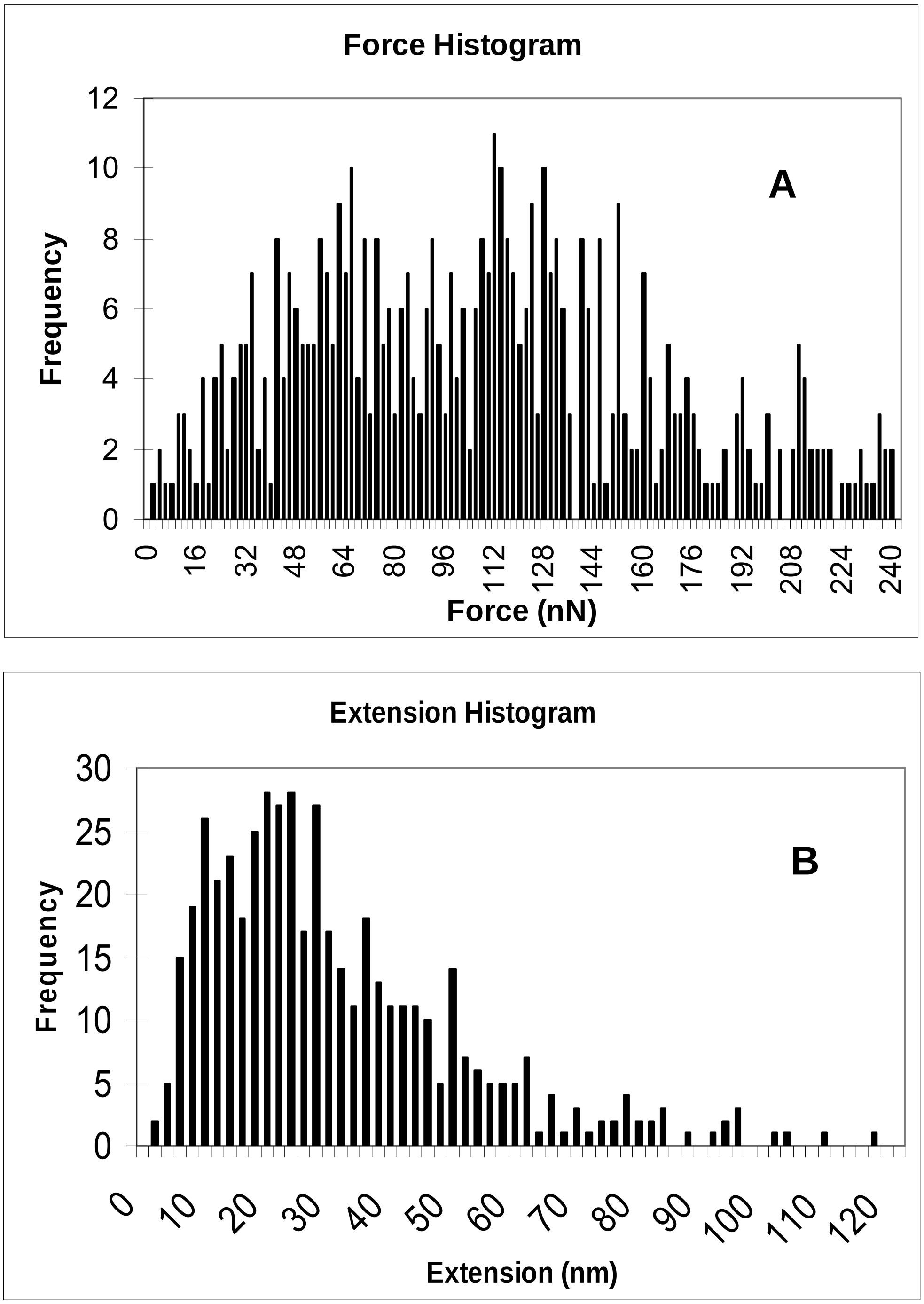

Figure 5.4: (a) Histogram of reasonable (see section 5.2.2) force data representing ‘pulling’ events of a TmGH1 mechanical force experiment. (b) Histogram of reasonable (see section 5.2.2) extension data from the same experiment.

In section 5.2.2 the data is considered without separating data based on pulling speed, which is defined as:

$$Pulling\,Speed\,(nm/s) = \frac{tip\,travel\,(nm)}{sweep\,time\,(s)} \qquad (19)$$

The pulling speed is an important parameter, because higher pulling speeds exert more force on force-sensitive biological samples. The data is analyzed in terms of the pulling speed in section 5.2.4. The complete dataset of force values, extension values, standard deviations and population sizes of various sub-sets of the described data is shown in Appendix C.

5.2.3 Force versus Extension Data

As exemplified in Figure 5.3, AFM data of specific events are presented in deflection-extension curves or force-extension curves. Using the dataset in Appendix C, a new force versus extension graph has been created to represent the average tip-TmGH1 interactions. I have used the average force and extension values for all the non-specific and specific events, with the latter grouped according to the event number; this graph is shown in Figure 5.5 a and b. The Figure 5.5 b shows the experimental error assocated with the data in Figure 5.5a.

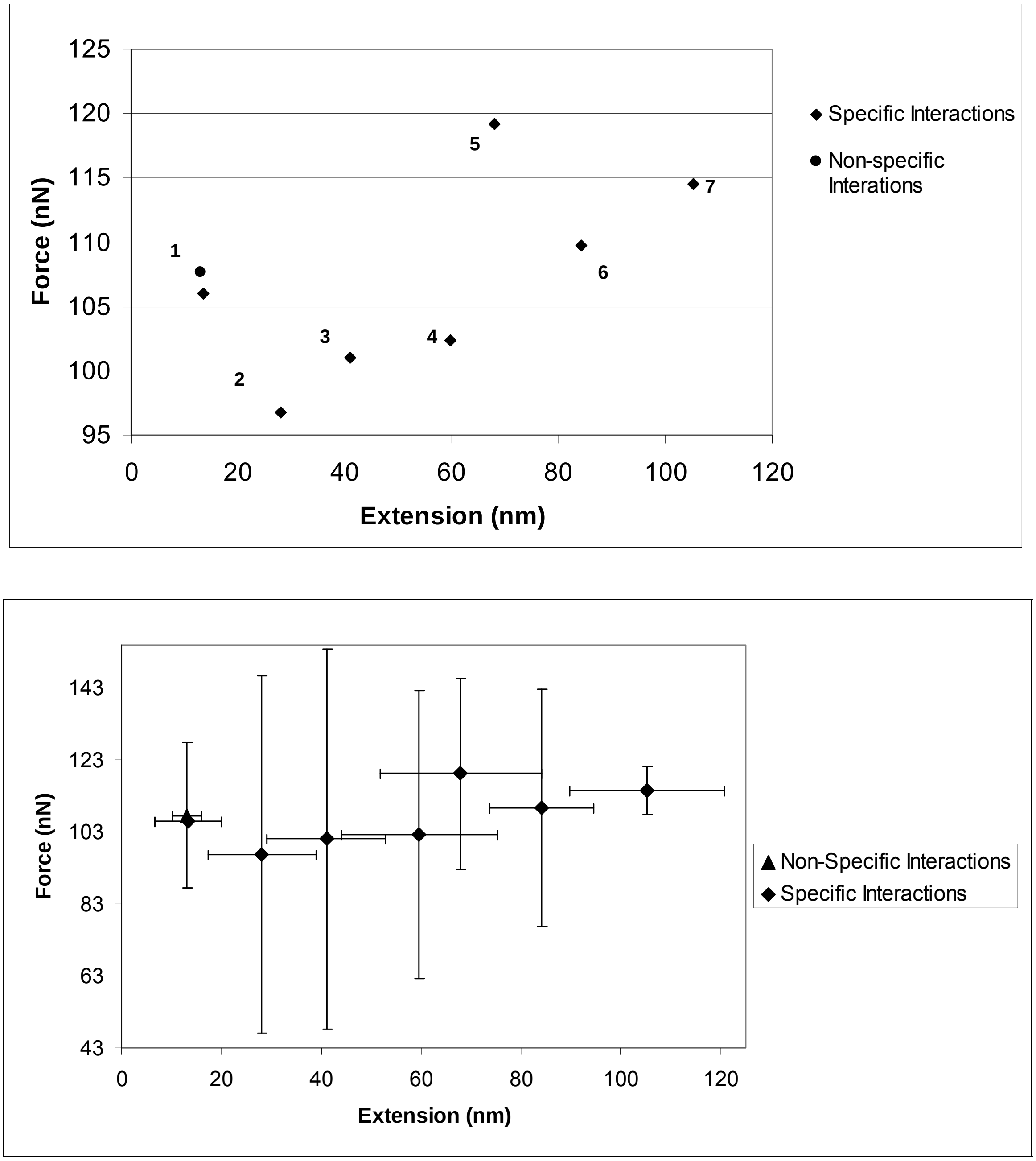

Figure 5.5: a) Force versus Extension graph for the TmGH1 pulling experiment. All reasonable (see section 5.2.2) non-specific and specific data have been included. b) the same plot as Figure 5.5a, but standard deviations of data has been included.

Figure 5.5 reinforces the observation of both non-specific and specific events. The average force and extension data (FE data) of all non-specific events is located at a force of 107.7 nN (± 57 nN) and an extension of 13.1 nm (± 7 nm). This value is similar to the average FE values of specific event 1 (106.01 nN (± 57 nN), 13.5 nm (± 7 nm). Using an unpaired T-test (2-tailed, Type 3), it was found that both the force data (P=0.91) and the extension data (P=0.53) is not statistically different between these two sets. This suggests that the first extension event is non-specific in nature, regardless of the general data classification.

Non-specific tip-sample interactions need to be minimized, but it is clear that they do occur with large data population sizes; what is the nature of this non-specific tip-sample interaction? We can generally rule out tip–sample interactions between the tip and the ester-terminated, NH_2-terminated and Sulfo-EMCS terminated portions of the surface, since the extension length is greater than the theoretical thickness of any of these substrate types (e.g. length of Sulfo-EMCS is 0.9 nm). It is most likely that this non-specific event is a tip-protein interaction with a short extension, but relatively strong interaction force; for example a favorable interaction that does not lead to unfolding of the protein or the pulling, but not unfolding, of more than one protein.

The second feature of Figure 5.5 is that there are a series of FE points that corresponds to multiple events, suggesting that they are specific tip-sample interactions. The FE points are separated by an average extension of 15.4 nm (± 5 nm) between events 2 through 7. The forces within this series start at ~97 nN (event 2) and rise to ~114 nN (event 7); event 5 seems to be an outlier, as explained later. The overall trendline through events 2 – 7, without event 5, has a linear regression R^2 value of 0.97. The linear relationship between events 2-4 and 6-7 are consistent with the sequential pulling of a protein with a number of unfolding pathways. It is also possible that some of these events represent the pulling of more than one protein in an oligimer structure, in a chain or grouped on the surface.

Event 5 in Figure 5.5 does not seem to be consistent with the other events tabulated. The extension value is consistent with the other events, but I do consider the force data for event 5 to be an erroneous result. It does not seem to be a true outlier, since a statistical Grubb's test of the presented force data of events 2 through 7 did not exceed the critical value for an outlier of a group of N=6 datapoints. It may be representative of protein mis-folding events, protein oligimers, and protein chains producing erroneous FE curves in the literature.[37] It is possible that many of the individual events representing the aggregate datapoint are examples of the above types of FE events.

In order to retain the clarity of Figure 5.5, the standard deviation error bars have been removed. However, it is important to note that the errors for both the force and extension values were large, relative to some published data by others.[11, 36, 37] The average error was ~55% and ~28%, respectively, for force and extension data presented in this section. Also, the data presented in Figure 5.5 represented only ~5-10 % of the total data collected, but this is consistent with collected data of other AFM protein-pulling experiments. A final consideration is that the force data presented here is in units of nN, whereas many literature examples report forces on the order of pN. While this may be unique to TmGH1, it is also possible that the tip is not calibrated with the correct force constant (k = 24.2 N/m), despite evidence to the contrary. Force curve data of proteins are known to be influenced by lateral and twisting forces on the tip and this would be a source of error, particularly at low pulling speeds. The quality of the obtained data could be improved through repetition and comparison to other similar datasets in future projects.

5.2.4 Pulling Speeds

The pulling speed of a tip towards and away from a biological sample is an important parameter to consider. High pulling speeds are known to damage biological samples and they are known to provide inadequate time for protein adsorption onto a tip during experiment.[34] As well, there is evidence of a relationship between the pulling speed and unfolding forces as demonstrated by Carrion-Vazquez *et al.* and others.[36, 40, 94] The pulling speed is compared to the force and extension data, as well as the number of specific and non-specific events that occur at each pulling speed. The pulling speeds (sweep times) that were used were 320 nm/s (5 s), 640 nm/s (2.5 s), 1600 nm/s (1 s), 3200 nm/s (0.5 s), and 8000 nm/s (0.2 s). It should be noted that traditional force curve experiments on non-biological samples, using AFM or CFM, by our group, are done on the order of 3000 – 8000 nm/s, in order to eliminate any interference due to twisting forces or hysterisis of the tip mechanism. The errors in the data are on a similar order to those discussed in Section 5.2.3 and the reasons for these errors are discussed there.

Figure 5.6 shows a comparison between the number of specific events observed and the pulling speed:

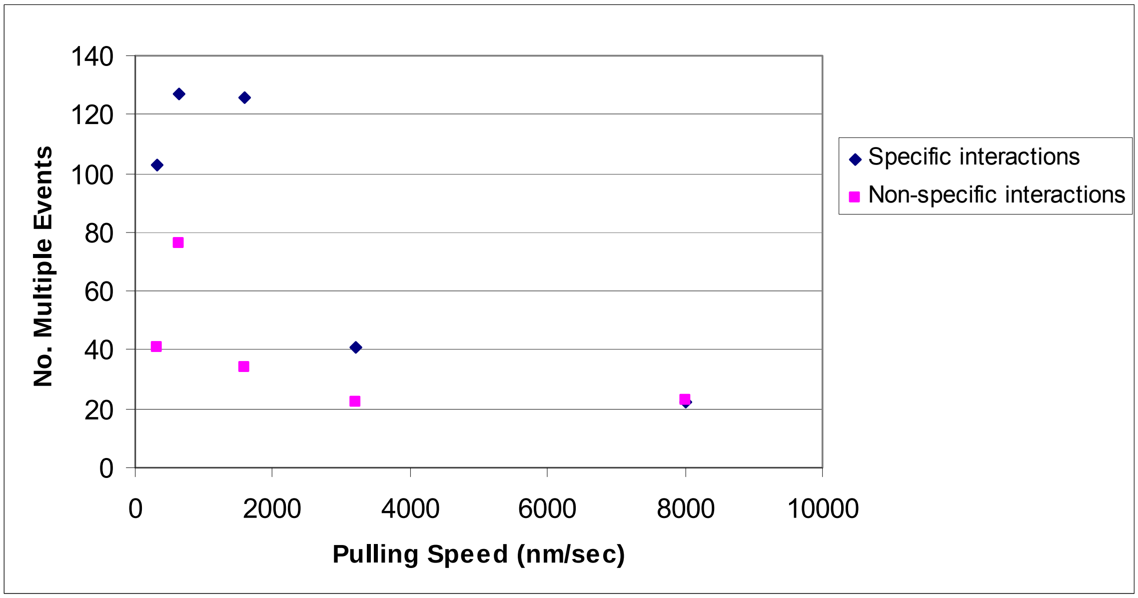

Figure 5.6: Number of Events versus Pulling Speed (nm/s) graph for the TmGH1 pulling experiment. Data has been classified into specific and non-specific interactions.

At low pulling speeds (<1600 nm/s) approximately 100-130 specific events are observed, but at higher pulling speeds (~ >1600 nm/s) there are only 20-40 specific events seen. An increased number of non-specific events can be seen as low pulling speeds as well, but at the low pulling speeds the number of non-specific interactions is lower than specific interactions. These result is consistent with pulling speeds used by other researchers to obtain specific tip-protein interactions; specific interactions are more favorable at lower pulling speeds.[36] Higher pulling speeds probably affect the ability of the tip to specifically attach to a protein, due to sample damage by tip approach force or by a lack of protein to tip adsorption time.

Figure 5.7 shows the relationship of the extension values for specific and non-specific interactions as a function of pulling speed.:

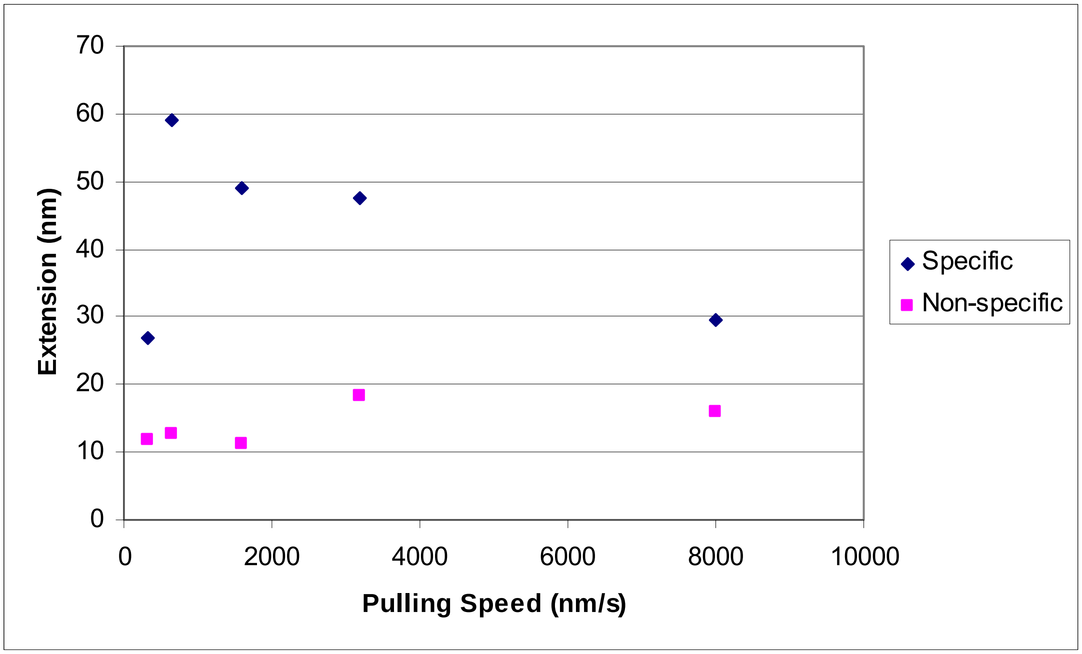

Figure 5.7: Extension (nm) versus Pulling (nm/s) plot for the TmGH1 pulling experiment. Data has been classified into specific and non-specific interactions. Standard deviations of extension data ranges ± 7 – 16 nm.

Again we see that there is a difference between the plots for the specific and non-specific events. The specific event plot includes a variety of extensions ranging from a maximum of 59.0 nm (± 14nm) at 640 nm/s to minimums of ~30 nm for 320 nm/s and 8000 nm/s. A consistently high extension value is apparent for pulling speeds between 640 nm/s to 3200 nm/s. On the other hand, non-specific events do not show as much variance in its plot in Figure 5.7. The values for the non-specific set fall in the range of 10-20 nm for all chosen pulling speeds. This helps confirm the idea that the non-specific interaction does not involve the residue from the Sulfo-EMCS modification (length of Sulfo-EMCS is 0.9 nm). Moreover, the consistent extension of the non-specific interaction indicates that the surface might be covered with a reasonably dense layer of proteins. As previously mentioned, these results seem to indicate that the specific events are unique and show some dependence on the pulling speed that seem to be consistent with unfolding events within a protein.

Figure 5.8 compares the relationship between the force data and the pulling speed for both the specific and non-specific tip-sample interactions. According to the observations of Fowler *et al.* [31]and Carrion-Vazquez *et al*.,[36] the unfolding forces should rise in a linear manner as pulling speed is increased. A linear regression was performed on each of the specific and non-specific datasets and their R^2 values are 0.7 and 0.2 respectively. This comparison shows that the specific event data better represents the optimal protein unfolding experiment than does the non-specific event data. The poor correlation of the non-specific forces suggests that the events lead to similar extensions, but require different forces. This idea would be consistent with the random interaction between a tip and multiple proteins on the surface. It would also be consistent with a tip interaction with a portion of the protein which does not lead to folding. Of course, there could be many such interactions within a single protein structure, so the forces for each of these non-specific interactions should be different.

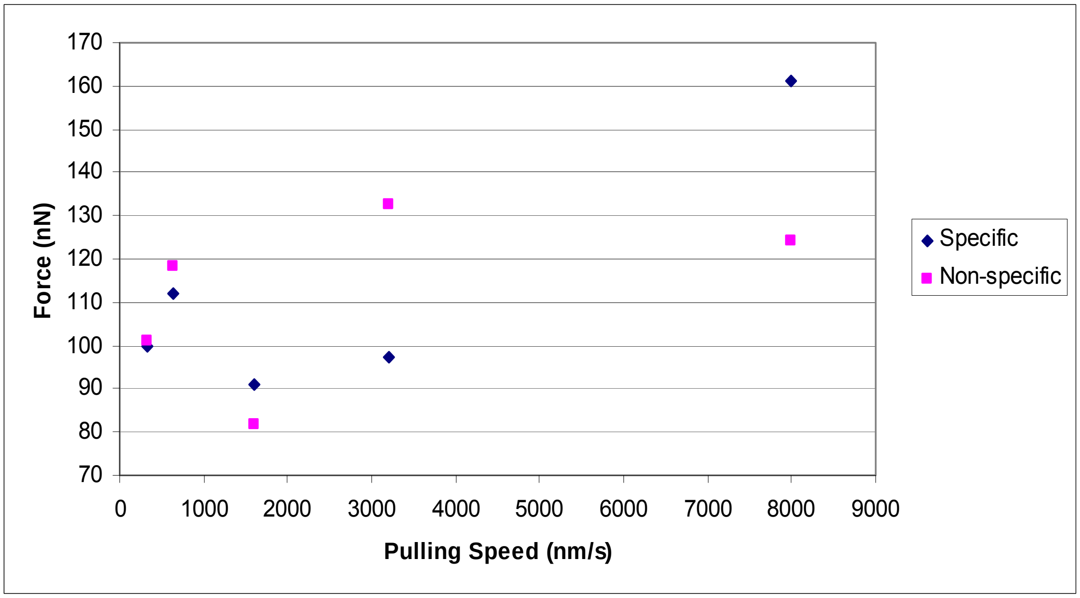

Figure 5.8: Force (nN) versus Pulling (nm/s) plot for the TmGH1 pulling experiment. Data has been classified into specific and non-specific interactions. Standard deviations of the force data range between values of ± 7 – 60 nN.

From the results of this section, we can make a few statements about this and future protein pulling experiments. First, pulling speeds should be kept as low as possible, while maximizing the probability of viewing a specific interaction. In our case, that seems to be at pulling speeds that are between 640 nm/s and 1600 nm/s, but lower speeds will also be suitable. Higher pulling speeds are inappropriate for these studies and they should also be avoided when initially approaching the sample to obtain a contact regime at the beginning of an experiment. Second, it seems that the concentration used for the proteins in this AFM experiment is appropriate for obtaining a selection of non-specific and specific forces to analyze. Third, the results of Figure 5.5 (extension versus pulling speed) suggest that the non-specific interaction has an extension between 10-20 nm, but this and other data, such as the force data, are insufficient to determine what this initial non-specific interaction actually represents - aside from the fact that it is not an extension of underlying substrate layers, due to the large extension length.

5.2.5 Evidence for a Covalent Bond between TmGH1 and modified-PMMA

In Chapter 3, XPS evidence for a covalent bond between modified-PMMA and TmGH1 was presented. There the evidence was not complete and mechanical force experiments were a further requirement to determine whether there was indeed a covalent bond. I have obtained evidence of specific tip-sample interactions between a dodecanethiol tip and a TmGH1-terminated surface which has just been presented. Specific and non-specific interactions were found with adhesive forces on the order of 80 – 100 nN and extensions on the order of 10 - 60 nm. Previous experiments of proteins attached to Au through a Au-S bond generated adhesive forces on the order of 100 pN.[31,36,37] The obtained forces and those in the literature differ by three orders of magnitude due to the higher force constant of the calibrated tip used in these experiments. This forces are evidence for either for a stronger single protein-tip interaction or an interaction between the substrate and multiple proteins linked together. Regardless, since the general adhesive force between TmGH1 and the tip is greater than ~100 pN, it is very likely that it is attached to the surface through a covalent bond. The protein has to have a platform in order to resist the retraction force applied to it by the tip. It is likely that these forces would be much smaller if the proteins were not attached to the surface (non-adhesive interaction, Figure 5.3a). In addition, the extension values are also evidence for a covalent bond between TmGH1 protein and the modified-PMMA substrate. The first extension value is ~13 nm, which is larger than the thickness of a modified-PMMA layer terminated by Sulfo-EMCS (~4 - 7 nm). This suggests that there is a layer of TmGH1 above the surface that has not been washed away by the buffer solution by the procedural washing steps or the experiment itself. This is confirmed by the contact-mode images of TmGH1-terminated surfaces. This layer of TmGH1 seems to be robust and can interact in a specific manner with a modified-AFM tip; this is characteristic of a robust, covalent interaction between TmGH1 and a modified PMMA substrate.

Chapter 6
Conclusions

An experimental study of proteins, particularly *Thermatoga* maritime β-Glucosidase Hydrolase 1 (TmGH1), on poly(methyl methacrylate) (PMMA) surfaces is described within this thesis. An optimized methodology for creating TmGH1-terminated surfaces which retain the bioactivity of the protein is presented. The surfaces were characterized for their chemical composition by X-ray photoelectron spectroscopy (XPS). Atomic force microscopy was used to probe the response of TmGH1 to mechanical force and it was used to image the surfaces characterized throughout this thesis. The methods presented here provide a platform for the use of PMMA as a substrate for thiol-terminated proteins for a variety of analytical or bio-physical chemistry applications.

An optimized methodology for the attachment of thiol-terminated proteins to PMMA has been developed in this work. The key features are an initial exposure of PMMA to hexamethyldiamine (in DMSO), which resulted in the formation of $-NH_2$ sites on the surface by aminolysis. These sites were then reacted with the hetero-bifunctional cross-linker Sulfo-EMCS. The N-hydroxysuccinimide ester terminal and maleimide terminal groups of Sulfo-EMCS could then react with surface amine groups and sulfhydryl-containing proteins respectively. A maleimide-terminated surface was then able to react with TmGH1 and phnH to create protein-terminated surfaces. It was important to ensure that the modification steps were successful and that the platform for protein adhesion could be used in a protein pulling experiment by AFM.

The XPS technique was used to determine the thickness and chemical composition of the modified samples. The C1s, O1s, N1s, and S2p regions of Mg Kα

XPS (1253.6 eV) scans were analyzed and compared between samples. The C1s spectra showed evidence for sequential modification of a PMMA surface as it was exposed to various chemical modifications. It was shown that features in the C1s region corresponded to surface chemistry, particularly in the ether (286 eV) and carbonyl region (~289 eV). The N1s spectra were extremely useful, since the sequential modification of PMMA added nitrogen to all of the surfaces. The O1s spectra was not as useful to the results, but the S2p region contained evidence of an orientation of TmGH1 on the surface, such that the sulfur containing terminal cysteine was pointing towards the surface. It is possible that methionine sulfur is contributing to the S2p signal as well, but it is thought that a majority of this type of S2p signal is attenuated by the bulk of the protein. Collectively, this data is evidence for a favorable covalent bond between TmGH1 and the maleimide group of the underlying Sulfo-EMCS-terminated surface.

The presence of a covalent bond between TmGH1 and modified-PMMA substrates could be probed through a protein pulling experiment using AFM. These particular experiments require a robust bond between the protein and the substrate, so that the proteins can properly resist the forces being applied to them by a retracting AFM tip. There was only one successful TmGH1-pulling experiment conducted, despite various attempts to do so. This success was due to the use of a dodecanethiol-terminated Au cantilever, which did not represent the traditional AFM method (unmodified silicon or silicon nitride cantilevers) – essentially, the experiment has become a chemical force microscopy (CFM) experiment. Deflection-extension curves were obtained and the data was classified and analyzed to obtain force-extension information about the probed TmGH1-terminated surface. TmGH1 seems to be adhered to the surface through a bonding regime (probably covalent) that is able to provide a platform for the protein to resist forces of 80 – 100 nN and extensions of ~10-60 nm. The fact that force-extension information could be obtained demonstrates the promise that the methodology presented in this thesis has for further experimentation with TmGH1-terminated surfaces. More detailed experiments are required to ensure reproducibility and to explore the various interactions that are possible with chemical force microscopy (CFM). This is a less developed technique within the field of protein response to mechanical force, but it has the potential to provide chemical information about protein surfaces (e.g. interaction forces, binding sites, etc.).

Protein-terminated surfaces have become important platforms for many analytical and biophysical experiments. The use of PMMA to develop a platform for TmGH1 is essential for the use of this protein within PMMA based analytical devices (e.g. microfluidics). Moreover, the use of PMMA as a substrate, rather than Au or Si means that a variety of routine experiments can become more affordable to researchers. It is also unique that a cross-linker was used to attach proteins to a modified-PMMA substrate. This opened the possibility that protein-pulling AFM experiments could be conducted without the need to engineer chains of repeating protein units. The ultimate goal is to probe a single protein in a manner that produces chemical information. The protein pulling results presented in this thesis is a contribution towards the further development of less complicated, and more chemically meaningful, protein-AFM studies.

References

1. Brown, L., Koerner, T., Horton, J. H., and Oleschuk, R. D.; *Lab Chip* **6**, 66-73 (2006).

2. Silvertand, L. H. H., Machtejevas, E., Hendriks, R., Unger, K.K., van Bennekom, W.P., and de Jong, G.J. *J. Chrom. B.;* **839**, 68-73 (2006).

3. Henry, A. C., Tutt, T.J., Galloway, M., Davidson, Y.Y., McWhorter, C.S., Soper, S.A., and McCarley, R.L.; *Anal. Chem.* **72**, 5331-5337 (2000).

4. Bai, Y., Koh, C.G., Boreman, M., Juang, Y.J., Tang, I.C., Lee, L.J., and Yang, T.; *Langmuir* **22**, 9458-9467 (2006).

5. Chen, S.H., Sung, W.C., Lee, G.B., Lin, Z.Y., Chen, P.W., and Liao, P.C.; *Electrophor.* **22**, 3972-3977 (2001).

6. Wang, B., Oleschuk, R. D., Petkovich, P. M., and Horton, J. H.; *Coll. Surf. B.: Biointerfaces* **55**, 107-114 (2007).

7. Tao, S. L., Lubeley, M. W., and Desai, T. A.; *J. Biomed. Mater.* **67A**, 369-375 (2003).

8. Fixe, F., Dufva, M., Telleman, P., and Christensen, C. B. V.; *Lab Chip* **3**, 191-195 (2004).

9. Wolfenden, R., Lu, X., and Young, G.; *J. Am. Chem. Soc.* **120**, 6814-6815 (1998).

10. Gloster, T. M., Macdonald, J.M., Tarling, C.A., Stick, R.V., Withers, S.G., and Gideon, D.J.; *J. Bio. Chem.* **47**, 49236-49242 (2004).

11. Best, R., B., Li, B., Steward, A., Daggett, V., and Clarke, J.; *Biophys. J.* **81**, 2344-2356 (2001).

12. Goddard, J. M., and Hotchkiss, J. H.; *Prog. Polym. Sci.* **32**, 698-725 (2007).

13. Strother, T., Cai, W., Zhao, X., Hamers, R. J., and Smith, L. M.; *J. Am. Chem. Soc.* **122**, 1205-1209 (2000).

14. Strother, R., Hamers, R. J., and Smith, L. M.; *Nuc. Acid. Res.* **28**, 3535-3541 (2000).

15. Boukherroub, R., and Wayner, D. D. M.; *J. Am. Chem. Soc.* **121**, 11513-11515 (1999).

16. Hauslling, L., Ringsdork, H., Schmitt, J., and Knoll, W.; *Langmuir* **7**, 1837-1840 (1991).

17. Patel, N., Davies, M.C., Hartshorne, M., Heaton, R.J., Roberts, C.J., Tendler, S.J.B., Williams, P.M.; *Langmuir* **13**, 6485-6490 (1997).

18. Ng, J. M. K., Gitlin, I., Stroock, A. D., and Whitesides, G. M.; *Electrophor.* **23**, 3461-3473 (2002).

19. Li, H., Oberhauser, A., F., Fowler, S., B., Clarke, J., and Fernandez, J., M. *PNAS* **97**, 6527-6531 (2000).

20. Pugmire, D. L., Waddell, E. A., Haasch, R., Tarlov, M. J., and Locascio, L. E.; *Anal. Chem.* **74**, 871-878 (2002).

21. Johnson, T. J., Ross, D., Gaitan, M., and Locascio, L. E.; *Anal. Chem.* **73**, 3656-3661 (2001).

22. Wang, B., Oleschuk, R. D., and Horton, J. H.; *Langmuir* **21**, 1290-1298 (2005).

23. Wang, B., Chen, L., Abdulali-Kanji, Z., Horton, J. H., and Oleschuk, R. D.; *Langmuir* **19**, 9792-9798 (2003).

24. Schulz, U., Munzert, P., and Kaiser, N.; *Surf. and Coat. Tech.* **142**, 507-511 (2001).

25. Patrito, N., McCague, C., Chiang, S., Norton, P. R., and Petersen, N. O. *Langmuir* **22**, 3453-3455 (2006).

26. van Saarfoos, Paul P., Vernon, C. F., Chirila, T. V., and Klauber, C.; *Poly. Bull.* **33**, 331-338 (1994).

27. Grimblot, J., Mutel, B., Moineau, V., Colson, T., Dessaux, O., Goudmand, P.; *Surf. Interface Anal.* **30**, 415-419 (2000).

28. Groning, P., Collaud, M., Dietler, G., and Schlapbach, L.; *J. Appl. Phys.* **76**, 887-892 (1994).

29. Cheng, J. Y., Wei, C. W., Hsu, K. H., and Young, T. H.; *Sensors and Actuators B* **99**, 186-196 (2004).

30. Barrett, T., Suresh, C. G., Tolley, S. P., Dodson, E. J., and Hughes, M. A.; *Structure* **3**, 9 (1995).

31. Fowler, S., B., Best, R.B., Toca Herrera, J.L., Rutherford, T.J., Steward, A., Paci, E., Karplus, M., Clarke, J.; *J. Mol. Bio.* **322**, 841-849 (2002).

32. Binnig, G., Quate, C. F., and Gerber, C.; *Phys. Rev. Lett.* **56**, 930-933 (1986).

33. Zhuang, X., and Rief, M.; *Curr. Op. in Struc. Bio.* **13**, 88-97 (2003).

34. Zlatanova, J., Lindsay, S. M., and Leuba, S. H.; *Prog. Biophys. and Mol. Bio.* **74**, 37-61 (2000).

35. Fotiadis, D., Scheuring, S., Muller, S. A., Engel, A., and Muller, D. J.; *Micron* **33**, 385-397 (2002).

36. Carrion-Vazquez, M., Oberhauser, A.F., Fowler, S.B., Marszalek, P.E., Broedel, S.E., Clarke, J., and Fernandez, J.M.; *Proc. Natl. Acad. Sci. USA* **96**, 3694-3699 (1999).

37. Oberhauser, A., F., Marszalek, P., E., Carrion-Vazquez, M., and Fernandez, J., M.; *Nature: struc. bio.* **6**, 1025-1028 (1999).

38. Yang, G., Cecconi, C., Baase, W.A., Vetter, I.R., Breyer, W.A., Haack, J.A., Matthews, B.W., Dahlquist, F.W., and Bustamante C.; *Proc. Natl. Acad. Sci. USA* **97**, 139-144 (2000).

39. Li, L., Wetzel, S., Pluckthun, A., and Fernandez, J. M.; *Biophys. Lett.* **90**, L30-L32 (2006).

40. Fisher, T., E., Oberhauser, A., F., Carrion-Vazquez, M., Marszalek, P.E., and Fernandez, J., M; *TIBS* **24**, 379-384 (1999).

41. Briggs, D., and Grant, J. T.; Surface Analysis by Auger and X-ray Photoelectron Spectroscopy. , 899 (2003).

42. Charles, D. W. *et al*. NIST X-ray Photoelectron Spectroscopy Database. (2005).

43. Ton-That, C., Shard, A. G., Teare, D. O. H., and Bradley, R. H.; *Polymer* **41**, 1121-1129 (2001).

44. Drummond, I. W. in *Surface Analysis by Auger and X-ray Photoelectron Spectroscopy* (eds. Briggs, D. & Grant, J. T.) 117-144 (IM Publications and SurfaceSpectra Ltd., Charlton, U.K., 2003).

45. Davies, G., and Henrissat, B.; *Structure* **3**, 853-859 (1995).

46. Kim, S. Y., and Kim, I. S.; *Structure* **11**, 121-127 (2004).

47. Zechel, D. *et al*.; *J. Am. Chem. Soc* **125**, 14313-14323 (2003).

48. Zhu, J., Withers, S. G., Reichardt, P. B., Treadwell, E., and Clausen, T. P.; *Biochem. J.* **332**, 367-371 (1998).

49. Vincent, F. *et al*.; *Chem. Bio. Chem.* **5**, 1596-1599 (2004).

50. Adams, E. L., Kroon, P. A., Williamson, G., Gilbert, H. J., and Morris, V. J.; *Carbo. Resear.* **339**, 579-590 (2004).

51. Alattia, J. R., Shaw, J. E., Yip, C. M., and Prive, G. G.; *CPNAS* **104**, 17394-17399 (2007).

52. Briggs, D., and Grant, J. T. in *Surface Analysis by Auger and X-ray Photoelectron Spectroscopy* (eds. Briggs, D. & Grant, J. T.) 1-30 (IM Publications and SurfaceSpectra Limited, Charlton, United Kingdom, 2003).

53. Moulder, J. F., Stickle, W. F., Sobol, P. E., Bomben, K., and Chastain, J.; Handbook of Photoelectron Spectroscopy (Perkin-Elmer, Physical Electronics Division, 1993).

54. Wagner, C.D. et al.; *Anal. Chem.* **51**, 466-482 (1979).

55. Schofield, J. H.; *J. Electron Spectrosc. Relat. Phenom.* **8**, 129 (1976).

56. Tanuma, S. in *Surface Analysis by Auger and X-ray Photoelectron Spectroscopy* (eds. Briggs, D. & Grant, J. T.) 259-294 (IM Publications and SurfaceSpectra Ltd., Charlton, U.K., 2003).

57. Powell, C. J.; and Jablonski, A.; *Surface and Interface Analysis* **33**, 211-229 (2002).

58. Seah, M. P. in *Surface Analysis by Auger and X-ray Photoelectron Spectroscopy* (eds. Briggs, D. and Grant, J. T.) 345-376 (IM Publications and SurfaceSpectra Ltd, Charlton, U.K., 2003).

59. Grant, J. T. in *Surface Analysis by Auger and X-ray Photoelectron Spectroscopy* (eds. Briggs, D. and Grant, J. T.) 57-88 (IM Publications and SurfaceSpectra Ltd., Charlton, U.K., 2003).

60. Seah, M. P. in *Surface Analysis by Auger and X-ray Photoelectron Spectroscopy* (eds. Briggs, D. and Grant, J. T.) 167-190 (IM Publications and SurfaceSpectra Ltd., Charlton, U.K., 2003).

61. Briggs, D. in *Surface Analysis by Auger and X-ray Photoelectron Spectroscopy* (eds. Briggs, D. and Grant, J. T.) 31-56 (IM Publications and SurfaceSpectra Ltd., Charlton, U.K., 2003).

62. Fairley, N. in *Surface Analysis by Auger and X-ray Photoelectron Spectroscopy* (eds. Briggs, D. and Grant, J. T.) 397-420 (IM Publications and SurfaceSpectra Ltd., Charlton, U.K., 2003).

63. Geller, J. in *Surface Analysis by Auger and X-ray Photoelectron Spectroscopy* (eds. Briggs, D. and Grant, J. T.) 89-116 (IM Publications and SurfaceSpectra Ltd., Charlton, U.K., 2003).

64. Kudo, M. in *Surface Analysis by Auger and X-ray Photoelectron Spectroscopy* (eds. Briggs, D. and Grant, J. T.) 145-166 (IM Publications and SurfaceSpectra Ltd., Charlton, U.K., 2003).

65. Tougaard, S. in *Surface Analysis by Auger and X-ray Photoelectron Spectroscopy* (eds. Briggs, D. and Grant, J. T.) 295-344 (IM Publications and SurfaceSpectra Ltd., Charlton, U.K., 2003).

66. Shirley, D. A.; *Phys. Rev. B.* **5**, 4709 (1972).

67. Proctor, A. and Sherwood, P. M. A.; *Anal. Chem.* **54**, 13-19 (1982).

68. Vegh, J.; *Surf. Sci.* **57**, 220-228 (2005).

69. Tougaard, S.; *Surf. Sci.* **216**, 343 (1989).

70. Tougaard, S.; *Surf. Interface Anal.* **11**, 453 (1988).

71. Tougaard, S.; *Solid State Comm.* **61**, 547 (1987).

72. Tougaard, S.; *Surf. Interface Anal.* **25**, 137 (1997).

73. Thermo Fisher Scientific Ltd.; Avantage. **2.0**.

74. Powell, M. J. D.; *The Computer Journal* **7**, 155-162 (1964).

75. Edgell, M. J., Paynter, R. W., and Castle, J. E.; *Surf. Interface Anal.* **8**, 113 (1986).

76. Doniach, S. and Sunjic, M.; *J. Phys. C.* **3**, 285 (1970).

77. Wagner, C. D. *et al*.; *Surf. Interface Anal.* **3**, 211 (1981).

78. Adams, M. A. *et al*.; *Journal of Bacteriology* **190**, 1072-1083 (2008).

79. Kelly, M. A. in *Surface Analysis by Auger and X-ray Photoelectron Spectroscopy* (eds Briggs, D. and Grant, J. T.) 191-210 (IM Publications and SurfaceSpectra Ltd., Charlton, U.K., 2003).

80. Yip, J., Chang, K., Sin, K. M., and Lau, K. S.; *Appl. Surf. Sci.* **205**, 151-159 (2003).

81. Thornburg, D. M., and Madix, R. J.; *Surf. Sci.* **226**, 61-76 (1990).

82. Wan, Y. Z. *et al*.; *J. App. Pol. Sci.* **99**, 949-956 (2006).

83. Lebugle, A., Rovira, M., Rabaud, M., and Rey, C.; *Journal of Mat. Sci. : Mat. in Med.* **7**, 223-226 (1996).

84. Baer, D. R., Englehard, M. H., Lea, A. S., and Gaspar, D. J. in *Surface Analysis by Auger and X-ray Photoelectron Spectroscopy* (eds. Briggs, D. and Grant, J. T.) 843-856 (IM Publications and SurfaceSpectra Ltd., Charlton, U.K., 2003).

85. Sandhyarani, N. and Pradeep, T.; *Chem. Phys. Lett.* **13**, 33-36 (2001).

86. Cavalleri, O., Oliveri, L., Dacca, A., Parodi, R. and Rolandi, R.; *Appl. Surf. Sci.* **175-176**, 357-362 (2001).

87. Fixe, F., Dufva, M., Telleman, P., and Christensen, C. B. V. *Nuc. Acids Res.* **32**, (2004).

88. Binnig, G., Quate, C. F., and Gerber, C.; *Phys. Rev. Lett.* **56**, 930-933 (1986).

89. Maganov, S. N. and Whangbo, M.H. in *Surface Analysis with STM and AFM* (VCH, Weinheim, 1994).

90. Noy, A., Vezenov, D. V., and Lieber, C. M.; *Annu. Rev. Mater. Sci.* **27**, 381-421 (1997).

91. Sader, J. E., Chon, W. M., and Mulvaney, P.; *Rev. Sci. Instrum.* **70**, 3967 (1999).

92. Cleveland, J. P., Manne, S., Bocek, D., and Hansma, P. K.; *Rev. Sci. Instrum.* **64**, 403 (1993).

93. Hutter, J. L., and Bechhoefer, J.; *Rev. Sci. Instrum.* **64**, 1868 (1993).

94. Li, H., Carrion-Vazquez, M., Oberhauser, A. F., Marszalek, P. E., and Fernandez, J. M.; *Nature: struc. bio.* **7**, 1117-1120 (2000).

95. Mengistu, T. Z., Goel, V., Horton, J. H., and Morin, S.; *Langmuir* **22**, 5301-5307 (2006).

96. Ratner, B.D.; *Ann. Biomed. Eng*. **11**, 313-336. (1983).

97. Merrett, K., Cornelius, R.M., McClung, W.G., Unsworth, L.D., and Sheardown, H.; *J. Biomat. Sci*. **13**, 593-621 (2002).

98. Margalit, R. and Vasquez, R.P.; *J. Protein. Chem.* **1**, 105-8 (1990).

99. Browne, M.M., Lubarsky, G.V., Davidson, M.R., and Bradley, R.H.; *Surf. Sci*. **553**, 155-167 (2004).

100. Ratner, B.D.; *Surf. Inter. Anal*. **23**, 521-528 (2004).

101. Selmer, M., Al-Karadaghi, S., Hirokawa, G., Kaji, A.; *Science* **17**, 2349-2352 (1999).

102. Rief, M., Gautel, M., Oesterhelt, F., Fernandez, J.M., Gaub, H.E.; *Science* **276**, 1109-1112 (1997)

Appendix A

XPS Datasheet

The table contained in this appendix summarizes the general data from all the XPS samples considered for this thesis. There are some points to consider before viewing this table:

- Charging effects were determined from calibrating peaks to the Au 4f 7/2 peak (84.0 eV) and the C1s peak (285.0 eV) adn the error is approximately 0.25 eV (resolution of the spectrometer) for each individual value.
- The thickness values are explained in section 3.1.
- The only samples that were exposed to 1 M sulphuric acid were those with the label prefix ‘PMMA OX’.
- With the exception of the entries labelled with a star, the cross-linker/buffer solutions were reacted with the substrates for 2 hours. All other exposures to the protein buffer solutions took place for 30 minutes.
- All the N1s and S2p XPS spectra for samples prior to S1 were taken with a dwell time of 60 ms and all samples after this one used a value of 120 ms.

									Charging Effects (eV)				
Full Descriptive Label	Label	Number of Drops of PMMA in CH_2Cl_2	Droplets (µL)	[Ethylene-diamine] (M)	Amination/Oxidation Treatment time (min)	Temp. (K)	[Sulfo-EMCS] (mM)	[Protein]	Au 4f$_{7/2}$ peak	C1s peak #1	Valence Background (counts/s)	Ratio (VBs/Vbo)	Thickness (nm)
Flame Annealed Au Blank	J					298			20	19.62	11511	1.00	0.00
Au Blank	I					298			10.61	9.85	11233	0.98	0.55
PMMA Control 1	A1	2	200	0	0	298			8.51	8.23	10735	0.93	0.87
PMMA Control 2	A2	2	200	0	0	298			8.23	8.18	10449	0.91	1.07
PMMA Control 3	A3	2	200	0	0	298			10.36	10.09	11460	1.00	0.79
PMMA Control 4	A4	2	200	0	0	298			7.78	7.56	9376	0.81	1.81
PMMA Control 5	A5	2	200	0	0	298			8.54	8.31	9952	0.86	1.28
PMMA Control 6	A6	2	200	0	0	298			9.27	9.09	10929	0.95	1.09
PMMA 1 x200 µL	R1	1	200	0	0	298			9.2	8.51		0.00	
PMMA 1 x 100 µL	R2	1	100	0	0	298			8.61	8	8963	0.78	1.89
PMMA3 x 100 µL	R3	3	100	0	0	298			7.23	7.38	8249	0.72	2.30
PMMA6 x 100 µL	R4	6	100	0	0	298			8.38	8.22	8965	0.78	1.93
PMMA OX 1 min 298K	S1	1	200	0	1	298			0.97	-0.05	6387	0.55	4.46
PMMA OX 5 min 298K	S2	1	200	0	5	298			3.76	1.6	7543	0.66	2.52
PMMA OX 20 min 298K	S3	1	200	0	20	298			9.76	8.58	6353	0.55	2.42
PMMA OX 20 min 333K	S4	1	200	0	20	333			0.56	-0.41	11758	1.02	2.54
Round 1 Aminated 1 min 298K 1.0 M 60 ms	B1	3	100	1	1	298			4.85	5.41	6876	0.60	3.85
Round 1 Aminated 5 min 298K 1.0M 60 ms	T1	3	100	1	5	298			6.14	6.38	8769	0.76	1.72
Round 1 Aminated 20 min 298K 1.0M 60 ms	T2	3	100	1	20	298			4.9	5.18	8082	0.70	2.66
Round 2 Aminated 5 min 298K 1.0M 120 ms	U1	3	100	1	5	298			6.59	6.61	8732	0.76	2.32
Round 2 Aminated 20 min 298K 1.0M 120 ms	U2	3	100	1	20	298			5.68	5.98	9026	0.78	2.19
Round 2 Aminated 20 min 298K 2.0M 120 ms	U3	3	100	2	20	298			6.43	6.72	9358	0.81	1.49
Aminated 3rd Round PMMA	V1	3	100	0	0	298			7.98	7.97	9692	0.84	1.80
Aminated 3rd Round 5 min 1M NH2 298K	V2	3	100	1	5	298			7.32	7.26	8286	0.72	1.80
Aminated 3rd Round 20 min 1M NH2	V3	3	100	1	20	298			7.94	7.98	10058	0.87	1.84
Amination 1 - 1 min 298 K	B2	2	200	1	1	298			8.48	8.38	10499	0.91	0.72
Amination 1 - 2 min 298 K	W1	2	200	1	2	298			8.94	8.68			
Amination 1 - 5 min 298 K	W2	2	200	1	5	298			8.44	8.27	9887	0.86	1.48
Amination 2 - 1 min 298 K	B3	2	200	1	1	298			8.53	8.37			
Amination 3 - 2 min 298 K	W3	2	200	1	2	298			10.26	10.33	10983	0.95	0.54
Amination 4 - 5 min 298 K	W4	2	200	1	5	298			7.73	7.62	9282	0.81	1.18
Amination 5 - 10 min 298 K	W5	2	200	1	10	298			8.33	8.41	9982	0.87	0.96
Amination 6 - 20 min 298 K	W6	2	200	1	20	298			10.03	9.76			

Full Descriptive Label	Label	Number of Drops of PMMA in CH_2Cl_2	Droplets (µL)	[Ethylene-diamine] (M)	Amination/Oxidation Treatment time (min)	Temp. (K)	[Sulfo-EMCS] (mM)	[Protein]	Charging Effects (eV)		Valence Background (counts/s)	Ratio (VBs/Vbo)	Thickness (nm)
									Au $4f_{7/2}$ peak	C1s peak #1			
DT # 1 PMMA Blank (1 x 200 µL)	K1	1	200	0	0	298			7.33	7.6	9430	0.82	1.88
DT #2 1 x 200uL 1 min NH2, 298K	X1	1	200	1	1	298			7.26	7.43	9365	0.81	1.90
DT #3 2 x 200uL 1 min NH2, 298K	B4	2	200	1	1	298			7.28	7.5	10131	0.88	1.71
DT #4 3 x 200uL 1 min NH2, 298K	X2	3	200	1	1	298			8.34	8.59	10799	0.94	1.24
CLET#1 1 min NH2, 298K, <0.1mM CL	M1	2	200	1	1	298	<0.1 *		6.16	6.37	8749	0.76	2.31
CLET#2 2 min NH2, 298K, <0.1mM CL	M2	2	200	1	2	298	<0.1 *		6.53	6.4	8068	0.70	2.60
CLET#3 3 min NH2, 298K, <0.1mM CL	M3	2	200	1	3	298	<0.1 *		6.79	6.79	7487	0.65	3.12
CLE#1 1 min NH2, 298K, 0.1mM	Y1	2	200	1	1	298	0.1		5.83	5.96			
CLE#2 1 min NH2, 298K, 0.1mM	Y2	2	200	1	1	298	0.1		8.1	8.18			
CLE#3 1 min NH2, 298K, 0.1mM	Y3	2	200	1	1	298	0.1		7.81	7.92			
CLE#4 1 min NH2, 298K, 1mM	Y4	2	200	1	1	298	1.0		5.83	6.01			
CLE#5 1 min NH2, 298K, 1mM	Y5	2	200	1	1	298	1.0		8.01	8.3			
CLE#6 1 min NH2, 298K, 1mM	Y6	2	200	1	1	298	1.0		7.32	7.55			
CLE#7 1 min NH2, 298K, 10mM	Y7	2	200	1	1	298	10.0		5.65	5.84			
CLE NH2 Blank 1 min NH2 298K	Y8	2	200	1	1	298			8.34	8.37			
CLE Au Blank	Y9	2	200	0	0	298			7.61	6.99			
CLE2 #1 PMMA Blank	K2	2	200	0	1	298			6.29	6.33	8583	0.75	2.56
CLE2 #2 1 min NH2, 40C, 1mM CL	C1	2	200	1	1	333	1.0		6.52	6.46	7975	0.69	3.11
CLE2 #3 1 min NH2, 40C, 1mM CL	C2	2	200	1	1	333	1.0		7.68	7.61	8432	0.73	2.88
CLE2 #4 1 min NH2, 40C, NaOH, 1mM CL	N	2	200	1	10	333	1.0		5.73	5.74	7654	0.66	2.99
CLE2 #5 10 min NH2, 40C, 1mM CL	O1	2	200	1	10	333	1.0		7.3	7.1	7891	0.69	2.72
CLE2 #6 10 min NH2, 40C, 1mM CL	O2	2	200	1	10	333	1.0		8.08	7.71	9462	0.82	1.35
CLE2 #7 10 min NH2, 40C, NaOH, 1mM CL	P	2	200	1	1	333	1.0		7.02	6.55	7923	0.69	2.48
TmGH1 #1 1 min NH2, 298K, 1mMCL	D1	2	200	1	1	298	1.0	3.73 µM	4.63	4.64	6246	0.54	7.23
TmGH1 #2 1 min NH2, 298K, 1mMCL	D2	2	200	1	1	298	1.0	3.73 µM	4.31	4.53	7534	0.65	5.46
TmGH1 #3 1 min NH2, 298K, 1mMCL	D3	2	200	1	1	298	1.0	3.73 µM	4.65	4.64	7322	0.64	6.38
TmGH1 #4 1 min NH2, 298K, 1mMCL	D4	2	200	1	1	298	1.0	3.73 µM	4.66	4.67	7051	0.61	6.22
phnH (7.2µm)	Q	2	200	1	1	298	1.0	7.2 µM	3.62	3.76	4402	0.38	13.78
phnH (1.66µm) #1	E1	2	200	1	1	298	1.0	1.66 µM	4.02	4.16	7067	0.61	6.64
phnH (1.66µm) #2	E2	2	200	1	1	298	1.0	1.66 µM	3	3.54	3249	0.28	16.72
TmGhH1 on Au/mica	F1	2	200	1	1	298		3.73 µM	16.33	16.49	8900	0.77	4.39
TmGhH1 on Au/mica	F2	2	200	1	1	298		3.73 µM	16.17	16.59	9744	0.85	4.68
TmGH1 on PMMA	G	TmGH1 on PMMA directly without modification for 30 minutes				298		unk.	20.72	20.84	10955	0.95	2.89
TmGH1 on NH2 - PMMA multiple C1s peaks	H1	TmGH1 on NH2 PMMA directly without modification for 30				298		unk.	17.83	17.74	9471	0.82	4.69
TmGH1 on NH2 - PMMA one set of C1s peaks	H2	TmGH1 on NH2 PMMA directly without modification for 30 minutes (unknown TmGH1 concentration but higher than usual) -				298		unk.	16.93	16.77	8479	0.74	5.20

Appendix B

Electron Attenuation Length NIST Database

Database Program Obtained From:

C.J. Powell and A.Jablonski, *NIST Electron Effective-Attenuation Length Database* – Version 1.1, National Institute of Standards and Technology Gaithersburg, MD (2003)

In order to determine the practical electron attenuation length and the means escape depth values necessary to determine the thickness of PMMA on Au, the following parameters were entered into the NIST EAL Database Program (footnotes apply to some parameters; also note that the same procedure can be modified to address the other elements or EAL issues discussed in this thesis):

Input Parameters entered:

Electron Kinetic Energy = 969 eV[1] (for C – for O, N or other elements see footnote)
$\beta = 2.00$[2]
Name: PMMA
Stoichiometric Coefficients: C:H:O is 5:8:2 (based on a PMMA fragment)
Formula: G-1 equation from Gries[3] (Gries, W. H., Surf. Interface Anal. 24, 38 (1996))
Length unit: Nanometers
Density of PMMA: 1.19 g/cm^3 (from a MSDS provided from Bangs Laboratory)
Detector/Sample Angle: 60^0
Type of Practical EAL value:
    Overlayer Thickness (as opposed to a depth of a thin layer)[4]

---

[1] This value is approximately equal to the Mg Kα energy minus the binding energy of the element (in the case of carbon: 284.4 eV) Carbon provides the bulk of the PMMA structure, so it is probably practical to use it as the value for the electron energy. The value for the C binding energy was found in Appendix A of the NIST database user's guide.

[2] This was the recommended value for C, based on Appendix A of the NIST database user's manual

[3] This formula was recommended by the user guide for studies that require a practical EAL.

[4] The question asks for a thickness determination, so I thought that this was the most appropriate parameter to use here.

After entering these values, Practical EAL values were calculated for a variety of thicknesses. I chose a thickness halfway between 0 and 28 nm to calculate the Average Practical EAL value. It should be noted that the EAL values for PMMA at an electron energy of 969 eV are generally the same across all thicknesses.

Results, Related Parameters and Input Parameters shown on results screen:

Results

Practical EAL: 2.69 nm (for a film of 14 nm)
Substance signal intensity: 5.49×10^{-1} % of value for uncovered substrate
Average EAL (Lave): 2.702 nm (for film thickness between 1 – 14 nm)

Related Parameters:

Mean escape depth: 2.747 nm
EAL for quantitative analysis: 2.875
$Q_x = 0.989$ [5]

Input Parameters shown on results screen:

Energy : 969 eV
IMFP: 2.852
TMFP: 40.88
Alpha: 0
Theta: 60
Beta: 2

How the program calculated the IMFP λ value (or Practical EAL λ if elastic scattering is considered)

The program calculates the Practical EAL by first finding the IMFP (λ) using G-1 Equation[6] :

---

[5] This value is a correction term that accounts for reduce yield of photoelectrons due to elastic electron scattering (from user's manual)

[6] Gries, W. H.; *Surf. Interface Anal.* **24**, 38 (1996).

$$\lambda = 10k_1(V_a / Z^*)E/(\log E - k_2)$$

where λ is the IMFP (inelastic mean free path), $k_1 = 0.0018$ for organic compounds like PMMA, $k_2 = 1.00$ for organic compounds like PMMA[7], (both k_1 and k_2 will be discussed later), E is the electron energy, V_a is the atomic volume (in $cm^3\ mol^{-1}$; $V_a = M/\rho$, where M is the molecular mass and ρ is the density of the substance), but it is calculated in a different way for multi-element samples as discussed below. The value Z^* is "empirically" equal to $Z^{1/2}$, where Z is the atomic number of an element.[8] In order to translate this parameter to multi-element substances, it seems that Gries employed a summation of relevant terms. The same approach was taken to convert the atomic volume to V_a, which is the atomic volume of multiple elements:

$$Z^* = (pZ_A^{1/2} + qZ_B^{1/2} + ... + Z_C^{1/2})/(p + q + ... + r)$$

$$V_A = (pM_A + qM_B + ... + rM_C)/\rho(p + q + ... + r)$$

where, the formulas related to a compound $A_pB_q...C_r$, thus A, B, … C are elements and p, q … r are stoichiometric coefficients. The values $Z_A....Z_c$ and $M_A....M_C$ are, respectively, the corresponding atomic numbers and molecular weights of the elements in the compounds.

---

[7] From Appendix A of user's manual in the section on the "G-1 Equation of Gries". They are both just a fitting parameters within the equation and were found from fits of the Gries equation to that of Tanuma *et al.* (The TPP-2M Equation of Tanuma, Powell and Penn; for further explanation, see the user manual of the NIST EAL database)

[8] NIST EAL Database user's manual, page EAL-41

Shigeo Tanuma, in Briggs *et al.*[9] indicates that k_1 is found by using the following formula:

$$k_1 = \frac{5.24 \times 10^{-5} Z^*}{\beta N_v} = \frac{1.51 \times 10^{-3} Z^{1/2}}{M_{tot}^2}$$

Please note that some of the variables are familiar and that the β value is one of the input parameters of the EAL Database program. N_v is the number of valence electrons per molecule in the material. And for k_2

$$k_2 = - \log \gamma$$

I am not sure what γ stands for and may have missed it in the literature. Regardless, $k_1 = 0.0018$ and $k_2 = 1$ for organic compounds. A table in Tanuma's article in Briggs *et al*. (page 269) indicates the values of k_1 and k_2 for a variety of compounds.

From the above description of the G-1 formula, we can already see that some of my input parameters are linked to the formula. Identification of the elements in a studied compound is necessary to determine V_a and Z^*. Stoichiometric coefficients of PMMA, along with its density were also entered. The electron energy, E, and beta value was entered. The parameters k_1 and k_2 were automatically chosen.

---

[9] Briggs and Grant. Surface Analysis by Auger and X-ray Photoelectron Spectroscopy. (IM Publications; UK, 2003)

The practical EAL was determined using an equation identified in the NIST EAL Database user's manual. Now, as Tanuma explains, the Practical EAL equation is related to the Local EAL equation, but in the former case elastic scattering contributions are taken into account. :

$$L = \frac{1}{\cos\alpha}\frac{t}{\ln I_s^0 - \ln I_s)} = \frac{1}{\cos\alpha}\frac{t}{[\ln\int_0^\infty \phi(z,\alpha)dz - \ln\int_r^\infty \phi(z,\alpha)dz]}$$

where α is the angle between the sample and the detector with respect to the surface normal, t is the thickness of the overlayer, I_s^0 is the intensity of the uncovered substrate, I_s is the intensity of the covered substrate. The symbol φ (z, α) is the emission depth distribution function (EDDF); this is a term that applies to a measured signal from a surface and it is the probability that a "particle leaving the surface in a specific state and direction, originated from a specific depth measured normally from the surface to the material".[10] Essentially this equation is relating the difference between the logarithm of the entire EDDF and the logarithm of the EDDF at a specific thickness to each other. Methods for calculating the EDDF are given in the Tanuma article on page 284. The output of this equation is the distance by which the EDDF (or photoelectron signal intensity) is close to the value of $e^1 = 2.71$.

The above was a general overview and explanation of the formulae used to calculate the practical EAL in the NIST EAL database program.

---

[10] Tanuma in Briggs *et al.* (2003), page 261.

Thickness of the PMMA Layers

Using the calculated Practical EAL value from the NIST database program, 2.69 nm, we can calculate the overlayer thickness using the following formula:

$$t = \lambda \cos \alpha \ln\left(\frac{I_s}{I_0}\right)$$

where t is the thickness of the overlayer, λ is the average practical EAL[11], α is the angle between the detector and the sample with respect to the sample normal, I_s is a peak signal from the sample with the overlayer, and I_0 is the peak signal from the control sample (no overlayer). I will use values $\lambda = 2.69$ nm and $\alpha = 60^0$. The results of my calculations are shown in Appendix A.

Errors and Considerations of the Practical EAL calculations and thickness values

There are a number of uncertainties involved with the Practical EAL values and EAL values in general that are calculated using the NIST database. The assumption that the overlayer and the underlying substrate have similar electron scattering properties (e.g. IMFP values) would not be entirely valid for an overlayer of PMMA on Au. The IMFP for Au is approximately 7.4 nm, which is about four times the calculated Practical EAL value for PMMA. This difference in IMFP value introduces an uncertainty. Another uncertainty is introduced by the angle between the detector and the sample.

---

[11] Briggs and Grant. (2003), page 288.

According to the NIST EAL database handbook, angles of less than 60 degrees introduces errors of 1 – 4% and angles larger than 60^0 (like that used in the XPS spectrometer in Chernoff (~75^0)) have larger uncertainties. Surface structure is also an uncertainty, since no surface is uniformly flat and various thicknesses along the surface would change the Practical EAL of ejected photoelectrons from the bulk.

I chose to use the G-1 formula to calculate the Practical EAL in this exercise, despite the indication that the TPP formula of Tanuma, Powell and Penn could be more accurate.[12] The attractive benefit of the G-1 formula is the density of PMMA was the only physical requirement to enter into the program. The TPP-2M formula would have required an estimate of the number of valence electrons per molecule of the material and the band-gap energy. I am sure that these values could be found in the literature, particularly the latter, since XPS studies on PMMA are well known. The limitations of the G-1 formula are described in the paper in footnote 12. The G-1 formula is inaccurate in the range of 50 – 200 eV, but this is not a consideration for PMMA photoelectrons having an energy near that of carbon. Also, the G-1 formula is affected by material dependences and discrepancies between the G-1 value and optical data is up to 55% (see Table 2.1 in Tanuma *et al.*[13]) for some samples. In Table 3.1 of the cited paper, the Gries model was used to calculate the M_{tot}^2 term in the formula for PMMA and the uncertainty was 8% for this calculation. This may be caused by unaccounted physical effects in the studied sample, which according to NIST might include surface-electronic

---

[12] Tanuma, S, Powell, C. J., Penn, D. R.; *Surface and Interface Analysis* (1997), 25(1), 25-35.

[13] Tanuma, S, Powell, C. J., Penn, D. R.; *Surface and Interface Analysis* (1997), 25(1), 25-35.

excitation and surface refraction. The TPP-2M is recommended due to proof that it is a more applicable formula, but it is also inconvenient to use as it required input parameters relating to non-bulk quantities.

Appendix C

Force Curve Data (Summary Table)

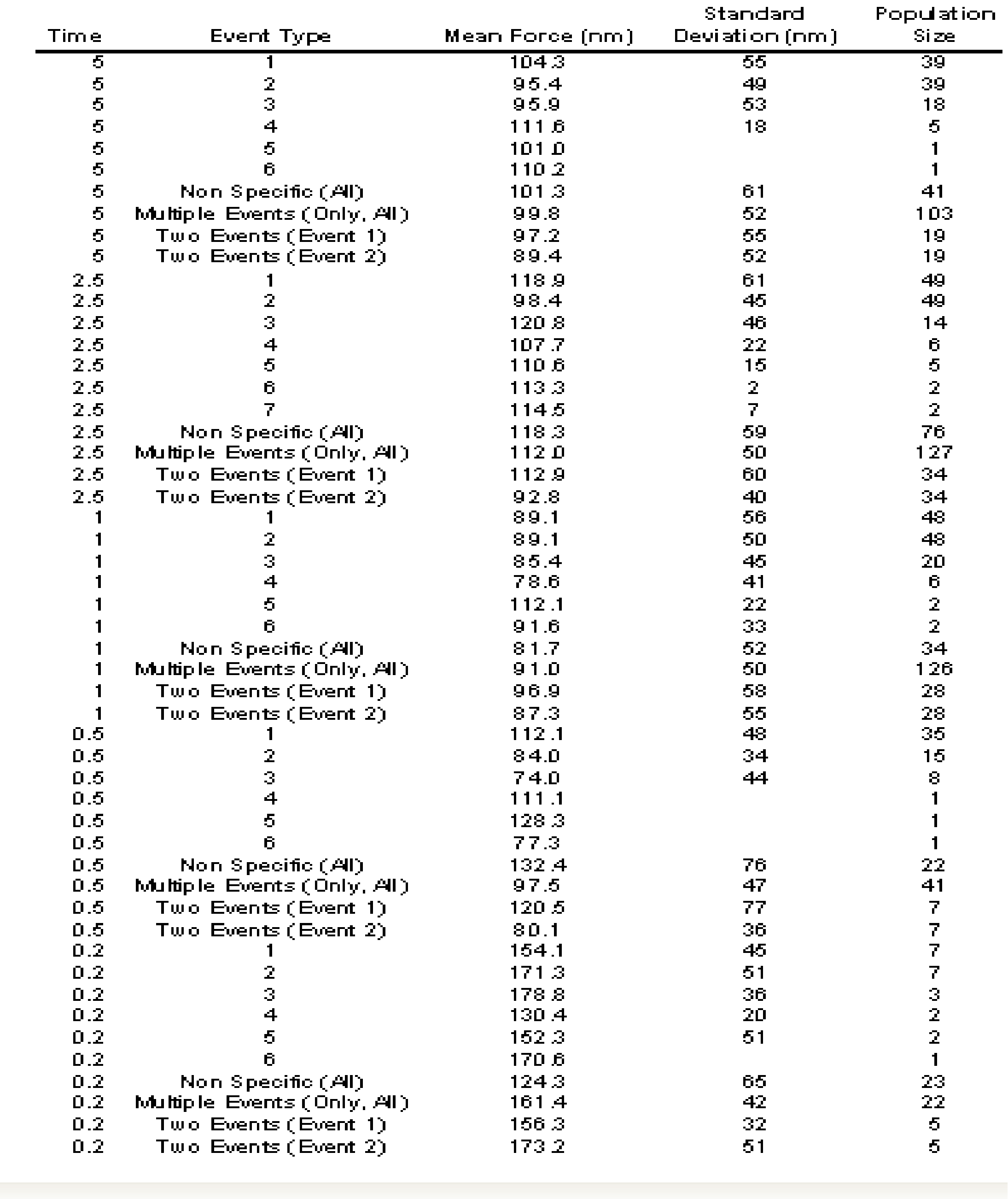

Time	Event Type	Mean Force (nm)	Standard Deviation (nm)	Population Size
5	1	104.3	55	39
5	2	95.4	49	39
5	3	95.9	53	18
5	4	111.6	18	5
5	5	101.0		1
5	6	110.2		1
5	Non Specific (All)	101.3	61	41
5	Multiple Events (Only, All)	99.8	52	103
5	Two Events (Event 1)	97.2	55	19
5	Two Events (Event 2)	89.4	52	19
2.5	1	118.9	61	49
2.5	2	98.4	45	49
2.5	3	120.8	46	14
2.5	4	107.7	22	6
2.5	5	110.6	15	5
2.5	6	113.3	2	2
2.5	7	114.5	7	2
2.5	Non Specific (All)	118.3	59	76
2.5	Multiple Events (Only, All)	112.0	50	127
2.5	Two Events (Event 1)	112.9	60	34
2.5	Two Events (Event 2)	92.8	40	34
1	1	89.1	56	48
1	2	89.1	50	48
1	3	85.4	45	20
1	4	78.6	41	6
1	5	112.1	22	2
1	6	91.6	33	2
1	Non Specific (All)	81.7	52	34
1	Multiple Events (Only, All)	91.0	50	126
1	Two Events (Event 1)	96.9	58	28
1	Two Events (Event 2)	87.3	55	28
0.5	1	112.1	48	35
0.5	2	84.0	34	15
0.5	3	74.0	44	8
0.5	4	111.1		1
0.5	5	128.3		1
0.5	6	77.3		1
0.5	Non Specific (All)	132.4	76	22
0.5	Multiple Events (Only, All)	97.5	47	41
0.5	Two Events (Event 1)	120.5	77	7
0.5	Two Events (Event 2)	80.1	36	7
0.2	1	154.1	45	7
0.2	2	171.3	51	7
0.2	3	178.8	36	3
0.2	4	130.4	20	2
0.2	5	152.3	51	2
0.2	6	170.6		1
0.2	Non Specific (All)	124.3	65	23
0.2	Multiple Events (Only, All)	161.4	42	22
0.2	Two Events (Event 1)	156.3	32	5
0.2	Two Events (Event 2)	173.2	51	5

Table C1: Summary of force data for specific and non-specific tip-sample interactions between a dodecanethiol-modified Au tip and a TmGH1-terminated sample. Reasonable events were chosen as indicated in section 5.2.2

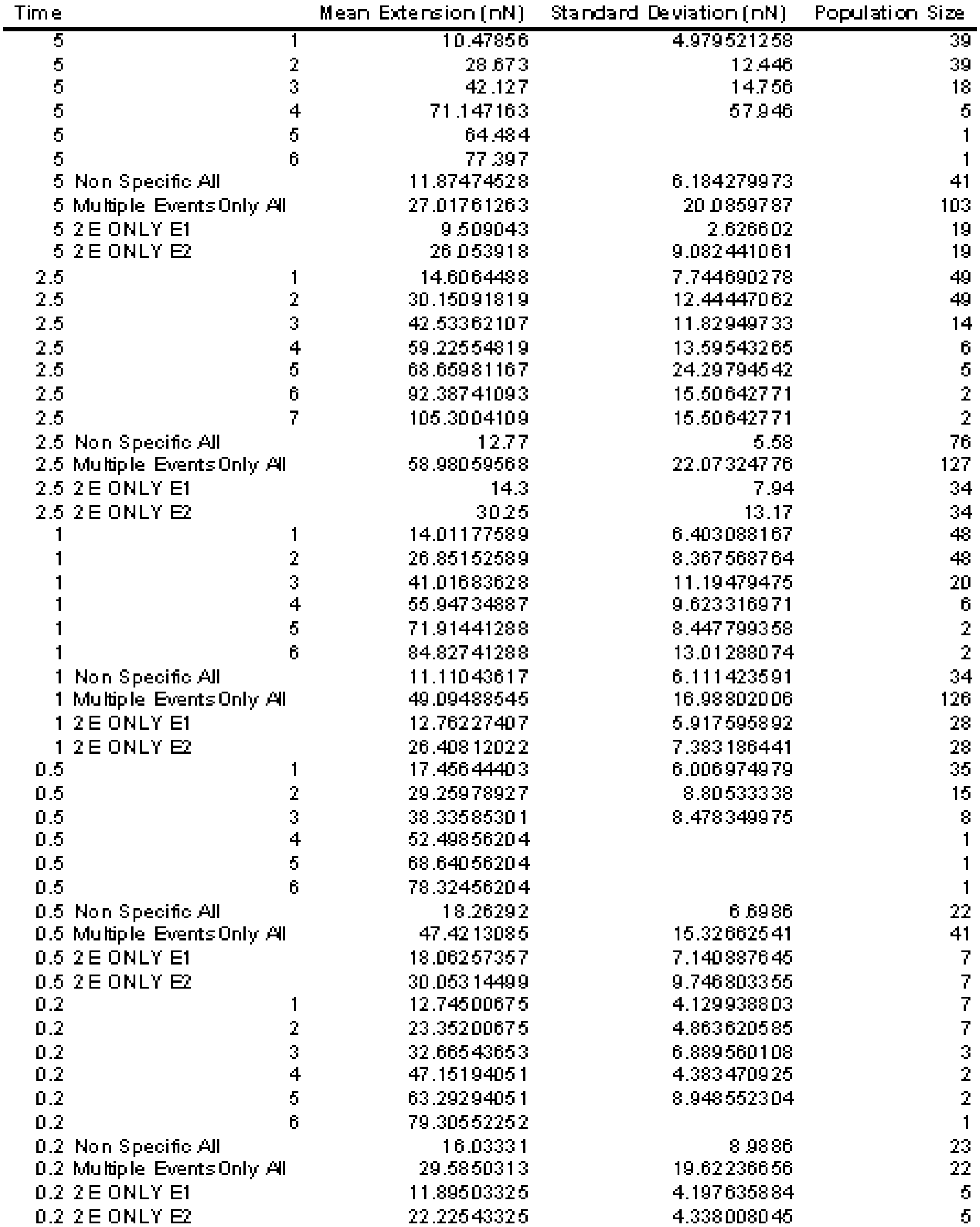

Time		Mean Extension (nN)	Standard Deviation (nN)	Population Size
5	1	10.47856	4.979521258	39
5	2	28.673	12.446	39
5	3	42.127	14.756	18
5	4	71.147163	57.946	5
5	5	64.484		1
5	6	77.397		1
5	Non Specific All	11.87474528	6.184279973	41
5	Multiple Events Only All	27.01761263	20.0859787	103
5	2 E ONLY E1	9.509043	2.626602	19
5	2 E ONLY E2	26.053918	9.082441061	19
2.5	1	14.6064488	7.744690278	49
2.5	2	30.15091819	12.44447062	49
2.5	3	42.53362107	11.82949733	14
2.5	4	59.22554819	13.59543265	6
2.5	5	68.65981167	24.29794542	5
2.5	6	92.38741093	15.50642771	2
2.5	7	105.3004109	15.50642771	2
2.5	Non Specific All	12.77	5.58	76
2.5	Multiple Events Only All	58.98059568	22.07324776	127
2.5	2 E ONLY E1	14.3	7.94	34
2.5	2 E ONLY E2	30.25	13.17	34
1	1	14.01177589	6.403088167	48
1	2	26.85152589	8.367568764	48
1	3	41.01683628	11.19479475	20
1	4	55.94734887	9.623316971	6
1	5	71.91441288	8.447799358	2
1	6	84.82741288	13.01288074	2
1	Non Specific All	11.11043617	6.111423591	34
1	Multiple Events Only All	49.09488545	16.98802006	126
1	2 E ONLY E1	12.76227407	5.917595892	28
1	2 E ONLY E2	26.40812022	7.383186441	28
0.5	1	17.45644403	6.006974979	35
0.5	2	29.25978927	8.80533338	15
0.5	3	38.33585301	8.478349975	8
0.5	4	52.49856204		1
0.5	5	68.64056204		1
0.5	6	78.32456204		1
0.5	Non Specific All	18.26292	6.6986	22
0.5	Multiple Events Only All	47.4213085	15.32662541	41
0.5	2 E ONLY E1	18.06257357	7.140887645	7
0.5	2 E ONLY E2	30.05314499	9.746803355	7
0.2	1	12.74500675	4.129938803	7
0.2	2	23.35200675	4.863620585	7
0.2	3	32.66543653	6.889560108	3
0.2	4	47.1519405 1	4.383470925	2
0.2	5	63.29294051	8.948552304	2
0.2	6	79.30552252		1
0.2	Non Specific All	16.03331	8.9886	23
0.2	Multiple Events Only All	29.5850313	19.62236656	22
0.2	2 E ONLY E1	11.89503325	4.197635884	5
0.2	2 E ONLY E2	22.22543325	4.338008045	5

Table C2: Summary of extension data for specific and non-specific tip-sample interactions between a dodecanethiol-modified Au tip and a TmGH1-terminated sample. Reasonable events were chosen as indicated in section 5.2.2